

Operational Use of Radar for Precipitation Measurements in Switzerland

Jürg Joss¹
Bruno Schädler²
Gianmario Galli¹
Remo Cavalli¹
Marco Boscacci¹
Edi Held¹
Guido Della Bruna¹
Giovanni Kappenberger¹
Vladislav Nespor³
Roman Spiess³

Locarno, 23.Sep.1997

¹ MeteoSvizzera, via ai Monti della Trinità 146, CH 6605 Locarno 5 Monti

² Landeshydrologie und -geologie, Papiermühlestrasse 172, CH 3003 Bern

³ Geographisches Institut der ETHZ, Winterthurerstrasse 190, CH 8057 Zürich

Table of Content

1.	Foreword, Summary, Zusammenfassung, Résumé, Riassunto	4
1.1.	Foreword.....	4
1.1.1.	Summary	5
1.1.2.	Zusammenfassung.....	5
1.1.3.	Résumé.....	6
1.1.4.	Riassunto.....	6
2.	Glossary, Abbreviations and Symbols	7
2.1.	Glossary.....	7
2.2.	Abbreviations	8
2.3.	Latin symbols	9
2.4.	Greek symbols.....	12
3.	Introduction (Joss, Spiess)	13
3.1.	Aim of project NOWRAD	13
3.2.	Aim of this report	14
3.3.	Milestones in the project	14
4.	Precipitation estimates by radar (Joss).....	15
4.1.	Introduction.....	15
4.2.	Accuracy of radar measurements.....	16
4.3.	Elimination of ground clutter	22
4.4.	Profile corrections.....	25
4.5.	Attenuation	28
4.6.	Interpolation of radar data (Spiess).....	29
4.7.	Past experience.....	31
5.	Swiss Weather Radars (Galli)	36
5.1.	Special Attributes of the Swiss Radars.....	37
5.2.	Compositing	47
6.	Products (Galli).....	50
6.1.	Type of Products	50
6.2.	Formats of Composite Products	63
6.3.	Coverage and coordinates of radars.....	68
7.	Archive (Galli)	73
7.1.	Concept for Archiving	73
7.2.	Software.....	76
8.	Operation (Cavalli, Della Bruna, Boscacci).....	82
8.1.	Concept for maintenance.....	82
8.1.1.	Calibration and Adjustment.....	82
8.2.	Status monitoring: Radwatch (Della Bruna).....	86
8.3.	Hard- and software (<i>Boscacci</i>).....	88
9.	Influence of the orography (Held, Kappenberger)	91
9.1.	Questions.....	91
9.2.	Instrumental and meteorological influence	91

9.3.	Corrections	92
9.4.	Results	93
9.5.	Alpine precipitation, past records (<i>Kappenberger</i>)	94
10.	Wind induced error of precipitation gauges (<i>Nespor</i>)	97
10.1.	Introduction.....	97
10.2.	Assumptions.....	98
10.3.	Results	100
10.4.	Comparison with measurements	103
10.5.	Conclusions.....	107
11.	References	108
11.1.	General References.....	108
11.2.	Special references to Swiss radars (being updated)	112
12.	Format of product data (<i>Galli</i>)	113
12.1.	Introduction.....	113
12.2.	Datafile Structure.....	113
12.3.	Decoder program	113
12.4.	Product identification	114
12.5.	Product Type.....	114
12.6.	Image format.....	115
12.7.	Pixel content.....	116
12.8.	Georeferencing	118
12.9.	Format of Wind Profile data.....	120
12.10.	Quality Indicator.....	121
12.11.	Visibility maps	121

1. Foreword, Summary, Zusammenfassung, Résumé, Riassunto

1.1. Foreword

Hydrologists need precipitation measurements. As simple as it looks, as difficult it is to obtain reliable data. We know that rain gauge measurements have errors, owing to the type of the instrument and to the site. Wind, snowfall, drop-size influence the results. But the largest problem is the areal representativeness. Measurements on a surface of 200 or 400 cm² are used to estimate the rainfall on areas in the order of magnitude of 100 km². Knowing the spatial variability of rainfall, especially during flood events, it is obvious that point measurements, even if the measurement itself would be correct, are heavily biased.

The hope of hydrologists is concentrated on radar measurements. Radar provides images of instantaneous rainfall intensity distribution over large areas. However, when trying to obtain the desired quantitative results one encounters a series of problems. Radar measures an echo, which is influenced by type, size and concentration of particles, all depending on the meteorological conditions, ground clutter, shadowing by mountain ridges, attenuation and parameters of the instrument itself. Calibration based directly on physical data is not possible, owing to the simple fact that no reliable data are available, since, as indicated above, rain gauge data are in error too. So one tries to obtain the best possible agreement with point measurements, being aware, that neither the gauge value nor the radar interpretation is necessarily correct. Therefore, radar is, and will be in future as well, a semi-quantitative measurement device.

However, despite of all these shortcomings, it is by far the best method to obtain information on areal precipitation. It allows to determine the relative weight of the individual rain gauge within the event. The size and the movement of thunderstorm cells can be observed, the height of the snowfall line can be interpreted from the received signal, thus making it an indispensable tool when flood forecasts are required at short time range ("nowcasting"). The areal information obtained was widely used in the NFP31 project "Klimatologie der Stürme anhand von Radar- und Schadendaten" carried out by Schiesser. Radar images enabled a better interpretation of the occurrence of debris flow events, as described in the NFP31 project by M. Zimmermann "Murganggefahr und Klimaänderungen". The practical value and the problems of application are described in these papers.

At the beginning of the NFP31 project it was intended to describe the use of the radar in nowcasting activities. However, numerous problems encountered when installing the new, third generation of Swiss weather radars, forced the authors to dedicate more time than planned to understand the physics of the instrument and the concept of measurements. Therefore, this publication became for a large part a manual for potential users, illustrating the state of the art of weather radars in Switzerland. The products, the problems and the available accuracy are described. Therefore, this publication is a basis for further applications in all activities which require areal information on rainfall. Users must be aware of the underlying principles of radar measurements and the problems which arise. Thus, the present application handbook is a basis for a wide range of research work in hydrology and meteorology.

Dr. A. Petrascheck, Prof. Dr. D. Vischer
Experts NFP 31

1.1.1. Summary

The precision desired and efforts needed for quantitative radar measurements in hydrology are considered - especially for estimating intense precipitation, aiming at flood warnings. This radar-application is far more demanding than the qualitative use of radar, e.g. for just following and extrapolating echoes in time and space.

The characteristics of the third generation of Swiss weather radars are discussed. This includes calibration, clutter elimination and the scan strategy adopted for optimum profile correction. The profile correction aims to eliminate the influence of clutter suppression and shielding on the weather: i.e. allows to extrapolate from regions, where the radar can "see" precipitation to - usually - lower regions where shielding eliminates real weather echoes and clutter produces additional, artificial echoes. Only after these corrections are applied, the true influence of the orography on the precipitation process itself can be investigated. First results are illustrated.

The last section estimates wind induced errors on measurements of precipitation gauges in rain and snow. These instruments are often the only direct source of information (ground truth) to adjust and verify radar data.

The formats, content, coordinates of and access to products are described. These are available in real time or from the archive over the wide area network of the Swiss Meteorological Institute.

1.1.2. Zusammenfassung

Fragen zur Genauigkeit für quantitative Niederschlagsmessungen mit Radar im Hinblick auf hydrologische Anwendungen (Hochwasseralarme) werden diskutiert. Solche Aufgaben sind wesentlich anspruchsvoller als die heute oft angewendete, reinqualitative Nutzung der Radardaten zur Extrapolation der Echos in Ort und Zeit.

Besprochen werden sowohl Eigenschaften der dritten Generation von Schweizerischen Radargeräten, deren Eichung, Bodenecho-Unterdrückung und die gewählte Abtaststrategie. Diese erlaubt, in optimaler Weise die Abnahme der Echointensität mit zunehmender Höhe zu korrigieren. Damit wird die Abschattung durch Gebirge und der negative Einfluss der Bodenecho-Unterdrückung auf die Erfassung des Niederschlages reduziert. Dies geschieht, indem man Werte von Orten, die vom Radar gesehen werden, in tiefer liegende Gebiete extrapoliert, d.h. in Gebiete, wo die Abschattung durch Berge (oder die Bodenecho-Unterdrückung) echte Wetterechos eliminiert hat. Erst wenn diese Korrekturen erfolgt sind, kann der wirkliche Einfluss der Orographie auf den Niederschlagsprozess untersucht werden. Erste Resultate werden vorgestellt. Der letzte Abschnitt befasst sich mit der Abschätzung des windbedingten Niederschlagsmessfehlers bei flüssigem sowie auch bei festem Niederschlag. Der Niederschlagsmesser stellt dabei zur Eichung und Verifikation von Radardaten oft die einzige Informationsquelle dar.

Formate, Inhalt, Koordinaten und Zugriff zu den Produkten sind ebenfalls beschrieben. Der Zugang zu den aktuellen (real time) sowie zu älteren Produkten erfolgt über das WAN (wide area network) der Schweizerischen Meteorologischen Anstalt.

1.1.3. Résumé

La précision des mesures *quantitatives* de précipitations par radar en vue d'applications hydrologiques, en particulier des avertissements du danger de crue, font l'objet de discussions. Ces objectifs sont infiniment plus exigeants que l'utilisation purement *qualitative* des données de radar destinées à l'extrapolation des échos en espace et en temps.

Les caractéristiques propres à la troisième génération d'instruments radar suisses ainsi que leur étalonnage, la suppression d'échos de sol et la stratégie de balayage permettant des corrections optimales des profils sont également discutées. Ces corrections éliminent l'influence négative de la suppression d'échos de sol (échos fixes) et de la projection d'ombre (suppression des échos réels) par les montagnes sur l'enregistrement de la précipitation; cela se fait par l'extrapolations des valeurs des lieux visibles au radar vers les régions invisibles (près du sol), ou les endroits où la suppression des échos fixes à éliminer des échos météorologiques réels. La vraie influence de l'orographie sur le processus de précipitation ne peut être étudiée avant que ces corrections soient effectuées. La dernière partie estime les erreurs dûs aux vents dans les mesures de précipitations par les pluviomètres et par les nivomètres. Souvent, ces instruments constituent la seule source d'information immédiate (réalité de terrain), apte à ajuster et vérifier les données de radar.

Les formats, les contenus et les coordonnées et l'accès aux produits sont décrits. Ces éléments sont disponibles en temps réel ou par les archives moyennant le WAN (wide area network) de l'Institut suisse de météorologie.

1.1.4. Riassunto

In vista di applicazioni idrologiche (allarmi alluvioni), saranno discusse le domande inerenti la precisione delle misure quantitative di precipitazioni con radar. Questi compiti sono essenzialmente più richiesti rispetto all'odierno uso qualitativo dei dati radar destinati all'esportazione di echi in tempo e spazio.

Sono discusse le caratteristiche degli impianti radar svizzeri della terza generazione, la relativa calibrazione, l'eliminazione di echi del suolo e la strategia scelta che con sente di correggere in modo ottimale la diminuzione dell'intensità dell'eco con l'altitudine. Queste correzioni riducono l'effetto dell'ombra delle montagne e l'influsso negativo dell'eco del suolo nel rilevamento delle precipitazioni. Questo avviene estra polando i valori di luoghi "visti" dal radar in altitudine per regioni vicino al suolo, dove l'ombra ha eliminato degli echi di precipitazione o dove, eliminando gli echi fissi, sono stati eliminati anche gli echi di precipitazione. Solo dopo l'applicazione di queste correzioni, potrà essere esaminato il vero influsso dell'origliarono sul processo della precipitazione. Sono presentati i primi risultati.

L'ultimo capitolo tratta la stima degli errori dei pluviometri causati dal vento in caso di precipitazioni normali come pure intense. Il pluviometro rappresenta spesso l'unica fonte di informazione per la calibrazione e la verifica dei dati radar.

Formati, contenuto e coordinate dei prodotti sono pure descritti. L'accesso ai prodotti attuali (tempo reale) come pure a quelli archiviati è possibile tramite l'ampia rete dell'Istituto svizzero di meteorologia.

2. Glossary, Abbreviations and Symbols

2.1. Glossary

Bin:

equivalent to gate (see there).

Bright band:

enhanced (bright), concentric rings visible on radar images produced by scanning the antenna in a cone and picking up higher echoes related to melting snow at altitudes below 0°C wet bulb temperature.

Cell:

space unit in polar coordinates of (1 deg) x (1 deg) x (1 km radial length).

Clutter, ground clutter:

contamination of measured echo (reflectivity, signal) by reflections of the emitted radiation at the ground.

Coherence:

attribute of received echoes with constant relative phase shift versus time (e.g. originating from non-moving targets), in contrast to the incoherent echoes received from many small targets moving relative to each other, as falling rain drops do.

Doppler frequency:

frequency of an echo reflected by a moving target; the Doppler frequency is primarily determined by the emitted frequency, but is modified depending on the radial velocity of the reflecting target: it is lowered by targets moving away from the radar, risen in the opposite case.

Decibel (dB):

a logarithmic expression for the ratio of two quantities, the mathematical expression being $\text{dB} = 10 \cdot \log(x1/x2)$. Depending from the physical quantity we denote dBm for the electrical power in [mW], dB_R for the rain intensity in [mm/h], dBZ for the reflectivity factor in [mm^6/m^3] when setting $x2=1$.

Gate:

element caused by the resolution in time of the receiver; the original time period during which the receiver is ready to record echoes originating from a certain distance: in our case a space unit in polar coordinates of ca. 83.3m radial length, related to the pulse length and the speed of light.

Pixel:

space unit in cartesian coordinates of (1km)x(1km)x(1km) e.g. for products RAIN or RAPID single radar or (2km)x(2km)x(1km) for composite products TODAY or OVERVIEW.

Radome:

Radar dome; shielding to protect the radar antenna.

Specs:

specifications and parameters of the radar equipment provided to and by the producer.

Volume:

entire volume scanned by one radar station in polar coordinates; for the new Swiss radars the volume over flat terrain would be a hemisphere of 230km radius, of which 200km x 200km x 12km are analyzed in cartesian coordinates.

Z-R relationship:

empirical relation between the radar reflectivity factor Z and the rain rate R ($Z=aR^b$, a : constant in Z-R relationship, typically a value of 316, b : exponent in Z-R relationship, typically a value of 1.5 (Z-R relationships, and see also Collier, 1996 or Sauvageot, 1992).

2.2. Abbreviations

ADU:

Analog to Digital Units; digitalized received signal of 12 bits size, characterizing the signal received for 1 pulse (pulses are transmitted $\sim 1/30$ degree in azimuth having a radial resolution of 1/12 km (in range)).

BITE:

Built In Test Equipment, used to evaluate system noise.

CAPPI:

Constant Altitude Plane Position Indicator; image of reflectivity in Cartesian coordinates from a volume of 200km x 200km x 1km; the 12 CAPPIs piled up constitute the product OVERVIEW (see Product processing).

LZW:

file compression format (after Lempel-Ziv-Welch)

MAP:

Mesoscale Alpine Programme.

NFP31:

Nationales Forschungs Programm 31, Swiss National Research Programme 31: "Climate Changes and Natural Hazards".

NOWRAD:

NOWcasting of precipitation with RADars: a project of the National Research Programme NRP31 about "Climate Changes and Natural Disasters".

PPI:

Plane Position Indicator; image of reflectivity or velocity or clutter in Polar coordinates resulting from the antenna scan at a fixed elevation angle.

PRF:

Pulse Repetition Frequency of transmitter; 600, 800 or 1200 Hz depending on elevation.

RF:

Radio Frequency.

SMA:

Schweizerische Meteorologische Anstalt: Swiss Meteorological Institute.

SRN:

Swiss Radar Network

VAD:

Velocity-Azimuth Display; algorithm to display the horizontal wind-vector calculated from the radial wind speed measured at high elevation (34 and 40 degree), as a function of azimuth and assuming horizontal homogeneity.

WAN:

Wide Area Network.

WBN:

Wide Band Noise; the wide band noise test is applied to detect second trip echoes and mark them as ground clutter (in the Doppler channel).

2.3. Latin symbols

a:

constant in Z-R relationship, typically a value of 316.

b:

exponent in Z-R relationship, typically a value of 1.5.

$c_{R,G}^2$:

square of correlation coefficient between radar-based ground-level rainfall estimates and precipitations measured with gauges, equal to the explained variance divided by the total variance of gauge-amounts at all analyzed points in the population

D [mm]:

rain drop diameter

G [dB]:

antenna gain

G₀ [dB]:

antenna gain on the beam axis

i:

E-W coordinate index (400 pixels corresponding to 400 kilometers) if Cartesian coordinates, or range index if polar coordinates.

j:

N-S coordinate index (400 pixels corresponding to 400 kilometers) if Cartesian coordinates, or azimuth index if polar coordinates.

h [km]:

height above sea level

H:

coordinate index of height of estimate (12 pixels corresponding to 12 km).

HG:

coordinate index of height of ground level (12 pixels corresponding to 6 km).

k1 . . . k3:

regression coefficients (units varying)

K_{H,HG} [-]:

12 x 12 values: Correction factors used to apply the vertical profile.

M:

number of azimuth samples for a single azimuth sector, usually M=33.

n [-]:

multiplication factor to correct for wind-induced errors of precipitation gauge measurements (see also: Wind induced error of precipitation gauges (Nespor))

N [m⁻³mm⁻¹]:

number of drops per m³ and mm

N_0 [$m^{-3}mm^{-1}$]:

as N [$m^{-3}mm^{-1}$], for $D=0$

Q_{3dB} :

radar aperture angle [deg], aperture angle at which the signal gain is reduced to half its value from beam centre

R [mm/h]:

corrected rainfall rate (see also: Wind induced error of precipitation gauges (Nespor))

$R_{i,j,H}$ [mm/h]:

400 x 400 x 12 values: Estimated precipitation rate using the Z-R relationship.

$RG_{i,j}$ [mm/h]:

400 x 400 values: Best estimate of precipitation rate at the ground.

R_H [mm/h]:

12 values: Best estimate of vertical profile of precipitation rate.

R_m [mm/h]:

measured rainfall rate (see also: Wind induced error of precipitation gauges (Nespor))

R_N [mm/h]:

rain rate corresponding to noise-equivalent power

R_{NS} [mm/h]:

rain rate corresponding to noise-source-equivalent power

R_{NS0} [mm/h]:

nominal value for noise-source-equivalent rain rate

R_P [mm/h]:

peak power-equivalent rain rate

$VIS_{i,j,H}$ [-]:

400 x 400 x 12 values: Visibility normalized to the maximum value at a given height level.

$VISIB_{i,j,H,t}$ [mm]:

400 x 400 x 12 values: Precipitation (mm) in each pixel of the volume integrated over time from the beginning (months to years) at time t .

v_f [m/s]:

wind speed (see also: Wind induced error of precipitation gauges (Nespor))

vv [m/s]:

vertical wind speed averaged over $18 \times 18 \text{ km}^2$

vw [m/s]:

vertical wind speed averaged over $80 \times 80 \text{ km}^2$

$W_{H,HG}$ [-]:

12 x 12 values: Weight, used to calculate the best estimate at ground-level, for each combination of **H** and **HG**.

$Z_{i,j,H}$ [$\text{mm}^6 \text{ m}^3$]:

400 x 400 x 12 values: reflectivity factor measured by the radar.

2.4. Greek symbols

$\Lambda\mu\beta\delta\alpha$ [mm^{-1}]:

parameter of the drop size distribution formula, depending on the rain rate

Καππα :

Ulbrich drop size distribution parameter; $k = -1$: small drops (typical for orographic rain), $k = 1$: large drops (typical for thunderstorm rain)

3. Introduction (Joss, Spiess)

3.1. Aim of project NOWRAD

At the beginning of project NOWRAD (NOWcasting of precipitation with RADar) the Swiss Meteorological Institute (SMA) had just ordered three new weather radars from Gematronik, Germany, with software from Lassen Research, California. The specs were based on the experience with the first two generations of weather radars in Switzerland. It also considered the conclusions and recommendations from COST-projects (COST72: Measurement of Precipitation by Radar, COST73: Weather Radar Networking and COST75: Advanced Radar Systems, still going on).

As explained in the introduction of Swiss Weather Radars (Galli) the specs at that time were far from being complete, but rather "visionary", based on the experience and extrapolated in the future: putting the equipment into operation, therefore, was rather a research than an operational task. The aim of the new radars included applications for nowcasting heavy precipitation and issuing of flood warnings. Therefore, the work already started fitted well in the new theme of the Swiss National Science Foundation "Climate changes and Natural Disasters" NFP31.

The goals, having been set up at the beginning of our project NOWRAD, were and still are correct for both efforts (NFP31 und SMA). But they were too ambitious and could not be reached fully in the time and with the effort available. Future work will have to continue the well started task. Here the Mesoscale Alpine Programme (MAP) will profit from what is already available and continue. Concrete plans exist to use the Swiss radars in the field-phase of MAP and in the sub-project CLIMPRA (CLIMatology of Precipitation from Radar and in-situ data over the Alps).

Important goals of the project NOWRAD have been reached: Our forecasting office has more and better products than before: the products OVERVIEW, RAIN and PROFIL are -- already just using first-guess-parameters -- of much better quality than the old TODAY-product, which has also been improved with the new results. Many of the algorithms still need their final testing, but preliminary results promise, that the new products fulfil our expectations: in spite of having calculated the default-parameters for calibration, clutter suppression and profile correction on the basis of the old pseudo-3D-data, the new results are already significantly better than the old ones. The new concept for data-transmission showed its merits: It allows modifications of parameters and algorithms via direct access to the software on the three radar stations. The new program "RADWATCH" was created to check the 171 operational parameters defined for each radar station. "RADWATCH" allows to indicate deviation from normal conditions in the unmanned radar equipment.

With this equipment and software the basis for long-term, real-time, reliable surveillance of precipitation in Switzerland was created. First steps for its application have also been made.

3.2. Aim of this report

This report presents in a nut-shell all information available on the Swiss radar system - or the access to it, referring to basic literature and the documentation elaborated during NOWRAD. It should help the user in form of a manual to better grasp the radar information, to understand its content and apply it to special needs.

To make it easier for non-german speaking users inside and outside Switzerland, we have written it in English. If you do not understand what we are trying to explain, it is not your fault, radar is a very complicated thing, and not easy to describe.

3.3. Milestones in the project

After starting NOWRAD in June 1992, E. Held and G. Della Bruna could be hired for 3 years each. E. Held finished his PHD-theses at the end of 1995 (see Influence of the orography (Held)). The project was going to end mid 1996, but in agreement with the conductors of NFP31 was continued until the end of 1996. This allowed us to hire Dr. V. Nespor (under the guidance of Prof. H. Lang, GIETHZ) who just had finished his PHD-thesis on:

"Investigation of wind-induced error of precipitation measurements using a three-dimensional simulation"

His object is to estimate wind induced errors of rain. Being the dominant source of error of our reference instrument at ground level, this is an important subject for the warmer season and lower altitudes. He agreed to continue his work and investigate wind induced errors in snow in the second part of 1996, supported by ETH and NFP31 (see Wind induced error of precipitation gauges (Nespor)). Snow is important in a large part of the radar volume and over a long time of the year.

It was an important task of NOWRAD to develop the concept of a user-friendly archive especially for NFP31-partners, for operational weather forecasting and for future research. This was done during the project, starting from a simple version (storing just one product in an ad-hoc way) to utilities for building a central data base of the raw data for future research as well as of some often used products for easy access, both for real-time and long-term storage (see Archive (Galli)). Products are described in some detail in Swiss Weather Radars (Galli) .

During the full duration of NOWRAD, archived data were provided for the collaboration with other NFP31-projects such as Zimmermann et al. (1997) and Schiesser et al. (1997). The administrative part of the project (effort involved as well as conclusions) is described by Haug et al. (1997).

4. Precipitation estimates by radar (Joss)

4.1. Introduction

Factors limiting the use of radar for quantitative work in an Alpine region are discussed. Obviously the precision needed for quantitative radar measurements in hydrology - especially for issuing flood warnings - is far more demanding than for a qualitative use of radar, e.g. for just following and extrapolating echoes in time and space. The concept of clutter elimination, calibration, profile correction and adjustment with rain gauges of the third generation of Swiss radars is described and first results are given. A preliminary step to quantify the influence of the Alpine orography on the radar data has been done (see Influence of the orography (Held)). The goal of our work is to set the basis for a full approach in assimilating many data sources, as discussed by Laroche and Zawadzki (1995) to analyze data in three dimensions and extrapolating it in time.

On one side the influence of some purely instrumental aspects - such as the stability of the radar hardware - on the accuracy of radar to estimate precipitation are fairly well known and can be kept stable (see Calibration and Adjustment). On the other hand a second class of instrumental attributes are far more difficult to detect and investigate, because the magnitude of the resulting error is influenced by meteorological processes and the orography. In other words, we have to separate the consequences of the precipitation process from effects of shielding of precipitation (optical horizon, curvature of the earth), ground clutter and the finite width of the radar beam. These combined effects, perhaps together with uncertainties of the Z-R-relationship in snow and rain, are far more difficult to handle and more limiting for the retrieval of precipitation amounts at ground-level than purely instrumental problems such as the calibration of the hardware. We often ignore the complex combinations of instrumental features and meteorological phenomena when we try to find answers with models which are too simple, e.g. by assuming that the reflectivity measured aloft can be directly transformed into rain rate at the ground. Here, for the optimum solution, we must use our knowledge about the various instrumental and meteorological processes involved.

Knowing the order of magnitude of the various uncertainties from analyses of data of the second generation of Swiss radars, the rather poor agreement between radars, rain gauges and river flow described in Past experience is understandable. An agreement within a factor of two for daily amounts was typical. Therefore, we conclude that we can significantly improve the use of radar for quantitative work by careful calibration of the radar, complete elimination of ground clutter, applying rigorous corrections for limited visibility and for variations of the vertical profile of reflectivity. Whenever feasible, these corrections were applied for test purposes off-line to the recorded data of the second generation of radars. The algorithms are now installed in the third generation of 3 Swiss radars. The last radar has been installed on La Dôle close to Geneva in autumn 1995. The software is working in all three radars, but in order to obtain optimal results, parameters still need adjustment. Nevertheless, the stability of the instruments, the access to calibration data and the clutter elimination could be improved significantly in the third generation. Much better correlation between radar and gauges are obtained, in spite of still using mostly default values (determined from the second generation) for the parameters controlling real-time tests and analyses of the data.

Need of, and concept for improvement are discussed in more detail later in this chapter and properties of the practical realization are listed in Special Attributes . Influence of the orography

(Held) shows ways to analyze the influence of the orography and consequences on the new way of analyzing the data.

4.2. Accuracy of radar measurements

4.2.1. Accuracy requirements for hydrological applications

A reasonable accuracy desired to estimate rain amounts for hydrological applications spans from a few tens of percent down to a few percent, depending on whether we discuss point values or quantities averaged over time and space. This is by far more demanding than the precision needed just to follow the and to extrapolate them qualitatively in time and space.

Apart from the distinction between applications involving point values and averages over time and space, we need to differentiate between systematic and stochastic errors. While the systematic errors (bias) are unaffected by integration, the stochastic ones are sensibly reduced (by the root of the number of independent samples). But stochastic errors can also produce a bias: in case of an integration in another "unit" than the variable of interest. E.g. if we integrate over the logarithm of the reflectivity (assuming a standard deviation of 7.5dB of the values of reflectivity), instead of the rain rate, we obtain a bias of 4.3dB (a factor of 2.7) for the rain rate. As a rule we should, therefore, perform all integrations in the "unit" of interest: i.e. the rain rate, in case we are interested in flood warning or the reflectivity in case of interest in echo strength. In other words, when interested in rain rate we should not average reflectivity, but do the transformation between Log Z and R as early in the process as possible.

Discussing the errors of radar and its verification we should not forget errors of the reference, i.e. gauges, river flow etc. Some aspects are discussed in Influence of the orography (Held) and in Wind induced error of precipitation gauges (Nespor) .

4.2.2. The concept to achieve the accuracy

To fulfill the need in accuracy for hydrological radar applications, our concept includes the following three steps:

a - Automatic calibration using microwave- and other test equipment to check the stability (relative accuracy) of all important components. Every 5 min crucial components are measured and, if feasible and reasonable, parameters for data analyses are automatically calibrated. The main aim of this first step is to obtain stability of the system: if the system does not perform according to the standards specified by the user (i.e. if preset thresholds of operating parameters are exceeded), an electronic mail is sent automatically to the maintenance staff, giving the necessary information for a rapid and efficient intervention, as described in more detail in Status monitoring: Radwatch (Della Bruna) .

b - The software eliminates clutter, corrects for beam shielding (e.g. topographically induced) in connection with the estimated vertical profile of reflectivity, using the best available information on the local visibility and on the Z-R relationship .

c - Finally the absolute accuracy of the quantitative precipitation measurements is achieved with the help of long-term correlation and adjustment with data from rain

gauges. The time needed to do this job depends on the number of gauges available and the desired precision. As different weather situations should be considered, we are talking at least of many hours, if not days or months with precipitation.

4.2.3. *Z-R relationships and representativity*

As used with the old radars, for the new radar software we set the exponent in the relationship $Z=AR^b$ to a constant value of $b=1.5$. This makes data analyses easier. It is also reasonable for physical arguments: in a large range of "natural" conditions the exponent b of a "population" of drop size distributions varies within narrow limits (10% around a mean value of around 1.50, see TABLE 3.1). These conditions include reasonable atmospheric variations of air pressure and temperature. They also include a variation of rain rate R within a factor of 10 as well as N_0 within a factor of 10 (assuming an exponential distribution: $N=N_0\exp(-\Lambda D)$ with Λ depending on the rain rate R). Considering that exponential distributions result from large sample sizes (as shown by Joss and Gori, 1978), the immense measuring-volume of operational weather radars (as compared to the small sample volume obtained e.g. from drop devices) should lead to exponential distributions. N_0 must, however, remain constant within the population for which the exponent b is assumed to be close to 1.5. This condition is met by definition for a single measurement cell of the radar, for which we may want to reduce the fluctuations of the radar signal caused by changes of position of the precipitation particles.

However, changes of N_0 correlated with R and Z (in the population of samples used to determine Z-R) do lead to a corresponding deviation of the exponent from 1.5. More details and first results of analyzing the immense data set recorded in Germany during 7 years are given in the paper by Doelling et al. (1996).

The proposed $b=1.5$ simplifies the implementation of the Z-R or R-Z relationship in every-days operational work considerably and, furthermore, allows easier comparison between different case studies (different authors). But not only physical reasons justify setting $b=1.5$. Often the determination of an exponent is not justified or may be in error because of truncation or statistical limitations (large fluctuations due to limited sample sizes). Smith et al. (1993) discuss consequences of small samples. They show that statistical fluctuations caused by limited sample sizes, resulting from a single population of drops can mimic (reproduce) a Z-R relationship just as reported for drop size devices in real rain. This means the Z-R-line in their simulation is caused only from too small a sample size! In fact, the single population of drops should result in just one point, not a line: one single value of rain rate belonging to one value of reflectivity.

TABLE 3.1: "Natural typical" variations of DSD-parameters.

The input variables in rows 1 to 4 and their influence on the power laws between parameters of the DSD. Dependences between the reflectivity Z [mm^6m^{-3}], the slope Λ [mm^{-1}] and the two-way attenuation A [dB/km] from the rain rate R [mm/h] are given in Rows 6 to 11, Columns B to M. The power laws, defined by the constant (pair-lines) and the exponent (impair lines) correspond to the straight line (in the Log-Log-plot), tangential to the curved line of the parameter versus rain rate R . Columns B and C show the results for extreme cases, column D for an average distribution, columns E,F the influence of the rain rate R , columns G,H the influence of N_0 , columns I,K the influence of the temperature T and columns L,M the influence of the air pressure p (for details see Doelling et al, 1997).

Operational Use of Radar for Precipitation Measurements in Switzerland

	A		C	D	E	F	G	H	I	K	L	M
1	R/[mm/h]	0.3	100	5	1	30	5	5	5	5	5	5
2	No[m ⁻³ mm ⁻¹]	30,000	1400	8000	8000	8000	1400	30,000	8000	8000	8000	8000
3	T/[°C]	0	0	10	10	10	10	10	0	20	10	10
4	p[hPa]	700	1050	850	850	850	850	850	850	850	800	900
5	A ^(a) /[mm ⁶ /m ³]	120	722	201	211	203	485	108	205	198	194	209
6	A/[mm ⁶ /m ³]	107	376	201	211	175	453	113	204	199	195	208
7	b in Z = A R ^b	1.406	1.642	1.499	1.463	1.543	1.542	1.469	1.503	1.496	1.497	1.502
8	c/[mm ⁻¹]	5.726	3.089	4.33	4.301	4.419	3.008	5.680	4.325	4.338	4.353	4.312
9	d in $\Lambda = c R^d$	-0.201	-0.235	-0.214	-0.209	-0.220	-0.220	-0.210	-0.215	-0.214	-0.214	-0.215
10	e/[dB/km] ^(b)	0.0044	0.0047	0.0048	0.0050	0.0048	0.0054	0.0046	0.0049	0.0048	0.0047	0.0050
11	f in A = e R ^f	1.016	1.187	1.084	1.058	1.116	1.115	1.062	1.087	1.081	1.082	1.086

(a) To calculate **A**, the exponent was set to **b**=1.5

(b) The relationship for two-way attenuation is given here for a wavelength of 5.6 cm. Note that at 10 cm wavelength the attenuation is ~5 times smaller, at 3.2 cm ~5 times larger (These factors depend on the drop size distribution and the temperature: here we assumed No= 8000m⁻³mm⁻¹, R=30mm/h, p=850hPa and T=0°C).

But what errors in estimated rainfall rate R are to be expected if the exponent **b** in the data analyses is kept constant (i.e. ignoring deviations from 1.5 in nature, caused by systematic variations of **No** with **R**)? The analyses shows that errors increase proportionally to the fraction of **No** (standard deviation) correlated with **R**. If we adjust **A** for each rain sample (e.g. according to the vertical reflectivity profile) no error occurs. Even with a "reasonable" correlation between **No** and **R** and with setting **A** to a constant value, the error for the average **R** will be smaller than the one caused by averaging the linear reflectivity or Log(**Z**), i.e. dB-values instead of averaging in the linear domain of rain rate!

Following Smith and Joss (1997) we find:

$$Z = A \cdot R^b \tag{3.1}$$

In the software we set for the analyses $b_f=1.5$ and adjust the A at the rain rate R_A with the corresponding Z_A

$$A = Z_A / R_A^{b_f} \tag{3.2}$$

If the actual rain rate R_a has a real exponent b_a different from the fixed one ($b_f=1.5$) used in the software, we obtain a deviation for the estimated rain rate R_f (fixed in the data analyses, assuming $b=1.5$), because:

$$Z/Z_A = (R_a/R_A)^{b_a} \quad \text{and} \tag{3.3}$$

$$Z/Z_A = (R_f/R_A)^{b_f} \tag{3.4}$$

combining Eq.3.3 and Eq.3.4 leads to the fractional error caused when b_a deviates from the assumed fixed exponent b_f set in the software:

$$R_f/R_a = (R_a/R_A)^{(b_a - b_f)/b_f} \tag{3.5}$$

Table 3.2 shows this ratio for a deviation of the actual exponent b_a of 0.2 from the value b_f set in the software. Note that this deviation is twice as big as found for exponential distributions with a single value of \mathbf{No} in the population of DSD (see TABLE 3.1). Doelling et al (1997) give details on how much \mathbf{A} and \mathbf{b} change for a given variation of \mathbf{R} , \mathbf{No} and other parameters.

TABLE 3.2: Ratio R_f/R_a for a fixed exponent $b=1.5$

of estimated R_f to the actual R_a precipitation rate for various deviations R_a/R_A (the actual R_a rate to the rate R_A where the adjustment of A has been made. No deviations are found ($R_f/R_a = 1$) if $R_a=R_A$ or $b=1.5$.

Ra/RA	b=1.3	b=1.5	b=1.7
0.1	1.359	1.000	0.736
0.316	1.166	1.000	0.858
1	1.000	1.000	1.000
3.16	0.858	1.000	1.166
10	0.736	1.000	1.359

When estimating precipitation in a river basin, the rain rate is varying from pixel to pixel. Frequency distributions are often found to be approximately exponential (e.g. Jones 1978). If $p(R) = p_0 R \exp(-R/R_e)$ then an integral of Eq.(3.6) over all rates will give the accumulated rainfall Q in the river basin. The integrand is one of the family of gamma distributions, which has a distinct mode at $R_m = 1.678 R_e$.

$$dQ = R * p(R)dR = p_0 R \exp(-R/R_e)dR \quad (3.6)$$

If in Eq.3.1 the exponent deviates from the estimated, fixed one (b_f) and we integrate over all rain rates, we find for the rain amounts Q_f/Q_a :

$$Q_f/Q_a = (R_e/R_a)^{(b_a - b_f)/b_f} \cdot |b_a/b_f|! \quad (3.7)$$

To make $Q_f/Q_a \sim 1$, we have to adjust the radar at the rain rate R_A :

$$R_A = R_e \cdot |b_a/b_f|!^{(b_a - b_f)/b_f} \quad (3.8)$$

For $b_f=1.5$ and $1.3 < b_a < 1.7$ we find $R_A = 1.53 R_e$, (within less than 1%). Having adjusted the radar at $R_A = 1.53 R_e$, the errors-boundaries given in Table 1 are also valid for integrals (precipitation amounts) over distributions of rain rate Eq.(3.6), with R_e/R_A replacing R_a/R_A in TABLE 3.2

For example the radar assuming in the software a $b_f=1.5$, it indicates a precipitation amount Q_f which is 0.736 times smaller (-26.4%) than Q_a , if the real exponent is $b_a=1.3$ and the mode-rain-rate R_e is ten times larger than assumed, when the radar was adjusted: indeed a small error for a large deviation of mode intensity as well as of mode exponent! This is because the error ratio has a "self-compensating" feature: any overestimate on one side of R_A tend to be offset by underestimates on the other side.

In short, it means we should adjust the Z-R-relation where we need it in our application. Then the small, natural variations of the exponent b are unimportant, thus making data analysis much easier (just needing to adjust the linear constant A).

Atlas et al. (1996) discuss variations of drop sizes in TOGA COARE. As revealed by simultaneous samples at ground level and aloft (airborne), they find significant differences. This leads to the difficult, but important, question about the representativity of single point- or line-samples for a larger area (samples from ground-based/airborne drop sampling devices and vertical pointing radar).

An attempt to summarize our knowledge on DSD's and on experiments needed to answer open questions are discussed in Joss and Zawadzki, 1997.

For an operational radar, we need to know the "representative" Z-R-relationship in the whole range of interest. An obvious and reasonable solution may consist in analyzing the volumetric data of the radar itself (better than point- or line-measurements?). Fabry and Zawadzki (1995) interpret the vertical profile, giving reasons for its variability, and Henrich et al. (1996) propose to extract an estimate for Z-R-parameters from the vertical profile of reflectivity.

Our problem of representativity will be solved, if we succeed to estimate the needed Z-R-parameters in the full volume of our operational radar from vertical profiles measured by the operational instrument itself. This could be done by adapting the results of Henrich et al. (1996). Based on data from a vertical pointing, 3cm wavelength research radar and a distrometer, they show how the shape of the vertical profile of reflectivity can be used to obtain information on the R-Z relationship. The procedure of deducing the precipitation rate at the ground would then imply two steps: 1) extrapolation of the reflectivity aloft to ground level and 2) transformation of this best estimate of the reflectivity at ground level into rain-rate. Note that for both steps the local vertical

distribution of reflectivity is needed and therefore has to be estimated (locally?) from full-volume radar data. With increasing distance (decreasing resolution of the beam, limitations by the radar horizon) this becomes more and more difficult. Then it may be better to extrapolate profiles estimated at close ranges or to use climatological profiles. The future will show the best compromise and how well precipitation can be estimated using such information.

4.2.4. The errors of discretization

The measured data during the various processing phases will be discretized (quantified). This causes uncertainties which are to be set in relation with other sources of errors like fluctuations in observed reflectivity fields.

For instantaneous reflectivity measurements of 1km x 1degree gates values delivered to the users are available in classes of constant width W in units of dBZ. If this width is small enough (typically 3 dBZ in rain) the distribution of the observations within the class can be assumed as log-uniformly distributed. The standard deviation will be $SDq=W/\sqrt{12}$ and thus the variance $VARq=W^2/12$.

Reflectivity observations of C-band weather radars typically fluctuates with a standard deviation of 5.5 dBZ (~ 3dBR). If we assume a beamwidth of 1 degree, use a volume scan of 33 pulses per azimuthal degree and take gates of 83.3 m we may estimate a number of 4 independent samples in azimuth for 1 degree in azimuth (assuming a decorrelation time of 10ms and an antenna rotation speed of 30 ms/degree) and 8 valid observations in radial direction for 1 km in range (assuming 2 of 12 gates are contaminated by clutter). The variance will be $VARf=3^2/(4*8)=\sim 0.3dBR^2$.

The variances from the quantization error and from the fluctuation effects sums up giving the total variance of $VARt=W^2/12+0.3(dBR)^2$.

Choosing a quantization step of 2dBR (~3dBZ) we become:

$VARt=4/12+0.3=\sim 0.63(dBR)^2$ thus the pixel value will have an uncertainty of \sqrt{VARt} or ~ 0.8dBR (factor of 20%).

Taking a volume scan each 5 minutes and building average values of 1 hour (12 measurements) we obtain a variance of $VARt/12$; the pixel value will have an uncertainty of $\sqrt{VARt/12}$ or ~ 0.24dBR (factor of 5.6%).

Conclusion:

the fluctuations of the observed reflectivity fields and the variability in time and space of the precipitation fields are dominant with respect to the error introduced by the discretization of the transmitted measured values for the scales of time and space considered here. Spatial and temporal aggregations (averages) helps further in reducing quantization effects.



Tables of quantisation errors for 3-bit versus 4-bit at different distances from the radar station and under different assumptions for the decorrelation time which is mainly a function of the wind shear, of the illuminated volume and of the fall velocity of the hydrometeors are under construction ...

4.2.5. Z-R relationships and representativity

As used with

4.3. Elimination of ground clutter

4.3.1. Clutter elimination concept

It seems best to utilize all information available in the clutter elimination algorithms, rather than to use a single, perhaps sophisticated, scheme. This is particularly important with rapid-scan systems, since these systems require compromises in PRF because of the combined intensity-Doppler measurements, and hence suffer to a greater extent from problems of range and velocity ambiguity. The following sections describe three aspects of a new approach which produces data with a quality suitable for use in the profile-correction algorithm. The procedure is successfully implemented in the third generation of Swiss radars, first results are described by Lee et al., 1995.

4.3.2. High range resolution

One approach to clutter reduction is to use high range resolution to take advantage of the rapid decorrelation of clutter echoes in space, seeking clutter-free returns close to clutter echoes. The raw polar data has 83-m resolution (2760 gates at 230-km range), so that a total of twelve measurements can be checked over each 1-km range interval while seeking a single clutter-free return.

The computational steps used to obtain the 1-km clutter-free estimates from the raw data emphasize clutter *detection* followed by complete *elimination*, rather than *suppression* of clutter by *subtraction* (Joss and Lee, 1993). All clutter-free measurements in each 1km window are averaged to produce the precipitation estimate. The efficiency in eliminating clutter is high because of the high probability that at least one of the twelve gates in each 1-km range bin is clutter-free, and because a single clutter-free 83-m measurement is sufficient for precipitation estimation in each 1-km range bin.

4.3.3. Decision tree

The signal processing algorithm is based on a decision-tree classification system, so that the processing algorithm used for a given range gate of 83-m depends upon the characteristics of the data in that gate. At each step in the decision tree an attempt is made to classify the signal as rain, clutter, or system noise; if a conclusive decision can be reached the testing is completed and the data for that 83-m gate is marked as one of the three mentioned signal types; if not, then the next test in the decision tree is executed. The clutter elimination algorithm is controlled by a number of parameters and thresholds under user control, and a record of the decisions made is kept at each stage in the tree. This record is useful to adjust the 9 thresholds and parameters for optimum signal classification. First, encouraging results on the success of the decision tree (values of thresholds and the percentages of gates classified in each test) are described in Lee et al. (1995). In the worst case the following five attributes are tested in sequence:

Minimum detectable signal test: The first algorithm classifies the received signal as noise if the signal is lower than a given threshold, set slightly above the system noise level; i.e. if no significant signal is detected the pixel is assigned a precipitation rate of zero, and processing for that gate is terminated. If no signal is there, the clutter map can be decremented, since clearly no clutter was observed either.

Wide-band noise (WBN) test: The wide-band noise test is performed in the Doppler channel after a valid signal (above receiver noise) was detected in the previous test. If the coherence is high enough (WBN lower than a second threshold) the test is continued; if not, the pixel is marked as clutter, the clutter map is incremented, and processing for that gate is terminated.

Velocity algorithm test: The velocity algorithm is performed on signals which did not get a conclusive answer from the first two tests, and hence are known to be significant in magnitude and coherent. The test classifies a received signal as a usable precipitation measurement if the signal velocity is outside an adjustable band around zero velocity. Since this indicates that the echo is moving, the estimate is marked as precipitation, the clutter map is decremented (since no clutter was observed), and processing for that gate is terminated.

Statistical clutter-filter algorithm tests: These two tests are applied to signals known to be coherent but around zero velocity. The tests are to determine the probability that the signal is precipitation, based on the signal probability distribution. According to Geotis and Silver (1976) incoherent clutter detection using the mean-difference algorithm permits 70% of the clutter signals to be rejected with no loss in weather echoes, for a scanning antenna. The rejection rate is much higher for the stronger echoes, which concern us most. The remaining 30% of the echoes contaminated by clutter are mainly weak, causing only a negligible bias. Signals with statistical distributions indicating the possibility of clutter are marked as clutter, the clutter map is incremented, and processing for that gate is terminated (for more details and results, see Lee et al., 1995).

Gradient algorithm test: The gradient test is designed to discriminate against second-trip echoes and anomalous propagation by checking the change in signal power with height, i.e. from one elevation angle to the next. If the observed gradient is markedly higher than the climatological norms, it is likely that a second-trip or anomalous propagation echo has significantly biased the precipitation estimate. A high gradient indicates a false signal, therefore the pixel is marked as clutter, the clutter map is incremented, and processing for that gate is terminated.

frequently than clutter maps in earlier systems, where it was the only way to eliminate clutter, and being dynamic the adaptive clutter map contains far fewer blind spots than the static clutter map (since the map reflects only current clutter, not an integration of clutter over many months). If the clutter map indicates that the gate in question has evidenced significant clutter in the recent past then the measurement is marked as clutter, otherwise the measurement is accepted as precipitation.

4.4. Profile corrections

4.4.1. Concept

Under the term "profile corrections" we understand procedures used to remove artifacts caused by the sampling of the radar at different altitudes as well as for estimating the rainfall intensity at ground level from the calculated vertical echo distribution aloft. In Europe, much work has been done in this context. Koistinen (1986) recognized that the use of even a crude estimate of the vertical profile of rainfall rate can improve the agreement between radar and rain-gauges, and proposed deriving the profile from a 24-hour average of the best available radar measurements. Andrieu et al. (1995) proposed to correct for vertical profile effects through an inverse solution applied to radar data from at least two elevation angles. Diviak and Rakovec (1995) summarize procedures of using profile information to correct for over- and underestimation of radar precipitation. A total of 6 alternative ways of comparing radar data with those of 80 gauges during 3000 hours of precipitation are discussed. These efforts show that one should not simply take reflectivities aloft and use some Z-R relation to calculate the precipitation rate at the ground. Joss and Lee (1995) describe a more sophisticated concept, distinguishing between two "orthogonal" causes of error:

a - The horizontal contribution to the error, including the effects of visibility (earth curvature, topography), clutter, and beam-broadening with distance. In this contribution we include errors which at first approximation are fixed for a given installation, strongly variable in space but independent of the weather and, therefore, can be estimated in advance. A three dimensional array ($\mathbf{VIS}_{i,j,H}$) is needed, indicating the overall visibility of each element of the volume of interest. This may be obtained by integrating the precipitation observed in each cell over an extended period of time (see Procedure for treating the horizontal variation).

b - The vertical contribution to the error, on the other hand, is strongly variable in time, depending on the weather situation. Therefore, this variable must be estimated and corrected for, using - whenever feasible - real-time estimates of the profile from volume data, and otherwise climatological profiles: even the use of climatological profiles significantly reduces errors. Joss and Pittini (1991) discuss the climatology of vertical profiles recorded during the years 1986 to 1990 with the second generation of Swiss radars. This type of correction is described in Procedure for treating the horizontal variation.

The best estimate of precipitation at ground-level is derived from a weighted mean of the overlying, corrected precipitation estimates. Considering that the measurement error

increases with the height of the radar estimate, the weight is reduced with increasing distance (height) from the ground.

4.4.2. Definitions for cartesian coordinates

$Z_{i,j,H}$ [mm^6m^3]: 400 x 400 x 12 values: reflectivity factor measured by the radar.

$R_{i,j,H}$ [mm/h]: 400 x 400 x 12 values: Estimated precipitation rate using $Z=316 R_{i,j,H}^{1/5}$.

i: Coordinate: index E-W (400 pixels corresponding to 400 kilometers).

j: Coordinate: index N-S (400 pixels corresponding to 400 kilometers).

H: Coordinate: index of height of estimate (12 pixels corresponding to 12 km).

H_G : Coordinate: index of height of ground level (12 pixels corresponding to 6 km).

$RG_{i,j}$ [mm/h]: 400 x 400 values: Best estimate of precipitation rate at the ground.

R_H [mm/h]: 12 values: Best estimate of vertical profile of equivalent precipitation rate.

K_{H,H_G} [-]: 12 x 12 values: Correction factors used to apply the vertical profile.

W_{H,H_G} [-]: 12 x 12 values: Weight for each combination of H and H_G .

$VISIB_{i,j,H,t}$ [mm]: 400 x 400 x 12 values: Precipitation (mm) in each pixel of the volume integrated over time (months to years) to time t. $VIS_{i,j,H}$ [-]: 400 x 400 x 12 values: Visibility normalized to the maximum value at a given height level.

4.4.3. Procedure for treating the horizontal variation

Off-line: The precipitation is integrated over many storms (months to years) so that the variability caused by single storms in a given location becomes acceptably small. It is important to note that clutter and anomalous propagation echoes must be eliminated before this integration can be done. The product is saved daily to allow flexibility of data analyses. For every pixel in the volume (400 x 400 x 12) the following summation is done on a continuous basis:

$$VISIB_{i,j,H,\tau} = \sum_{t=0}^{t=\tau} R_{i,j,H,t} \quad (3.9)$$

From $VISIB_{i,j,H,t}$ we derive $VIS_{i,j,H}$. It is an estimate of the average percentage seen in a pixel, calculated for a given period from time $t = t1$ to time $t = t2$. It contains information for the volume. Depending on the experience yet to be made, the period will have to be optimized, e.g. for a month, the summer season, a year etc. For normalization the maximum-value (or a high

percentile-value) of all the pixels at a given altitude is used:

$$VIS_{i,j,H} = \frac{VISIB_{i,j,H,t2} - VISIB_{i,j,H,t1}}{\text{MAX}_{i,j,H}(VISIB_{i,j,H,t2} - VISIB_{i,j,H,t1})} \quad (3.10)$$

4.4.4. Real-time corrections for vertical variation

The mean vertical profile is calculated in real-time from data "close" to the radar (distance < 70km), the radar is at i=200, j=200):

$$R_H = \frac{\sum_{130}^{270} \sum_{130}^{270} R_{i,j,H}}{\sum_{130}^{270} \sum_{130}^{270} VIS_{i,j,H}} \quad (3.11)$$

The correction factor $K_{H,HG}$ is computed for each combination of height of measurement H and height of the ground HG (using a digital terrain map):

$$K_{H,HG} = \frac{R_{HG}}{R_H} \quad (3.12)$$

For stability reasons this correction factor is limited to a maximum value ($K_{max}=3$):

$$K_{H,HG} > K_{max} \text{ then } K_{H,HG} = K_{max} \quad (3.13)$$

The best estimate of the precipitation rate at the ground can then be calculated:

$$RG_{i,j} = \frac{\sum_{12} W_{H,HG} \times K_{H,HG} \times \|R_{i,j,H}\|_{\text{estimated}}}{\sum_{12} W_{H,HG} \times VIS_{i,j,H}} \quad (3.14)$$

A somewhat arbitrary function $W_{H,HG}$ is used to weight the contributions to the final (ground level) precipitation estimate as a function of the altitude of the estimates. This function reflects the practical experience that data taken closer to the ground are more accurate. Therefore Eq.(3.15)

emphasizes the measurements made at the lowest levels (note that for the weight is set to zero):

$$W_{H, HG} = \frac{1}{H + 1 - (HG)/2} \quad (3.15)$$

Note that the following identity exists for the estimate $R_{i,j,H}$ derived with the relationship mentioned in footnote 1 on page 29⁽¹⁾ from the reflectivity $Z_{i,j,H}$ deduced from the radar return:

$$\|R_{i, j, H}\|_{\text{estimated}} = \|R_{i, j, H}\|_{\text{real}} \times (\text{VIS}_{i, j, H}) \quad (3.16)$$

4.5. Attenuation

4.5.1. Correction for attenuation?

Attenuation occurs wherever radiation passes through media: it begins when transmitted radiation crosses the radome and is influenced by the meteorological conditions encountered in the volume to be scanned. Up to now, attenuation of transmitted and reflected radiation has not been taken into account in later processing, but we are evaluating, whether our understanding of the variability of attenuation already allows us to correct for it. There are several problems involved:

1. Factors such as the radar sensitivity, attenuation by the radome and the rain at close ranges, where the radar is not measuring, affect the measurement, and with it, the estimated attenuation to be corrected (Delrieu et al., 1997).
2. The relationship between reflectivity and attenuation is as variable as between rain rate and reflectivity.
3. Uncertainties concerning the representativity of estimated attenuation in time and space are still a matter of concern.
4. As already noted by Hitchfeld, W. and J. Bordan, 1954, errors of attenuation estimates may build up exponentially as the pulse travels through the rain.

These four problems make it extremely difficult to correct errors of attenuation larger than around 2dB two-way. The future will show what improvement can be achieved using more sophisticated way for estimating attenuation, such as differential phase shift, which is very closely related to attenuation, but rather involved and difficult in its measurement.

4.5.2. Uncertainty caused by wet radome

As long as the radome is dry, the specs of the manufacturer for the dry radome are relevant, but little is yet known on the attenuation and phase distortion of a wet radome in different weather- and wind-regimes. In heavy rain at 5cm wavelength a few dB of attenuation and beam distortions, amounting to a considerable part of the beam width, may occur. Obviously more effort has to be dedicated to this question, if we are interested in high precision and reliability. In a working document of COST 75 (Action on "Advanced Radar Systems") a brief summary on consequences of water, ice and mixtures of ice and water, representing the worst case, are given (Joss, 1996). It is probably is

impossible to correct for attenuation errors through a radome in a reasonable way in any real situation, because these errors may depend on the local rain rate, wind direction and speed, as well as on the direction of the radar beam relative to the wind - a truly complex situation.

FOOTNOTE 1 of page 29: *Equivalent precipitation rates are estimated from full-volume radar data using a single Z-R-relationship ($Z=316R^{1.5}$). This simple approximation may err in rain, but especially in snow or the bright band. This, however, does not hurt the quality of the final result, while significantly simplifying the calculations, as its main use is for extrapolating the estimates from aloft to the ground. The error of a given measurement is compensated if the profile is measured with the same relationship used for extrapolation. The Z-R-relationship must be corrected, of course, if the ice content aloft is to be measured.*

4.5.3. Choice of the wavelength

Errors influenced by the choice of wavelength should also be considered: we must compromise between errors caused by attenuation and resolution of the beam. At longer wavelength significantly more clutter is produced, either leading to higher antenna prices or to errors caused by inhomogenous beam filling. We opted for 5-cm waves, decided to postpone important parts for correcting these extra causes and concentrate on errors which are also important and solvable now.

4.6. Interpolation of radar data (Spiess)

4.6.1. Reason for interpolation

Gauges sample precipitation at selected points on the ground. These samples are usually very limited in number and placed in locations chosen for other reasons than representativity of the measurement. As precipitation intensity changes easily by a factor of ten per kilometer in a nonlinear way, the method of interpolation on a rectangular grid with equally spaced grid-points is very important. From these points we then derive precipitation totals, e.g. over a day into a river basin. Using radar data to obtain information on rain distribution (using the radar data as external drift), allows a deeper insight into the nonlinear pattern of precipitation distribution between the gauges, especially in convective precipitation. Very easily a gauge misses a narrow, but heavy precipitation cell.

4.6.2. Interpolation after corrections

The analysis clearly demonstrates that before using radar data to interpolate between gauges, it is extremely important to correct the data for instrumental artifacts. E.g. errors caused by clutter and shielding have to be eliminated as thoroughly as possible (see Elimination of ground clutter and Profile corrections). Results for improvements of instrumental corrections are illustrated in Corrections .

To improve estimates for poorly visible pixels, we can use two ways of interpolation:

a - extrapolate from higher pixels which are better visible (profile corrections) or

b - use pixels from horizontally adjacent regions for interpolation.

The second method has its merits if pixels with better visibility (better than the one of interest) are not too far away horizontally, whereas high-reaching weather situation and locations with rather good visibility ask for the first way. To decide we may look at the correlation between the pixel of interest and its neighbors in all directions. This was done in the vertical and led to the following result (TABLE 3.3): The cases analyzed showed by far better correlation between pixels at 3km and those above than below.

In many respects (profile corrections, smoothing) the results presented in Influence of the orography (Held) were confirmed with independent data and should be published in detail soon.

While the decrease of correlation to higher altitudes is reduced by the precipitation process (which obviously in this case is fairly well correlated and extending to high altitudes), below the altitude of three kilometers the decrease is caused by the visibility (horizon, beam shape and size) which is more irregular, e.g. depending on the azimuth and range. As a conclusion we must correct for the local visibility for optimum results, if we want to use low elevation angles. As at low elevations the chance of measuring in rain (instead of the snow aloft) is biggest, we have a strong need to consider visibility and develop ways of measuring it.

TABLE 3.3: Correlation between levels X and 3km.

X-Range	12km<- >3km	8km<- >3km	4km<- >3km	3km<- >2km	3km<- >1km
Correlation	0.44	0.83	0.96	0.81	0.54

4.6.3. Kriging versus regressions

Streit (1981) in his abstract puts the use and concept of Kriging in easy-to-understand words: "the Kriging method, basing on the theory of spatial stochastic processes, may serve to interpolate and extrapolate spatial hydrologic information. The characteristic features of the respective process, especially effects of persistence depending on the distance and direction, are analyzed by means of the variogram." Comparing Kriging with other multidimensional analyses - like multiple regression and determining spline functions - Streit (1981) finds the following attributes (translated and somewhat interpreted for our application):

1. Kriging weights "locally": values close to the point-of-interest are more important for the estimate. Note that in the multiple regression all samples receive exactly the same treatment.
2. As a result of Kriging we do not obtain a continuous surface (as for multiple regression and splining) but for each "Kriging effort" the best estimate at a grid-point is found. As a consequence, the mathematical effort is larger than for multiple regression and splining, an argument becoming less important as computing power increases.
3. Values at sample-points (gauges) are exactly reproduced with Kriging and splining, while this is not the case for the "over-determined" multiple regression.
4. Kriging can use additional data (from radar) as an "external drift" or by using Ko-Kriging. Both ways of Kriging provide interpolation between measured points at ground-level. When using radar data as external drift, radar data must be available at all rain gauge locations as well as at grid-points of interpolation, whereas for Ko-Kriging radar data is

- not needed at all points. Ko-Kriging is more involved than Kriging, which still needs more computing effort than multiple regression or spline functions.
5. Kriging gives an error of estimate for each evaluation. Multiple regression provides this too, but significant errors of estimating the error may occur because of auto-correlated residuals.

As a conclusion we may say that Kriging, by estimating each point separately, makes best use of the available information (available from surrounding points, thus considering persistence in time and space). The price is the effort involved to treat each point individually. Examples of applying this method to the spatial interpolation of hourly values of precipitation, temperature and snow on the ground can be found by Jensen, 1989.

4.7. Past experience

4.7.1. River-basin - gauge - radar

Making quantitative use of radar is especially difficult in Switzerland. Here results are reported such as were found before implementing the better clutter elimination, profile correction and calibration techniques used in the new Swiss radars. During a 7-year period, only 40% of the precipitation reaching the ground could be measured, country-wide by the old Swiss weather radars, primarily due to visibility and clutter effects (combined with the decrease of reflectivity at higher altitude). This is despite the fact that adjustments were made to force long-term agreement in regions near the radars. Algorithms, derived from retrospective analysis, promise substantial improvement for the fraction seen as well as its variation, through reducing clutter contamination and by real-time profile/visibility corrections.

But it is well known that visibility problems are not the only cause for disagreement with ground truth. This may be illustrated by analyzing five years of data over six river basins. Their sizes range between 25 and 356km², the average area being 130km². Monthly rain amounts estimated by different instruments were compared: basin-area integrated rainfall from radar (RR), two networks of gauges (GG and gg) and river flow (FF). About half of the precipitation was found to flow out of the river basin, leaving the rest - a reasonable amount - for evaporation and other effects. Three to twelve gauges (GG) were set up to be representative for each river basin. Independent from this first set, a second set of three gauges (gg) from the standard Swiss automatic network was used for each basin. The "variation" in TABLE 3.4 is defined as 100 times the standard deviation divided by the average of the 60 values in each basin. The correlation $C_{(XX, YY)}$ between monthly observations for variables XX and YY in each basin is also given. The average (AVG) and the standard deviation (STDEV) of the six basin-values are given in TABLE 3.4. We expected the correlation between the two networks of gauges $C_{(gg-GG)}$ to be higher than any other correlation and to be close to one. $C_{(gg-GG)}$ in fact is the highest, but it is significantly lower than one. Because of their location, the gauges (gg) are slightly less correlated with radar estimates and river flow than (GG).

Two interleaved networks of gauges and river flow: rather low correlation between 60 monthly averages during the years 1988-1992 was found.

TABLE 3.4: Comparison of radar and ground-truth.

Quantity in six basins	AVG	STDEV
Size of river basins	130km ²	114km ²
Distance from radar	60km	25km
Visibility above basins	1497m	395m
Height of basin	796m	190m
GG: amount in gauges for basins	118mm	25.9mm
"Variation"	50%	1.1%
gg: amount gen. purpose gauges	95mm	32.4mm
"Variation"	55%	6.2%
FF: am. river flow out of basins	59mm	20.9mm
"Variation"	60%	10.0%
RR: amount of radar over basins	114mm	31.3mm
"Variation"	62%	5.1%
$C_{(GG \leftrightarrow gg)}$ (Gauge ¹ \leftrightarrow gauge)	0.80	0.10
$C_{(GG \leftrightarrow FF)}$ (Gauge \leftrightarrow river-flow)	0.59	0.10
$C_{(GG \leftrightarrow RR)}$ (Gauge \leftrightarrow radar)	0.60	0.16
$C_{(gg \leftrightarrow FF)}$ (gauge \leftrightarrow river-flow)	0.55	0.18
$C_{(gg \leftrightarrow RR)}$ (gauge \leftrightarrow radar)	0.51	0.19
$C_{(FF \leftrightarrow RR)}$ (river-flow \leftrightarrow radar)	0.31	0.17

We conclude from the analyses that the rather poor correlation between all instruments including two networks of gauges can be attributed to the following factors:

1. Radar problems: measurement bias due to ground clutter, rain echoes obstructed by *beam blocking* (e.g. topographically induced shielding), by approximating the change of reflectivity with height (vertical profile) by a single climatological gradient, Z-R, etc.;
2. Gauge problems: under-sampling, with their representativeness further reduced by weather-dependent orographic effects;
3. Evaporation from the basin, depending on the distribution of rain in time and space;
4. River flow problems: variable delays and variable ground storage depending on current and past weather, storage in snow cover depending on season and terrain height.

While radar problems (1) can be significantly improved with algorithms described in the references, the rest are not influenced by radar, but are related to verifying the results (2) or are typical for estimates of river flow (3+4). Evapotranspiration, though important in this analyses, will be negligible in flash flood situations.

River flow problems strongly depend on the distribution of precipitation in space and time, i.e. the history of the distribution of precipitation up to many days before the flash flood. In this context, radar offers unique information.

A summary of the results in individual basins in English is given in Joss et al., 1995, details about this analyses are presented in German in Bürgi and Schädler, 1996. Their results, based on 12 river basins, show possibilities and limitations of the old, second generation radars, which had

just a clutter map for clutter suppression and no profile correction in real time. Both error sources were taken into account in later analyses. This work clearly shows that at least in a complicated orography, we should not just take reflectivity values aloft, use some Z-R-relationship and calculate precipitation at ground-level to estimate water input into river catchments.

4.7.2. Scan strategy

To obtain a well defined vertical profile of reflectivity, allow optimal extrapolation of reflectivity aloft to the ground-level and extract information on the Z-R-relationship (as indicated in Z-R relationships and representativity), we perform a volume scan and calculate 12-level Cartesian precipitation data.

To do so, the one-degree radar beam performs a continuous scan sequence in 20 elevation steps as described in Scan strategy and beam-width. The sequence is completed at five-minute intervals, to ensure that rapid storm evolution is not missed. A number of optimizations have been required to complete the scan in such a short period, without compromising the accuracy of the measurements:

1. The pulse repetition frequency (PRF) and scan rate of the antenna are increased with elevation angle, to maintain a constant number of around 33 pulses per degree of azimuth;
2. Doppler analyses are performed up to the maximum range used for clutter elimination in reflectivity measurements. For wind velocity information data only below 13km height and up to 120km distance are analyzed;
3. The first and second sets of 10 scans have interleaved elevation angles so that a complete 10-elevation volume is scanned each 2.5min, permitting a rapid-update product to be produced every 2.5 min.

Further details concerning the scan strategy of the Swiss radars can be found in Scan strategy and beam-width.

4.7.3. Vertical profile and CAPPI

In the past we had to determine the profiles in retrospect from processed data (pseudo-three-dimensional data consisting in three projections of maximum reflectivity). Furthermore, as full volume data was not available, tests could only be done on a daily base, i.e. daily averaged precipitation was corrected using daily determined profiles. Figure 3.2 shows results for summer (1) and winter (2), averaged over 7 years.

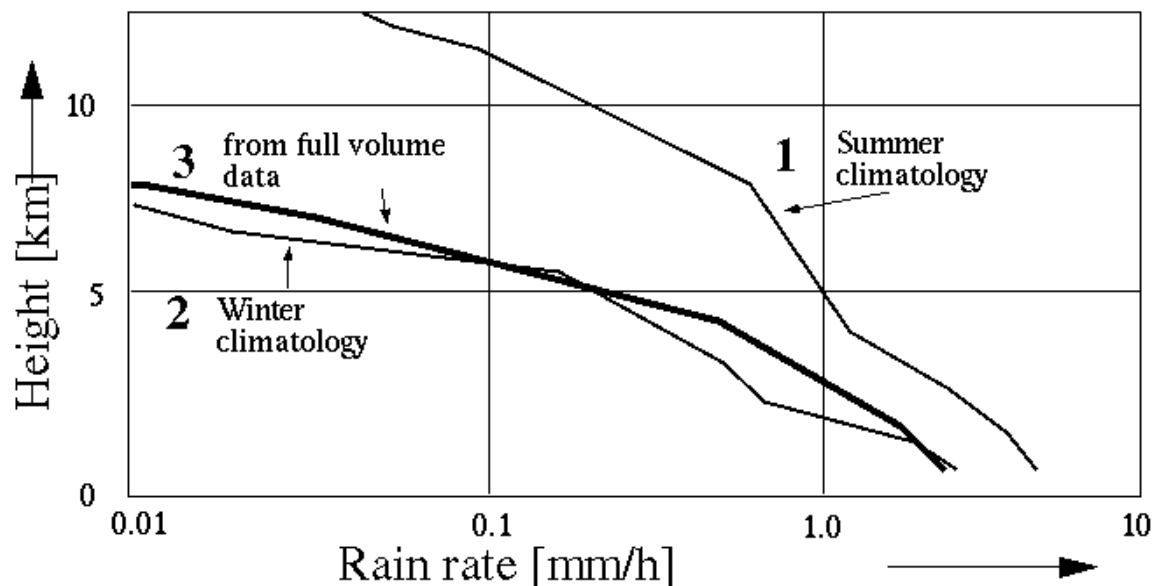
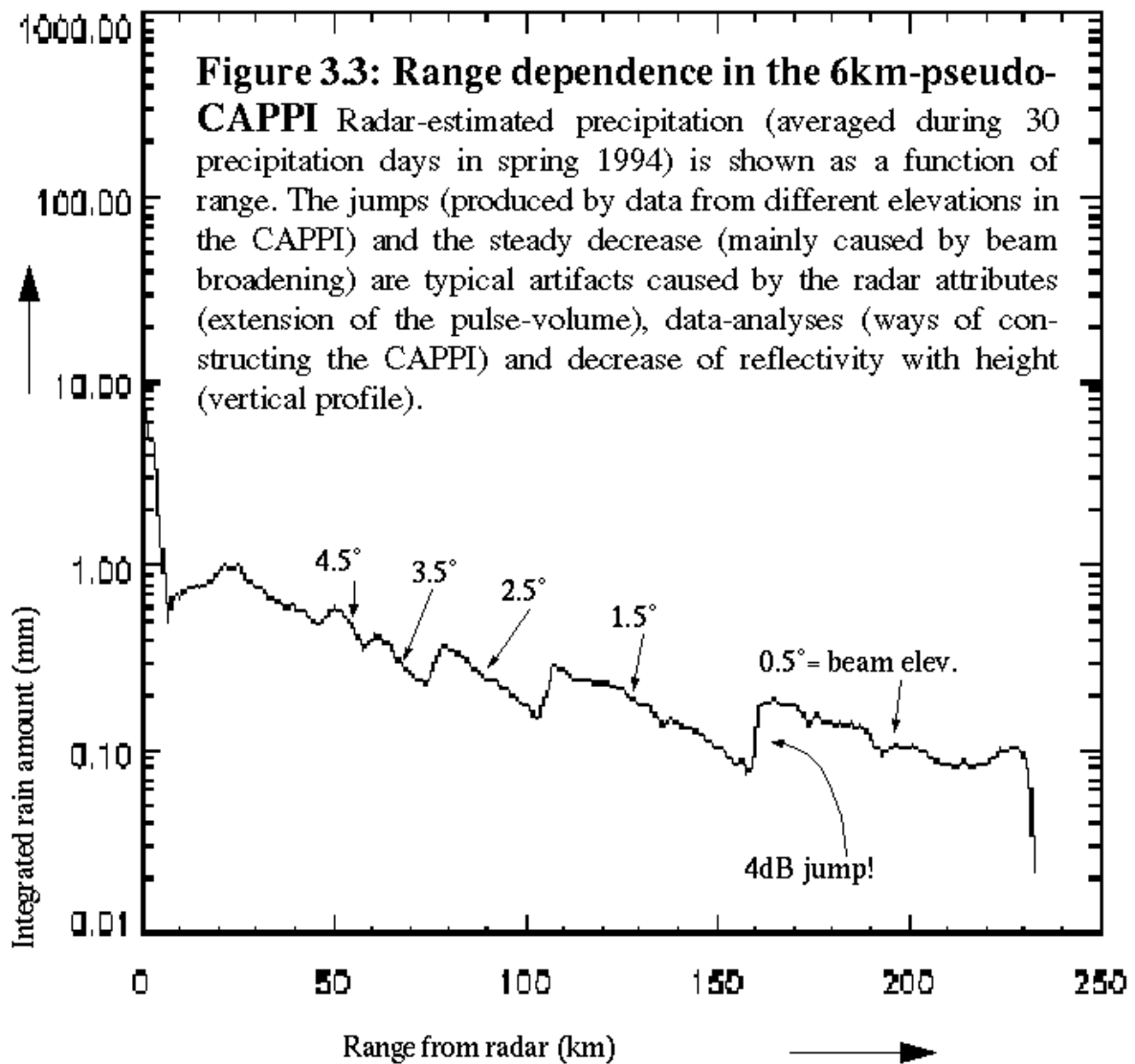


Figure 3.2: Average profiles of rain rate for summer (1) and winter (2), reconstructed from seven years of pseudo-three-dimensional data and profiles directly calculated from full volume data (3) from the new radar Lema (at 0930, 1.3.1994 using CAPPI's) show a similar decrease of rain rate with height

In all situations, in summer and winter, we find on average a significant decrease of reflectivity with height. At longer ranges (over 100km), the resulting errors in estimated ground level precipitation rate dominate all others, urging us to look for methods to correct for this apparent change of sensitivity of the radar, but in fact produced by the precipitation process: precipitation grows as it falls. Nearly any effort to correct for this decrease helps. But, as indicated by simulations and experiments with the new radars, the result may improve if the causes are analyzed and taken care of, but with that the effort involved increases also. We expect considerable improvement from corrections based on profiles retrieved in real time using full volume data as discussed in Profile corrections. As yet we have insufficient experience to evaluate cost/benefits of this method.



The pseudo-CAPPI Figure 3.3 illustrates the influence of the decrease of echo with height: it shows abrupt changes with range, caused by having to take the data from many elevations for each CAPPI. Within the 230km range of the radar, the 6km-CAPPI in Figure 3.3 requires 19 elevations with data originating from a height range between 3 to 9 km! This variation of height, far beyond of what we expect to find in a 6km-CAPPI, is caused by the vertical spacing of elevations and the 1° beam width. As an alternative to using CAPPI's, we are planning to interpolate between elevations and extract the vertical profile from the original polar data, taking into account the actual heights of the observations.

5. Swiss Weather Radars (Galli)

When in 1989 the specs of the third generation of three weather radars were defined, it was not yet possible to describe the algorithms for generating the products in detail. However, from past analyses (BYrgi and B.SchSdler, 1996, Bssch, R. 1993) it was clear that much effort was needed to use radars in hydrological applications:

- 1 - to eliminate ground clutter,
- 2 - to calibrate and monitor the radar system and
- 3 - to correct for the strong and systematic variations of radar echo with height: shielding by mountains and the systematic changes of radar sample volume with distance (extrapolation of the average, visible radar echo aloft to the non-visible echo at ground-level).

These fundamental problems were known. The solution was part of project NOWRAD and had to be developed with the hardware and software companies. First tests with the prototype radar station on Mt. Lema (installed in 1993) soon showed three more problems:

- 4 - important errors originated from the transformation of radar data into Cartesian coordinates (as it was done in the old, second generation of Swiss radars and as specified for the first software package). For best results, the algorithms in point 3 have to be applied to the raw polar data. The modification is now completed and installed, but it still needs final testing.
- 5 - attenuation in the radome (the protection of the antenna) and attenuation on the way to the rain of interest (some distance from the radar) has to be considered.
- 6 - the transformation of the extrapolated radar echo at ground level into rain rate. Errors caused by the first 5 points were so dominant that the software of the old radar generation assumed just a single transformation routine (Z=316R1.5). This needs research work before new methods can be used.

All six above mentioned aspects need to be considered to allow optimal use of radar in hydrology. At the end of NOWRAD (1996) problems 1-4 are ready to be tested; for items 5 and 6 plans for implementation should be further developed and tested within MAP (Mesoscale Alpine Project) during the period 1998-99.

After the prototype had been tested, the two old radars of the second generation were replaced (see Table 4.1). Thus, since end of 1995 all three radars are of the same hard- and software design, Lema still being used to test new combinations of parameters.

Start date of operational activity of the radar stations.		
Radar	II generation (end date)	III generation (start date)
Lema		13 September 1993
Albis	11 July 1994	20 October 1994
La Dôle	01 May 1995	07 November 1995

5.1. Special Attributes of the Swiss Radars

The radar equipment METEOR 360 AC from Gematronik (Germany) operates with the data processing system from Lassen Research (U.S.A.). The C-band Doppler weather radar was conceived to work continuously in an unattended operational environment and to supply high quality data even in presence of severe ground clutter.

With respect to the previous generation of operational Swiss weather radar equipment the following characteristics have been improved:

- 1 - time interval between measurements: from 10 to 5 minutes
- 2 - spatial resolution of the volume element: from 2x2x1 to 1x1x1 km³
- 3 - resolution in measured reflectivity: from 7 to 16 levels of rain-rate

The Doppler frequency is now also measured, thus permitting the detection of the radial motion of the targets.

Particular care has been given to design an automatic calibration of the radar. During normal operation the stability of the electronic components is checked; this is important to obtain good quantitative results from reflectivity data. Fast data acquisition and large computing power allows to eliminate more clutter by processing high resolution Doppler data. The full volume data is transmitted to the users and allows a better estimate of precipitation at ground level.

5.1.1. Sensitivity of reflectivity measurement

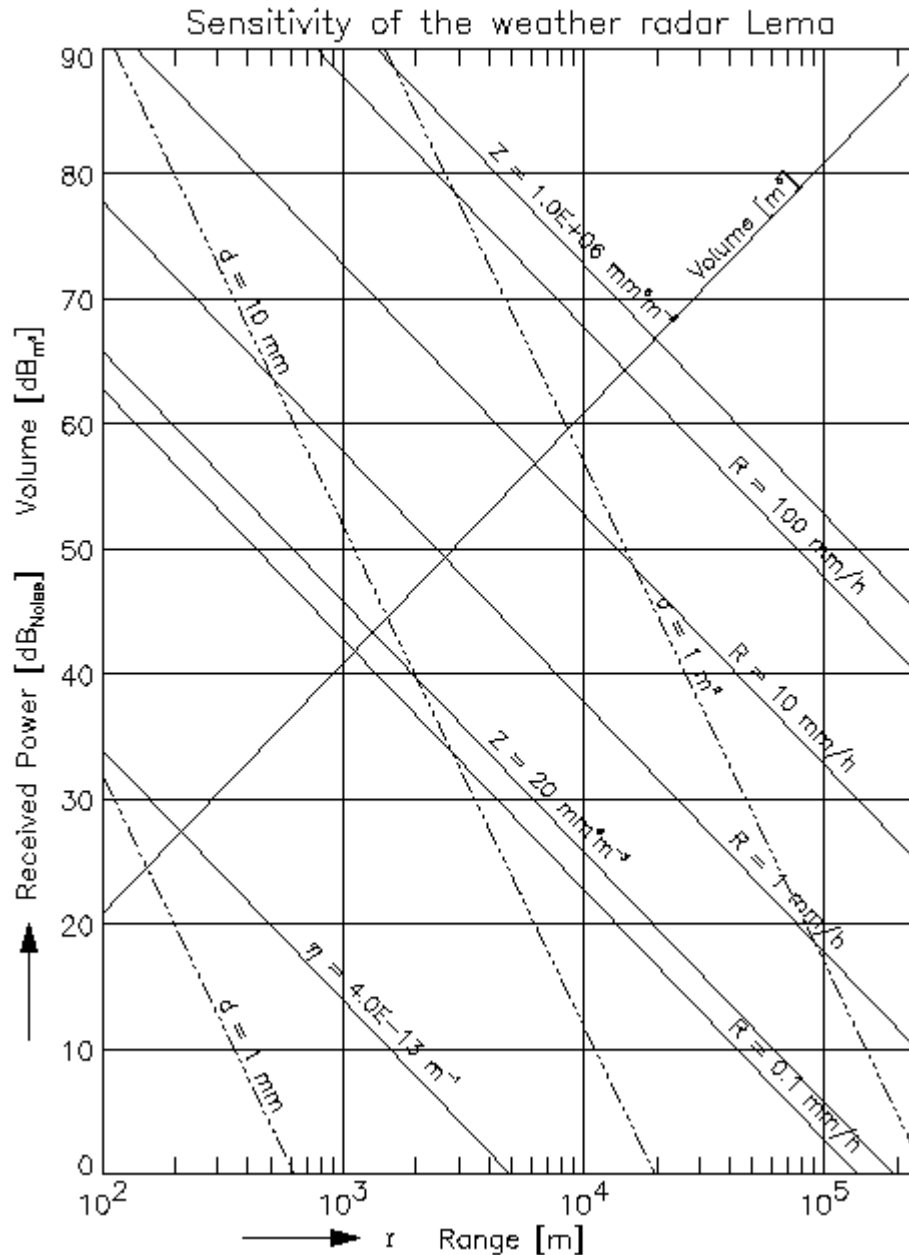
The microwave power reflected from objects depends on the number and size of objects in the illuminated volume. In precipitation the relation between reflectivity (Z) and precipitation rates (R) is called "Z-R relationship", see footnote(1) on page 29, which has been the object of many studies in the field of the radar meteorology. The "radar equation" is used to calculate the electrical power measured by the radar receiver, which is then transformed into an estimate of precipitation rate using the Z-R relationship. For more details we refer to the specialized literature, for example Collier, 1996 or Sauvageot, H. 1992 on pp. 116-119.

For various types of targets the signal-to-noise ratio is plotted in Figure 4.1. This figure is based on the **radar equation**, taking into account all relevant parameters of the radar listed in Table_4.1: frequency, transmitted power, pulse width, receiver bandwidth, antenna gain, beam-widths, distance of the target etc.

$$\text{Received echo power, relative to the receiver-noise [dBNoise]} = (\text{dB}_{\text{Sig}} - \text{dB}_{\text{Z(rec.-noise)}}) = \\ 10 \log(\text{Z}[\text{mm}^6/\text{m}^3] * \text{PT}[\text{kW}] * \text{F}[\text{MHz}]^2 * \tau [\mu\text{s}] * \Theta_{\text{H}} [-] * \Theta_{\text{V}} [-] * \text{G}[-]^2) \\ / (r [100\text{km}]^2 * \text{B}[\text{MHz}] * \text{NF}[-] * \text{Lossfactor} [-]) - 179.91\text{dB}.$$

The constant added at the end of the equation of 179.91dB results from radar equation and the units used in the equation and was confirmed within a few dB by comparison with rain gauges. The Lossfactor includes all types of losses in the system (from the transmitter to the receiver: wave-guide, radome etc.)

FIGURE 4.1: Sensitivity of Swiss radars.



Sensitivity and pulse volume of Swiss radars for volume targets (rain) and point targets (airplanes and insects) in function of range. The volume of the beam increases with the square of the range (beam width 1- in horizontal/vertical) and is constant in range (83m resolution cell). Values are given in logarithmic scale referred to the noise-equivalent power of the receiver and to 1m^3 for the volume. 10dB correspond to a change of a factor of 10 in magnitude. The graph is for Lema. Albis (longer wave- guide) is 4dB less and Dole (shorter wave- guide) 2dB more sensitive than the Lema-radar indicated in this figure (IDL-software written by Urs Germann).

5.1.2. Parameters of the Swiss radars

TABLE 4.1 gives the relevant characteristics describing the new radars. The symbols in the column on the right are used to calculate the results plotted in Figure 4.1 . "Nominal" reflects the average value which may slightly vary with the particular component used in a given equipment.

TABLE 4.1: Parameters of the third generation of Swiss radars.

Parameter	Value	Symbols
Antenna: half-power beam width	1.0 degree nominal (Q3dB)	Θ_V, Θ_H
Transmitted power	250 kW nominal	PT
Pulse length	0.5 μ s nominal	t
Transmitter frequency	5430MHz (Dole), 5440MHz (Lema), 5450MHz (Albis)	F
Bandwidth	2MHz nominal	B
Antenna gain	25'000 (44dB) nominal	G
Losses	5.7dB (Dole), 7.6dB (Lema), 12.3dB (Albis)	Losses dB
Noise Figure	1.52 (1.8dB) nominal	NF
Receiver noise k^*T^*B	-110.4dBm	
Sensitivity for rain at 230 km	0.16 mm/h nominal	
Number of elevations	20 in 5 min	
Antenna revolutions/min	3, 4 or 6 (depending on elevations)	
PRF (pulse repetition frequency)	600, 800 or 1200 Hz (dep. on el.)	
Wavelength	5.5cm	
Transmitter type	Magnetron	
Side lobes (excluding radome)	max -30dB	
Dry radome attenuation	less than 0.35dB one way nominal	
Receiver: log amplifier	90 ~ 0.5 dB nominal	
Samples per degree and per km	32 x 12	
Processed Video signals	I, Q, log-Z, resolution: 12 bits	
Clutter suppression	6 complem. tests, incl. dyn. map	
Calibration with noise source	every 2.5 min	
Calibration with signal generator	full automat, 121 points every 24h	
Profile corrections	visibility, profile estimated in real time	

Three Swiss- operational radars and some research radars: a French- (Ronsard), a US- (S-Pol), an Italian (Bric), and three ETH-radars. (Estimated parameters are marked with an asterisk*). Sensitivities are reflected in the maximum range of detection for a given type of target, calculated with the relevant radar equation. For example the maximum range for detection of 0.1mm/h rain was determined with the radar equation . The minimum detectable signal in dBZ and distances at

Operational Use of Radar for Precipitation Measurements in Switzerland

which the signal of a single bee, of a strong boundary layer or of a small air-plane is equivalent to the receiver noise, are also given.

TABLE 4.2: Sensitivity and coordinates of various radars.

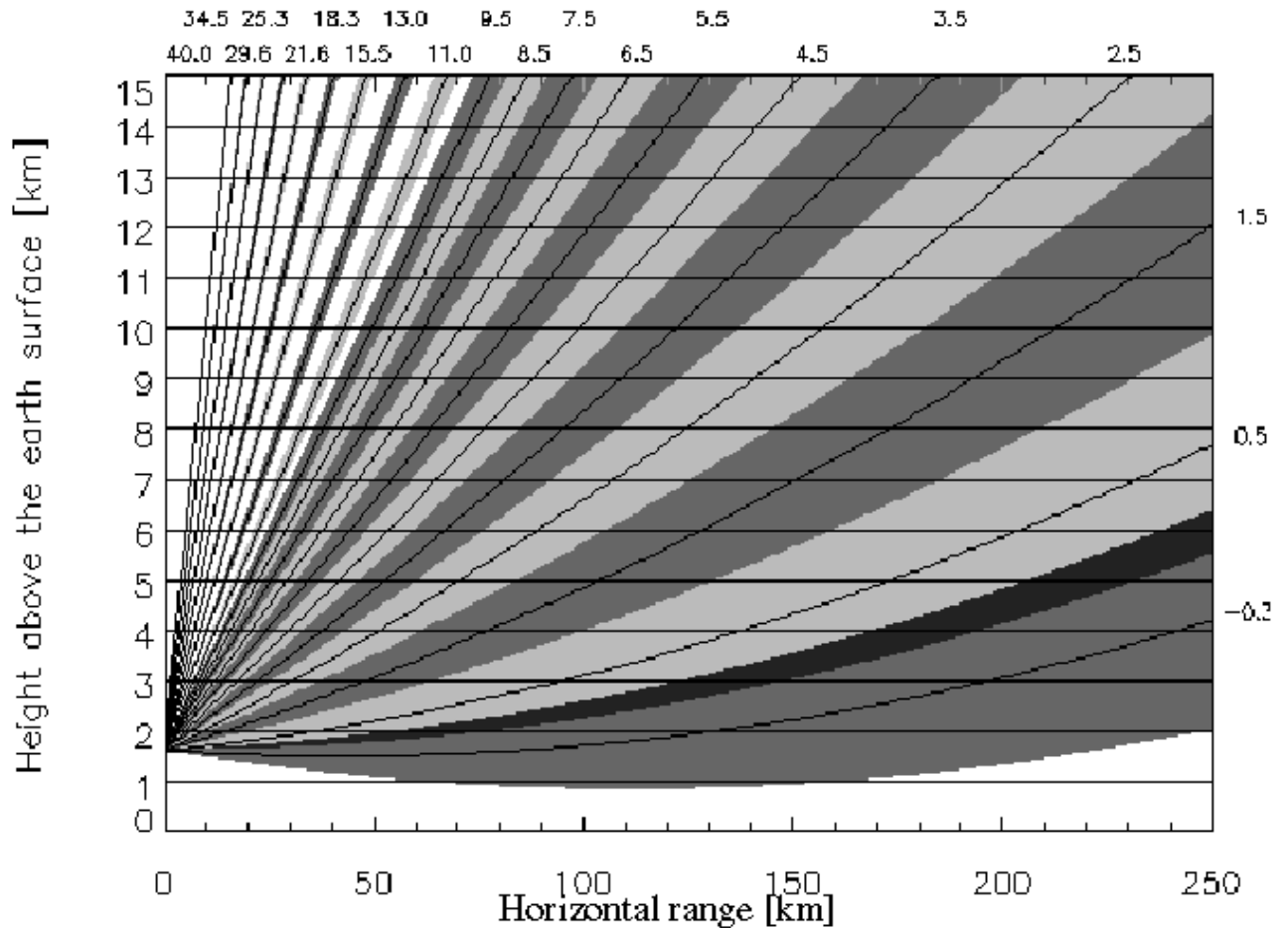
	Monte Lema SMA	Albis	Dole	Ron-sard F	S-Pol USA	Bric EEC old	ETH EEC	Fleder-maus ETH	Wind-profil. SMA/ETH
Antenna dia. [m]	4.2	4.2	4.2	4	8.5	2.5	2.5	1	2.7
Q: beam-width [$^{\circ}$]	1.0	1.0	1.0	0.89	0.91	1.65	1.65	2.4	6
G: Gain [dB]	44.7	44.7	44.7	44.4	44.05	40	40	36.6	29.5
PT: Peak power [kW]	251	292	303	250	1000	280	280	100	0.5
F: Frequency [GHz]	5.44	5.45	5.43	5.6	2.7-2.9	5.62	5.62	9.5	1.3
Wavelength [cm]	5.6	5.4	5.4	5.4	11	5.3	5.3	3	23
t : Pulse-width [μ s]	0.5	0.5	0.5	0.67	0.35-	0.5	0.5	0.25	2.8
Resolution [m]	75	78	78	100	38-	75	75	30	420
NF: Noise fig. [dB]	1.85	1.8	2.04	3.1	3.2*	6	6	7	1.2
B: Bandwidth [MHz]	2.0	2.08	2.11	1.5	0.74*	2.5	2.5	5	0.4
Losses: System [dB]	7.6	12.3	5.7	incl.	3*	5	3.6	4	1*
Min. det. [dBZ] signal @ 100km	7.3	11.4	5.0	.3.8	-1.4	14.1	12.7	23.6	39.9
Max. distance [km] single bee (5mm)	6.9	5.4	7.9	8.3	9.8	3.6	3.9	2.1	0.3
Max. distance [km] det. 0.1mm/h rain	136	85	178	205	373	62	73	21	3.2
Max. distance [km] clear air (4E-13/m)	4.9	3.1	6.5	6.8	44.2	2.1	2.4	0.3	1.6
Max. distance [km] det. of 1m ² sphere	262	206	299	305	723	133	144	45	45
Y [km]	707.96	681.22	497.1	684.5	700.5	623.2	680.93	680.93	680.93
X [km]	99.76	237.6	142.4	35.8*	63.8	-13.1	251.34	251.34	251.34
H [km]	1.63	0.93	1.68	0.165	0.29	0.73	0.60	0.60	0.60
Longitude	8.83	8.51	6.10	8.52	8.73	7.73	8.51	8.51	8.51
Latitude	46.04	47.29	46.43	45.47	45.72	45.03	47.41	47.41	47.41

5.1.3. Scan strategy and beam-width

The antenna scans the volume around the radar station at 20 different elevations, the lowest one being situated at 0.3 degrees below the horizon and the highest one at 40 degrees above it. Figure 4.2 illustrates the antenna elevations, showing the overlapping of consecutive antenna beams of one degree beam width.

Figure 4.2: Swiss scan strategy

The full volume scan is accomplished in two cycles, each lasting 2.5 minutes. During the first cycle (dark gray shaded), each second elevation is taken, starting with the lowest one (-0.3, 1.5, 3.5,...), the remaining elevations being taken during the second cycle (light grey shaded). The one-way beam-width is $\Theta_{3dB} = 1.0^\circ$ (shaded).



Note that the 3dB-beam-width (one way) is plotted in this figure: for our radar it amounts to 1.0. The two-way gain (G) of the antenna as function of the aperture angle Q may be approximated by:

$$G^2 = G_0^2 \cdot \exp\left(-8 \cdot \ln(2) \left(\frac{\Theta}{\Theta_{3dB}}\right)^2\right) \quad (4.1)$$

Operational Use of Radar for Precipitation Measurements in Switzerland

Applied to our antenna this means that 0.5- from the main axis (boundaries in the figure) the echo of a rain drop is attenuated by 6dB. At 1- from the beam axis the resulting 24dB attenuation may easily let pass strong echoes from the ground, thus echoes may be heavily contaminated by ground clutter. For our beam-width of $Q_{3dB} = 1.0-$ (the aperture angle where the emitted beam radiation decreases to half intensity), the equivalent beam width (with full gain inside the beam, zero outside), needed to calculate the pulse volume in the radar equation results as $0.85- [1-/\text{Sqrt}(\ln 4)]$.

TABLE 4.3 shows the chosen scan sequence allowing an aviation product every 2.5 min (two half-volume scans, calculated alternately from revolutions 1-10 and 11-20) and a full volume scan every 5 min (revolutions 1-20), without exceeding an antenna acceleration of $18^\circ/\text{s}^2$ and speed of $20^\circ/\text{s}$ in elevation ($36^\circ/\text{s}$ in azimuth). For each revolution n the table gives the elevation Elev, the elevation change ΔElev , the maximum range D_{max} to analyze the rain rate R and wind speed u , the rotation rate RPM, the time per revolution (Time), the time needed to change the elevation (Step), and the pulse-repetition frequency PRF. Calibrations take place during the elevations indicated with *. The wind-profile (+) over the radar station is estimated every 2.5 min from the highest elevation of each half-volume scan.

TABLE 4.3: Scan strategy: Attributes for scanning the antenna.

n	Elev.	Δ Elev.	$D_{\max R}$	$D_{\max u}$	RPM	Time	Step	PRF
-	[°]	[°]	[km]	[km]	[1/min]	[s]	[s]	[1/s]
1	-0.3	1.8	230	130	3	20	1.4	600
2	1.5	2.0	230	130	3	20	1.4	600
3	3.5	2.0	162	130	4	15	1.4	800
4	5.5	2.0	112	112	4	15	1.4	800
5	7.5	2.0	85	85	6	10	1.4	1200
6	9.5	3.5	68	68	6	10	1.7	1200
7	*13.0	5.3	51	51	6	10	2.0	1200
8	*18.3	7.0	37	37	6	10	2.2	1200
9	*25.3	9.2	27	27	6	10	2.4	1200
10	+ 34.5	-34.0	20	20	6	10	4.2	1200
11	0.5	2.0	230	130	3	20	1.4	600
12	2.5	2.0	205	130	3	20	1.4	600
13	4.5	2.0	133	130	4	15	1.4	800
14	6.5	2.0	97	97	4	15	1.4	800
15	8.5	2.5	76	76	6	10	1.5	1200
16	11.0	4.5	59	59	6	10	1.9	1200
17	*15.5	6.1	43	43	6	10	2.1	1200
18	*21.6	8.0	31	31	6	10	2.3	1200
19	*29.6	10.4	23	23	6	10	2.6	1200
20	+ 40.0	-40.3	18	18	6	10	4.5	1200

5.1.4. Data reduction

Reflectivity and Doppler signals from the receiver are processed in a dedicated signal processor: they are recorded for each pulse (in steps of $\sim 1/30$ degree in azimuth) and 1/12 km in range (~ 83.3 m) with values having a resolution of 12 bits (values in range 0-4095) called ADU (Analog to Digital Units).

Reflectivities are converted to rain-rates using a pre-defined Z-R relationship after subtraction of the receiver noise (measured during each volume scan) and after having been corrected for the

range attenuation (r^2 and atmospheric attenuation: 1.7dB/100km two-way). Clutter tests (see chapter 3.3) are applied and the data inside the 1-degree x 1-km sector (termed as "cells") found to be clutter free are normalized with respect to the transmitter peak power and to the power of a well known and stable noise source (calibration in absolute terms). When the tests are not passed (see chapter 4.1.6), the target is flagged as clutter. The averages of the (clutter-free) 83.3m-gate values are retained as polar data (POLAR-Z), every datum being representative for a cell.

Velocity values are estimated from a statistical analysis of the measured signal (from the auto-covariance function) e.g. 32 values inside an azimuthal angle of 1 degree; from all clutter free values at 83.3m resolution, the velocity of the sample with the strongest reflectivity value is retained as polar data (POLAR-U), representative for the 1-degree sector with 1-km radial extension.

For the VAD product (see below and Sec.5.1.4 "WIND: Sounding above radar and polar products" on page 56) gates at 83.3m resolution are taken before rejection by the clutter analysis to permit the wind being estimated also during clear weather situations.

5.1.5. Doppler analyses

The phase shifts from pulse to pulse (Doppler frequency shift) at the receiver is caused by the motion of the targets and permit the estimation of their velocity in the radial direction. Much effort was spent in the past to determine the wind field in three dimensions, a very logical application of the Doppler effect. However, with one radar - being able to estimate only one of three components - the reconstruction of a 3-dimensional wind vector is not obvious. Furthermore, displaying the results leads to pictures which are complicated and often disappointing for the user to grasp. Therefore, we left this task to groups with more man-power. Instead we have concentrated on extracting the vertical profile of the horizontal wind from the Doppler information (VAD = Velocity-Azimuth Display, see Sec.5.1.4 "WIND: Sounding above radar and polar products" on page 56). But the Doppler effect may also be used to distinguish between moving and stationary objects, i.e. for the elimination of ground clutter, explained in detail in Sec.3.3.1 "Clutter elimination concept" on page 23. It is this application of the Doppler effect which, at least at present, is most profitable, while in the field of wind speed analyses more research is desirable.

5.1.6. Clutter suppression

Both reflectivity and Doppler data are used to detect clutter (at a given elevation) in each element of 1-degree in azimuth and 1-km in radial range (see chapter 3.3). Different tests are applied to each data sample of the element.

The tests are based on the intensity value of the reflectivity (below a given threshold it is rejected, being classified as noise), on the Doppler frequency spectrum (not related to precipitation if too broad), on velocity of the target (if moving then accepted as precipitation) and on the spatial distribution (high gradients are assigned to clutter).

The average of all non-clutter samples in a given element is retained. Note that one sample classified as non-clutter data is enough to obtain a valid measurement in the mentioned element (1-km, 1-degree). This data reduction leads to the so called "polar data".

5.1.7. Volume resampling

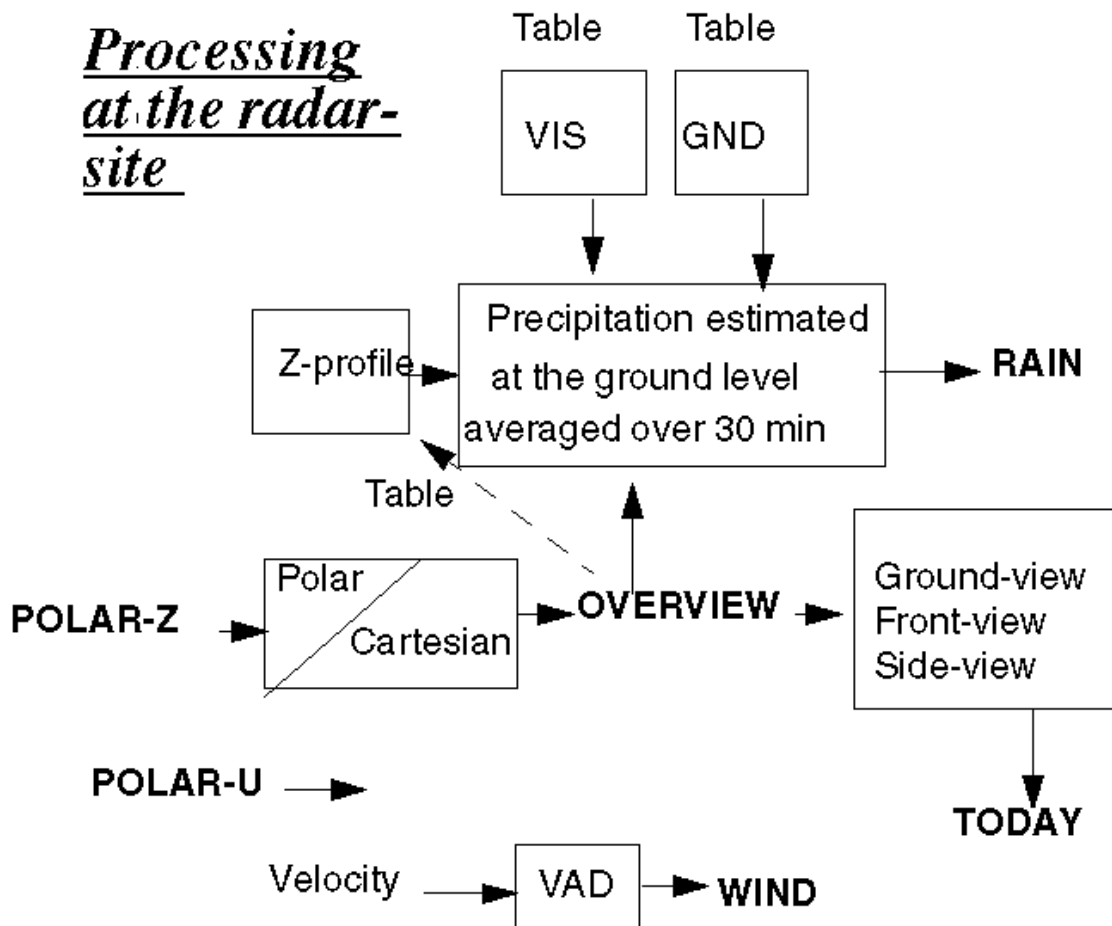
Because most user's products are based on 3 dimensional Cartesian coordinates associated with the Swiss national topographic projection, polar data need to be re-sampled. This is done by using a pre-calculated projection table converting data from the measured geometry (polar space) to the desired geometry (Cartesian space).

After this step the user can see the "volume data" in 12 horizontal planes of 1 km thickness extending from 0.5 to 12.5 km in altitude, containing elements of $1 \times 1 \times 1 \text{ km}^3$ or of $2 \times 2 \times 1 \text{ km}^3$, depending on the type of product.

5.1.8. Product processing

Products based on data originated from a single radar station are generated at the radar-site and successively transmitted to the central computing system where all composite products are constructed (Lassen Research 1994 on page 108).

Figure 4.3: Product generation at the radar station.



Polar reflectivity data (POLAR-Z) is used as source for product OVERVIEW. The reprojection of polar data into the Cartesian space is table-driven: this process includes the generation of the 12

CAPPI-images (Constant Altitude Plan Position Indicator) for product OVERVIEW correspondent to 12 height levels. Product TODAY is derived from OVERVIEW.

The most sophisticated product is RAIN representing the best-estimate of the precipitation on ground. It has OVERVIEW as source and takes into consideration the radar visibility (table VIS), the terrain topography (table GND) and the mean vertical reflectivity distribution (Z-profile) computed from OVERVIEW to estimate the precipitation at ground level. The data taken from the last 6 measurements (each obtained from a full volume scan) lead to this product, containing a gliding average of the precipitation rate during the previous 30 minutes, updated every 5min. The Z-profile is estimated using the mean precipitation amount from each of the 12 height levels of product OVERVIEW. This operation is performed within a range of 70 km side length, centered over the radar station.

The information flow between the raw data (polar reflectivity, polar Doppler velocity), the products and the processing algorithms are illustrated. All these operations are being done for every radar-site. Look-up tables reduce computing time.

Velocity data of type POLAR-U is currently not processed further.

The velocity data at resolution of 83m range-gates is the source for the product WIND, derived from the measurements of the two highest antenna elevations by means of a VAD algorithm (see chapter 5.1.4).

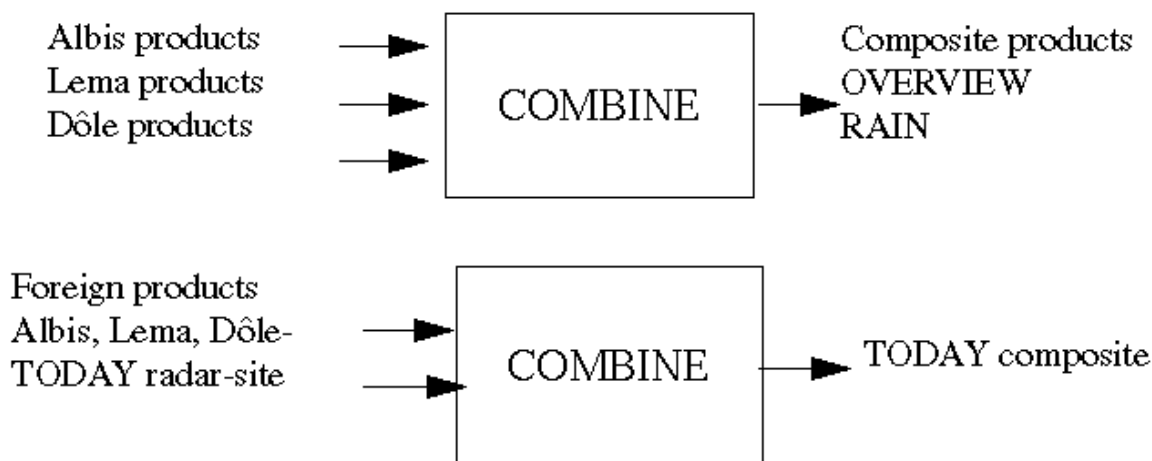
The products from the single radar sites are then combined or merged to create composite products, covering an area that contains the whole Swiss territory. The processing of these composite products (see chapter 4.2.1) takes into account the distance from the radar site and the radar visibility of the target point (height of lowest volume seen by the radar).

The products OVERVIEW and RAIN, resulting independently from every radar station (Albis, Lema and La D[tm]le), are processed through a combination algorithm to form the composite products having the same names. Data from all input sources are geo-referenced on the same projection map so that their combination in space is a matter of simple translation based on geographical coordinates.

For the product TODAY, data from foreign radars located near the Swiss national boundaries are also integrated to complete the TODAY-composite product on areas not covered by the national radars or in case of absence of data from them.

Figure 4.4: Product generation by the compositing computer.

Sketch of the information flow between radar-site products plus foreign radar data and composite products. The "COMBINE" method geographically positions the data from the different sites.



5.2. Compositing

5.2.1. Combining reflectivity from different radars

When generating a composite image, data from different radars of unequal quality and format (foreign radars) have to be merged (see Figure 5.9 on page 62). Variations in shielding (height of lowest volume visible to the radar) and size of the sample volume lead to changes of data quality. When composite images are created, the software takes this into account for every image pixel individually. The adopted algorithms are based upon a table (calculated offline) specifying the priorities on how to combine data from the available radars. This is important on areas "seen" by more than one radar and allows to make the best choice of available radar-information.

For reflectivity data the compositing task is straight forward: for each pixel of the composite image we have to choose the order of priorities for the radars to contribute to that location and whether to take the maximum or the mean value of available radar information having the same priority. For every pixel we obtain a list of priorities calculated from the "relative visibility" of precipitation seen from each site (influenced by the distance and/or the degree of shielding).

Since the Swiss radars operate within one uniform coordinate system, the problem of compositing is relatively simple: the data from the various stations are provided on the same 1x1x1-km or 2x2x1-km grid, so the compositing process reduces to the treatment of common grid points, i.e. points in areas with overlapping visibility of two or more radars. A flexible, table-driven scheme has been developed to allow the compositing of data from up to eight radars (three Swiss radars and up to five foreign radars). This algorithm allows up to four levels of priority to be assigned to each radar, at each data bin (pixel) in the composite product.

There is one priority table valid for all Swiss products, composed of 16-bit integers, with two bits assigned to each potential radar. The use of two bits for each radar provides three priority levels, in addition to not considering the radar (zero priority). The assignment of bits to the eight radars is shown in TABLE 4.4 (bits marked "11" signify bits used for radar number 1, and "xx" signifies bit patterns not used for the Swiss radars, but available for later expansion to foreign radars).

Bit pattern = (msb) 112233xxxxxxxx (lsb) [16-bit integer]

Bit value	TABLE 4.4: Composite priority levels
00	Zero priority: radar does not contribute to this data bin
01	Low priority: consider this contribution only if sources with priority 10 or 11 are not available; for multiple sources, average (or maximize) them
10	Medium priority: consider this contribution only if sources with priority 11 are not available; for multiple sources, average (or maximize) them
11	Maximum priority: top priority information; if multiple sources are available, average (or maximize) them

Whether we average or maximize depends on the type of product: for OVERVIEW and TODAY products the maximum value from different stations with equal priority is taken, thereby reducing computation time. For the product RAIN averaging is used to create composite images.

Each priority value is associated to one of the four possible states, as shown in TABLE 4.4. The table lookup algorithm for selecting measurements is designed to allow the averaging of logarithmically scaled (discretized) rain-rate data (see Sec.5.1.3 "RAIN: Precipitation amounts" on page 55): i.e. averaging values from different stations requires previous linearization of the data. To speed up processing, this is done by means of look-up tables.

The first implementation of this method (introductory phase) uses priorities for each radar based on a simple "distance criterium" which sets priority 3 (11 in TABLE 4.4) to all pixels within a square area of 100x100 km around the radar station, priority 2 to the area between 100 and 150 km and priority 1 outside 200km. The visibility of a pixel is not taken into account. This is applied for products OVERVIEW and RAIN, whereas for product TODAY the "old" way of combining images is used (simply the maximum value for "overlapping pixels" is taken).

In a successive phase we intend to use more sophisticated algorithms weighting distance and visibility for the setting of priorities; this method has first to be validated and calibrated with off-line trials using recorded data.

5.2.2. Combining Doppler radars

Many countries use Doppler radar techniques, but apart of a few attempts in research, little results of combining Doppler information has been successful so far. Even worse, Doppler products from single radars have proven to be far more complicated in operational use than anticipated. So after the initial effort of using and combining information of a network of Doppler radars, only the classical applications such as clutter elimination and Velocity-Azimuth-Display (see VAD, chapter Sec.5.1.4 "WIND: Sounding above radar and polar products" on page 56) remain in operational use on the display of the Swiss meteorologist.

Reasons for this situations are found in the immense complexity of the phenomenon weather and wind (at least six dimensions plus time) and in the fact that each Doppler radar measures only the radial velocity component, being complementary for every radar location. Because of this complementary attribute of each individual Doppler radar, it is considerably more difficult to combine velocity information of several radars - more difficult than combining just the scalar reflectivity information. For reflectivity, each radar works independently with its own data, whereas

Operational Use of Radar for Precipitation Measurements in Switzerland

to obtain 3-dimensional velocity components of the wind, the combination of three Doppler radars is needed. In practical terms this means that a given element in space must be well visible from at least three radars, a condition not easily met with today's density of European radars.

We find several open questions when processing Doppler information; e.g. complications caused by targets exceeding the unambiguous Doppler velocity, the influence of the pulse volume (broadening of the spectrum), of clear air echoes (birds moving relative to the air), fall speed of precipitation particles (vertical speed varying with size and shape of particles), of clutter contamination (no movement of echoes at all) and last but not least complicated coordinate systems for interpolation of the results in time and space.

For operational work we conclude that more research is needed before presenting Doppler data to the user or even solving of the "Doppler networking problem". We may want to combine Doppler radar data with independent "non-Doppler" information on wind (eventually obtainable from numerical models) or with interpreted reflectivity information (COTREC in Li L., W. Schmid and J. Joss, 1995), and pass it through some kind of multi-dimensional interpolation scheme, which uses the measured radial component of individual Doppler radars as weak or strong constraint for the interpolation, as discussed by Laroche and Zawadzki (1995).

6. Products (Galli)

6.1. Type of Products

TABLE 5.1: Radar-site products.

Product name	Content (resolution of pixel value)	Purpose
RAIN	Best estimation of the precipitation rates (4 bit)	User
OVERVIEW	Reflectivity volume, 12 constant altitude plans (4bit)	User
WIND	Vertical profile of the horizontal wind component (32 bit)	User
POLARZ	Reflectivity, 20 elevations (4 bit)	R+D
VISIBP	Daily reflectivity, 20 elevations (16 bit)	R+D
COUNTP	Daily clutter map, 20 elevations (16 bit)	R+D
STATUS	State of the system (8 bit)	Supervision
CALIB	Calibration report (8bit)	Supervision
TODAY	Maximum-reflectivity 3-views + geographic overlay (3 bit)	User
RAPID	Maximum-reflectivity vertical (4bit)	User
POLARU	Doppler velocity, 20 elevations (8 bit)	R+D

Products are generated either at the radar sites either at the composite center.

Data recorded at a constant elevation while the antenna is rotating for 360 degrees in azimuth (the so called polar data) are mainly used for Research and Development purpose. Some data contain information which are useful for the maintenance staff and for monitoring purpose. All other products are made at disposal of the users and consist of :

* An **OVERVIEW** consists of 12 images, each one corresponding to one height level, within a range of heights between 1-12 km. The full 3-dimensional information of the volume scanned by the radar is available, permitting any vertical or horizontal section to be analyzed.

* A best estimate of the precipitation rate at the ground called **RAIN** containing a running average over the past half hour, is updated every 5min. It is relevant for quantitative precipitation estimates and river flow predictions.

* An experimental product called **WIND** contains wind information over the radar station, calculated from data of the highest elevation of each half-volume scan (see chapter 5.1.4).

* For the identification of rapid changing phenomena and very short delays between measurement and data display (mainly for the aviation) a product called **RAPID** is a disposal

Operational Use of Radar for Precipitation Measurements in Switzerland

about 3 minutes after the observation on a 2.5 minutes interval, containing the vertical projection of the maximum reflectivity.

* For compatibility with the old generation of Swiss radars (reusability of user's equipment, interpretation skill of weather forecasters, etc.) the product **TODAY** is still supported. It has the same format and content as it previously did: it is formed by the three views (ground-, side- and front-view), each one containing a projection of maximum reflectivity.

The scale of rainfall intensity for OVERVIEW, RAPID and RAIN contains 16 equal steps on a logarithmic scale between 0.16 and 100 mm/h (see TABLE 5.2), i.e. the resolution is more than twice as good as in the old ones (TODAY). The original data of RAIN and RAPID are highly resolved in space with a pixel size of 1x1 km², having the corresponding radar station in the centre of the picture. The composite of these products as well as of OVERVIEW are of lower spatial resolution (2x2 km²). The fourth product, WIND is extracted from the Doppler data of the two top elevations over each radar station.

TABLE 5.2: Levels of intensity

for reflectivity and rain rate data subdivided into 16 classes as recommended by COST-73.

Class	Reflectivity [dBz]	Rain rate [mm/h]
00	<13	< 0.16
01	13 - 16	0.16 - 0.25
02	16 - 19	0.25 - 0.40
03	19 - 22	0.40 - 0.63
04	22 - 25	0.63 - 1.00
05	25 - 28	1.00 - 1.60
06	28 - 31	1.60 - 2.50
07	31 - 34	2.50 - 4.00
08	34 - 37	4.00 - 6.30
09	37 - 40	6.30 - 10.0
10	40 - 43	10.0 - 16.0
11	43 - 46	16.0 - 25.0
12	46 - 49	25.0 - 40.0
13	49 - 52	40.0 - 63.0
14	52 - 55	63.0 - 100.
15	> 55	> 100.

Products generated at the radar site (see TABLE 5.1, geographically centered over the radar station) are transmitted to a composite centre where the information originating from different sites are combined to form composite images. Both types of products (single and composite) are retransmitted to servers attached to the user's workstations.

Not all products are supported by the user's operational display program named "SRN-display": some products like POLARU or COUNTP contain raw data which is mainly used for monitoring

and research purposes. Table 5.3 presents the list of all products available to the SMA-users on their workstations for visualization with program SRN-display.

TABLE 5.3: Products supported by program SRN-display.

Product-name	single	composite	data-type	spatial aspect
OVERVIEW	-	x	Reflectivity	volume data
TODAY	x	x	Reflectivity	3 maximum projections
RAIN	x	x	Precip. rate	ground surface
RAPID	x	x	Reflectivity	maximum vertical projection
WIND	x	-	Horiz. wind	vertical profile (VAD)

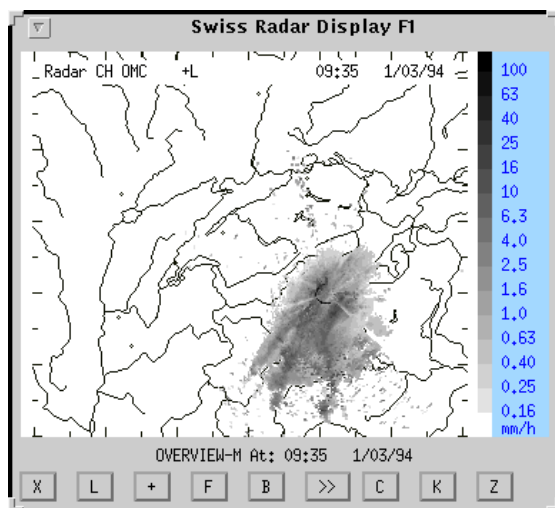
6.1.1. OVERVIEW: Full volume information

The product OVERVIEW contains full volume information of the reflectivity, updated each 5 minutes. It consists of 12 images corresponding to the heights 1 to 12 km above sea level plus one image with the "ground view", a projection of the maximum reflectivity in vertical direction. The levels 1 to 12 are named 1,2,...,9,A,B,C, the plane with the maximum projection is named M. This product is useful for example to obtain vertical sections in any desired azimuthal direction, to obtain a 3-dimensional impression of the weather or for numerical modelling purposes.

Polar reflectivity data are interpolated and projected on a Cartesian grid and converted to rain-rate values. The data at height 1 km (for example) contain measurements made between 0.5 to 1.5 km above sea level. Figure 5.1 shows an example of this product for the composite format with data from Lema (+L) only, OMC: O for OVERVIEW, M for Maximum projection C for Composite; image size and pixel resolution: 305x269 [2x2 km²].

Figure 5.1: OVERVIEW: Full volume information.

Image OVERVIEW composite (maximum vertical projection) as presented by the display program SRN-display. The data was taken on 1.March 1994 with contributions from Radar Lema only.

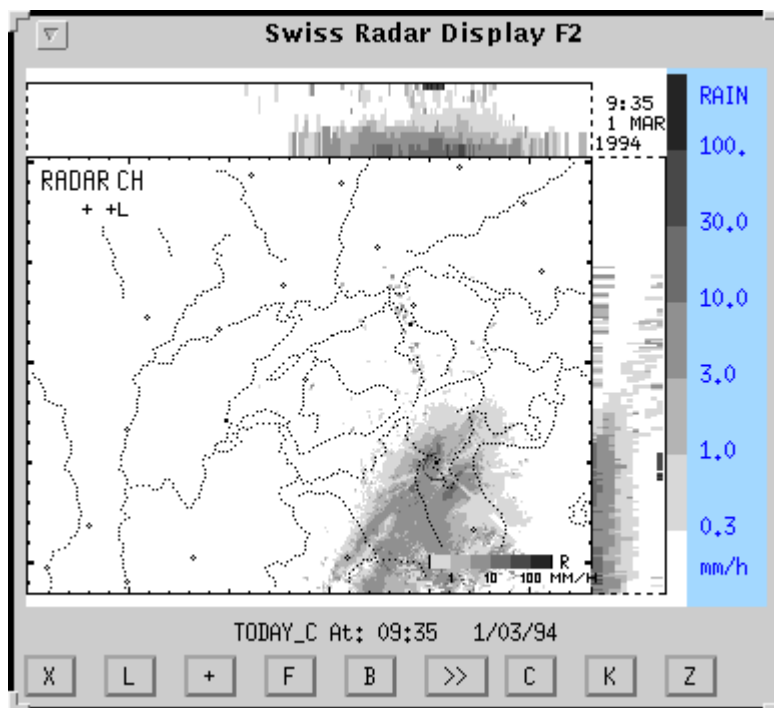


6.1.2. TODAY: Pseudo 3-D image

The product TODAY was retained from the previous generation of Swiss weather radars because of its content and in order to maintain compatibility of transmitted data format. It provides a summary of the precipitation, giving the spatial distribution of the echoes projected in 3 directions: vertical, West-to-East and South-to-North. For clarity the vertical scale is expanded by a factor of four. The three projections contain the maximum precipitation encountered and allow to judge the precise location and intensity of high and/or intense precipitation. However, compared to the product RAIN, the indicated rates are of reduced resolution: 7 levels of precipitation rates instead of 16 and a pixel size of km^2 instead of km^2 . The update rate of this product is 5 minutes. The user can display either the individual radar-site products or the composite.

Figure 5.2 shows an example for TODAY with data taken from the radar station Lema (+L) alone. The image was produced using the display program of Lassen Research; the product has the identification TGC (T for TODAY, G for Gap-format and C for Composite; image size and pixel resolution: 320×256 [$2 \times 2 \text{ km}^2$]).

Figure 5.2: TODAY Composite with Radar Lema only
1. March 1994 at 09:35 utc.



6.1.3. RAPID: 2D maximum Reflectivity

The product RAPID was conceived as quick available product with high repetition frequency for purposes of air traffic control.

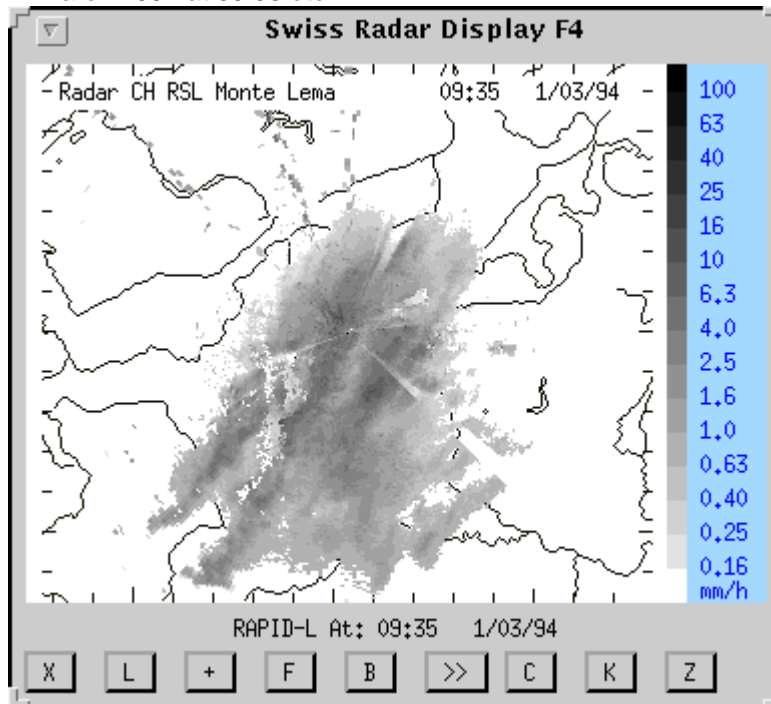
It uses the half volume scan data to deliver each 2.5 minutes the vertical projection of the maximum reflectivity coded in 16 levels of precipitation intensity. The spatial resolution

of the pixel is 1x1 km². The user can display either the individual radar-site products or the composite.

Figure 5.2bis shows an example for RAPID with data taken from the radar station Lema. The image was produced using the display program of Lassen Research; the product has the identification RSL (R for RAPID, S for Standard-format and L for Lema; image size and pixel resolution: 305x269 [1x1 km²]).

Figure 5.2bis: RAPID Lema

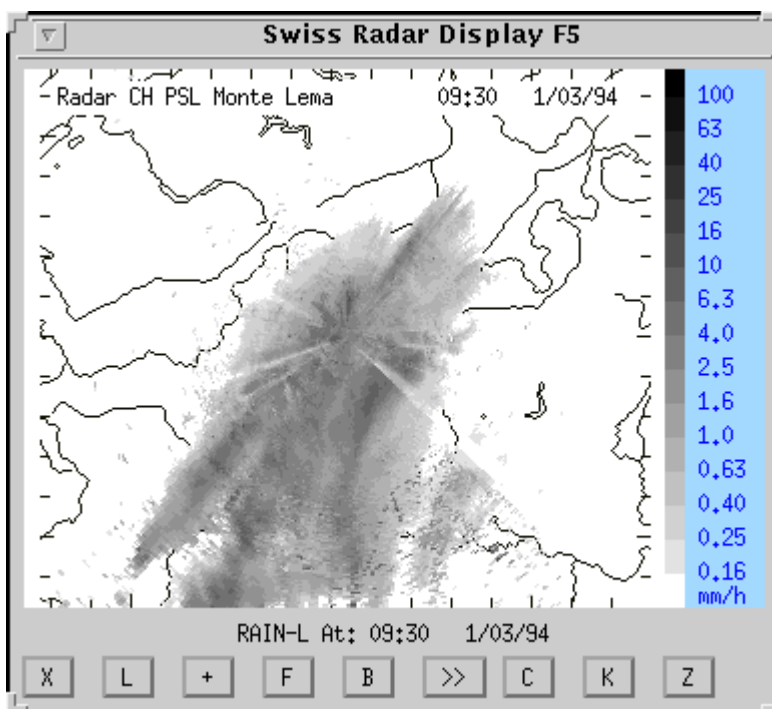
1. March 1994 at 09:35 utc.



6.1.4. RAIN: Precipitation amounts

The product RAIN displays the best estimate of the precipitation at ground level using the experience accumulated in the past. A running average over the last 6 samples (reflectivities of 6 successive volume scans) is calculated to improve representativity of the image and make the system less vulnerable to short losses of data communication channels. The product is updated every 5 minutes, covering the last 30 minutes by calculating a linear average of the available data. The image below shows data from the radar station Lema as displayed by SRN-software from Lassen Research (PSL: P for Precipitation, S for Swiss-format, L for Lema, image size and pixel resolution: 305x269 [1x1 km²]).

Figure 5.3: Product RAIN for radar Lema (1. March 1994 at 09:30 utc).



The precipitation over ground is estimated, taking into account all valid reflectivity measurements in the vertical column over each terrain pixel. The long-term averaged radar visibility and the terrain height will be considered together with a vertical reflectivity profile taken from the currently measured data (see "Real-time corrections for vertical variation" on page 28).

6.1.5. WIND: Sounding above radar and polar products

The product WIND is generated from velocities estimated from the Doppler measurements of the radar echo. It consists of a vertical profile of the horizontal wind component over the radar station. Updated every 2.5 minutes during the highest elevations (at sweeps 10 and 20, elevations 3400 and 4000), it is recorded with a resolution of about 165 meters in range (along the beam) between the radar station and a maximum altitude of 7 km.

This product uses an enhanced version of the wind profiling algorithm (VAD, described below) in the radar-site data system. Using the poly-pulse-pair algorithm this offers improved sensitivity to create wind profiles. With that it improves the chance of getting wind information in clear air. The increase in sensitivity is achieved through the use of several lags of the signal to calculate the complex auto covariance function, rather than with the single lag usually adopted with the classical pulse-pair algorithm.

Figure 5.4: WIND: Sounding (VAD) above radar.

Vertical profile of the horizontal wind component over radar Albis taken on March 27, 1995. Indicated are time of measurement (UTC) along the abscissa and altitudes above sea level on the ordinate. Note that the Albis radar is at 928m above sea level

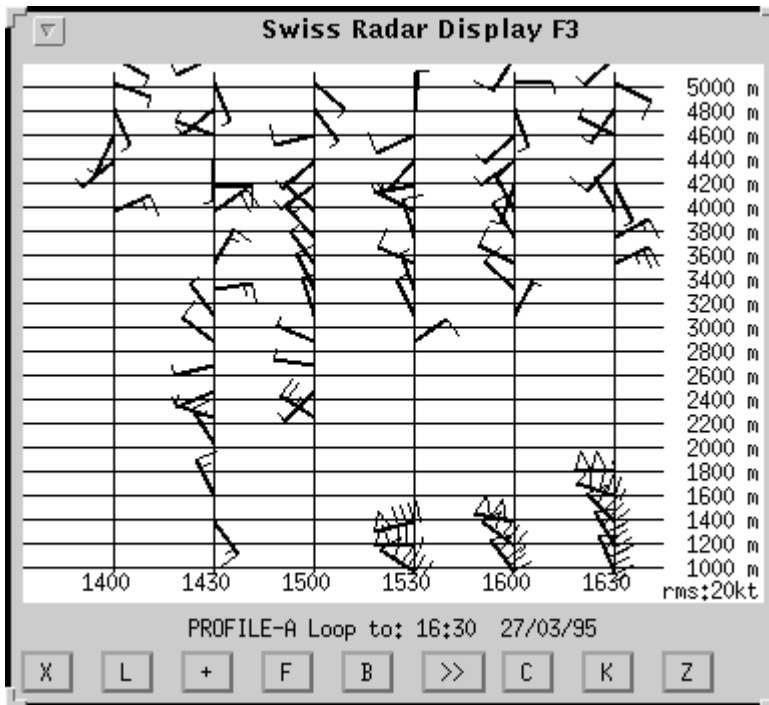


Figure 5.4 illustrates the wind profiles taken every 30 minutes from 14:00 to 16:30, March 27, 1995 over the radar station Albis, again presented by the SRN-display program of Lassen Research. The selected range of altitudes above the mean sea level is between 1 and 5km. Missing wind vectors in the example are caused by contradictory data. Data over a user-selected value is being discarded; in the example 20 knots rms-error was chosen (rms = "root mean square").

The VAD algorithm (Velocity Azimuth Display) examines the radial velocity measurements as a function of azimuth, under the assumption that the horizontal wind velocity and direction are constant at each height. If these assumptions are valid then the radial velocity at a given range (and hence at the height corresponding to that range and the elevation-angle) will be a simple sinusoid.

The measured radial velocities at the range in question are fitted by least-squares techniques to a sinusoid; The horizontal wind velocity estimate is simply the peak value of the best-fit sinusoid; the direction its phase-offset (angle, at which the best-fit sinusoid reaches its maximum value), the velocity of the wind toward the radar being defined as positive.

Doppler velocity in polar products:

In mid 1997 we are still discussing the resolution (number of bits) in our products. 4- and 8-bit velocity products exist. For the 4-bit version the Doppler velocities in the polar products (POLARU) are coded as unsigned integers shown in TABLE 5.5:

- velocity with code-value = 0 → data not defined (missing,clutter,shielded,noise);
- velocity of class "k" boundaries → $(V_n/7.5)*[(k-8)\pm 0.5]$ for $k=1..15$

Considering a wavelength λ of 5.515 cm the frequency shift which corresponds to a radial speed of 1 m/s is 36.27Hz. The maximum unambiguous velocity, the Nyquist velocity V_n , is dependent on the current PRF (Pulse Repetition Frequency) and the wavelength (λ): $V_n = \lambda*PRF/4$ (see TABLE 5.4).

TABLE 5.4: Unambiguous velocity range in antenna elevations (PRF's)

Elevation index:	1	2	3	4	5	6	7	8	9	10
Elevation index:	11	12	13	14	15	16	17	18	19	20
Vn [m/s]:	8.27	8.27	11.03	11.03	16.54	16.54	16.54	16.54	16.54	16.54

TABLE 5.5: Average Doppler velocity [m/s] in each class k (positive is toward the radar, for 4-bit resolution of the data)

k	1	2	3	4	5	6	7	8	9	10	11	12	13	14	15	0
Vn=8.27 m/s	-7.7	-6.6	-5.5	-4.4	-3.3	-2.2	-1.1	0	1.1	2.2	3.3	4.4	5.5	6.6	7.7	CL
Vn=11.0m/s	-10.3	-8.8	-7.4	-5.9	-4.4	-2.9	-1.5	0	1.5	2.9	4.4	5.9	7.4	8.8	10.3	CL
Vn=16.5 m/s	-15.4	-13.2	-11.0	-8.8	-6.6	-4.4	-2.2	0	2.2	4.4	6.6	8.8	11.0	13.2	15.4	CL

6.1.6. POLARZ: Reflectivity

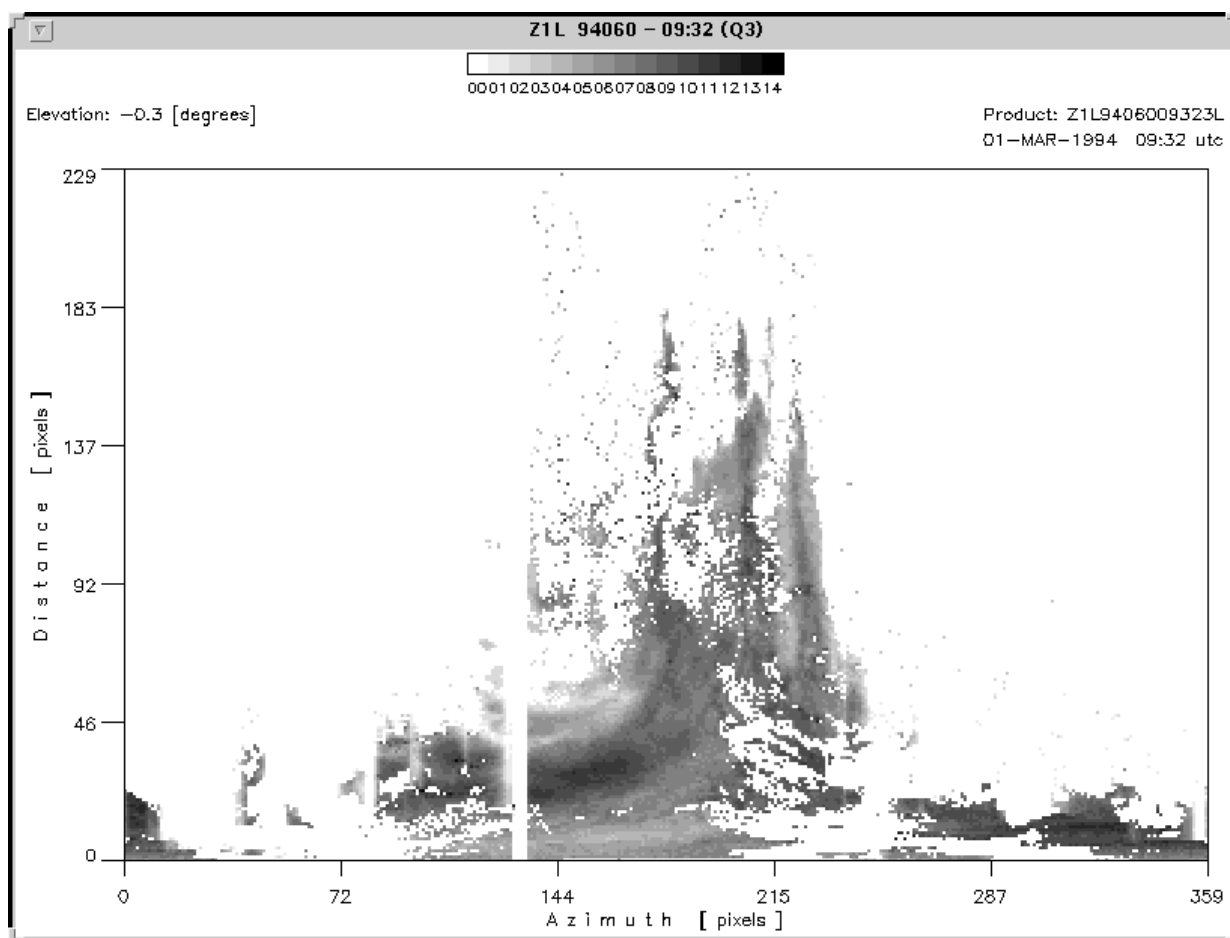
This product contains reflectivity data for all the antenna elevations of a full volume scan, updated each 5 minutes. One volume dataset is characterized by 20 image files, one for each elevation. POLARZ permits the access to the highest spatial resolution of the data which is accessible to the user (fine spatial resolution at short range, sparse at wide range).

The reflectivity assigned to a pixel belongs to a cell with extension of 1 degree in azimuth and 1 km in range on the conical surface scanned during the elevations. The center of each range gate along the radial beam is placed at every kilometer between 1km and a maximum range. The maximum range is elevation dependent, for the lowest elevations being of 230 km (TABLE 4.3 on page 44). The reflectivity is coded in range 0 to 15 corresponding to a linear scale in dB_Z (TABLE 5.2 on page 52).

The figure shows an example of this product for the radar station Monte Lema at the first elevation of the volume scan which is -0.3 degrees below the horizon; the data was taken at 09:32 utc time on 1. March 1994. The maximal measured reflectivity in this image reaches the class 52-55 dB_Z which is coded with value 14.

Figure 5.5: POLARZ: Reflectivity Image from Monte Lema

with polar reflectivity data, shown here in an azimuth-distance representation form used for the data analyses.



6.1.7. POLARU: Velocity

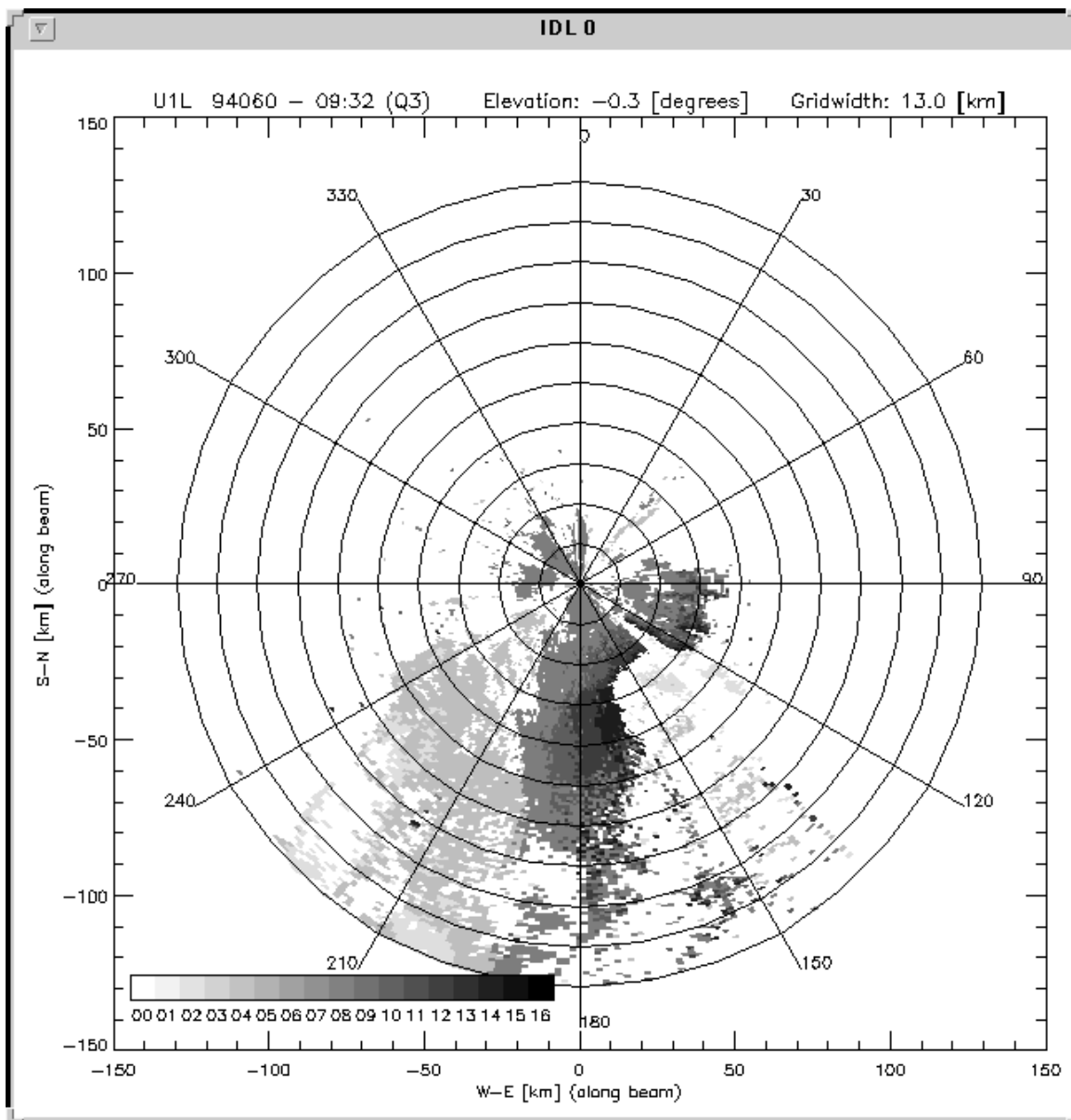
This product contains Doppler velocity data for all the antenna elevations of a full volume scan, updated each 5 minutes. One volume dataset is characterized by 20 image files, one for each elevation.

The Doppler velocity assigned to a pixel belongs to a cell with extension of 1 degree in azimuth and 1 km in range in the surface scanned during the elevations. The center of each range gate along the radial beam is placed at every kilometer between 1km and a maximum range. The maximum range is elevation dependent, for the lowest elevations being of 130 km (TABLE 4.3 on page 44). The velocity in each cell is coded in range 0 to 15 corresponding to a linear scale in fractions of the Nyquist velocity dependent from the active pulse repetition frequency (TABLE 5.5 on page 57).

The figure shows an example of this product for the radar station Monte Lema at the first elevation of the volume scan which is -0.3 degrees below the horizon; the data was taken at 09:32 utc time on 1. March 1994 (day of year: 060). The velocities coded 01 to 07 are negatives

(away from the radar), those coded 09 to 15 are positives (toward the radar), 08 is for zero (perpendicular to the beam) and 00 is for unknown velocity (clutter or shielding or noise).

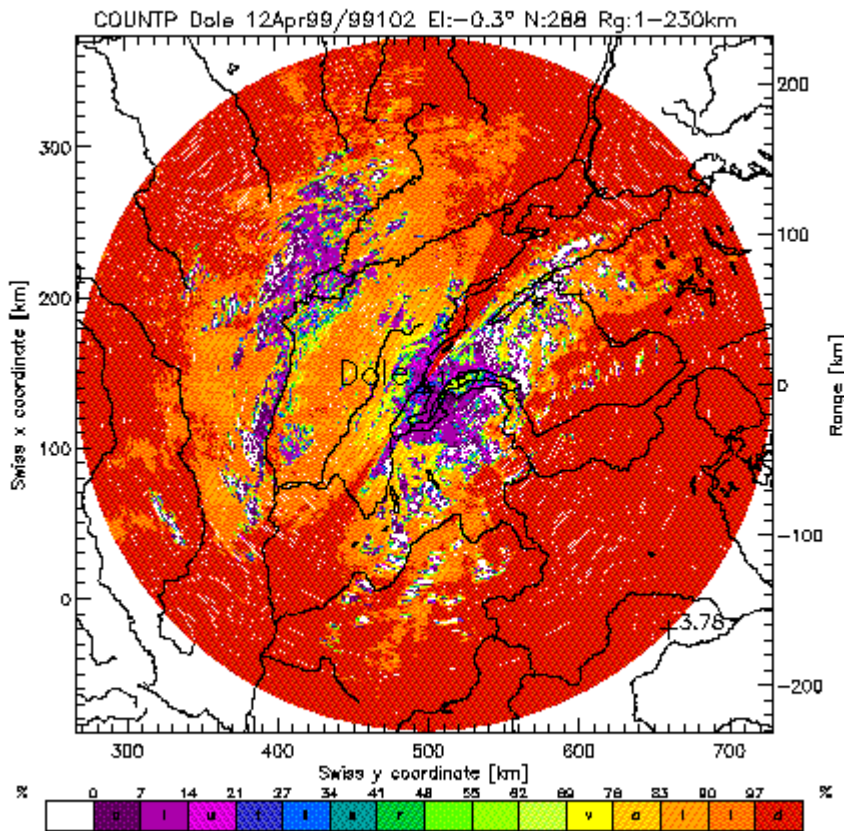
Figure 5.6: POLARU: Velocity Image from Monte Lema with Doppler velocity data shown here in a polar representation.



6.1.8. COUNTP: Cumulated Count of Valid Measurements

The COUNTP product counts how many times a polar pixel has been valid (not flagged as missing because of clutter contamination) during the last 24 hours. This product provides the daily percentage of valid data for each polar cell, which is useful, since

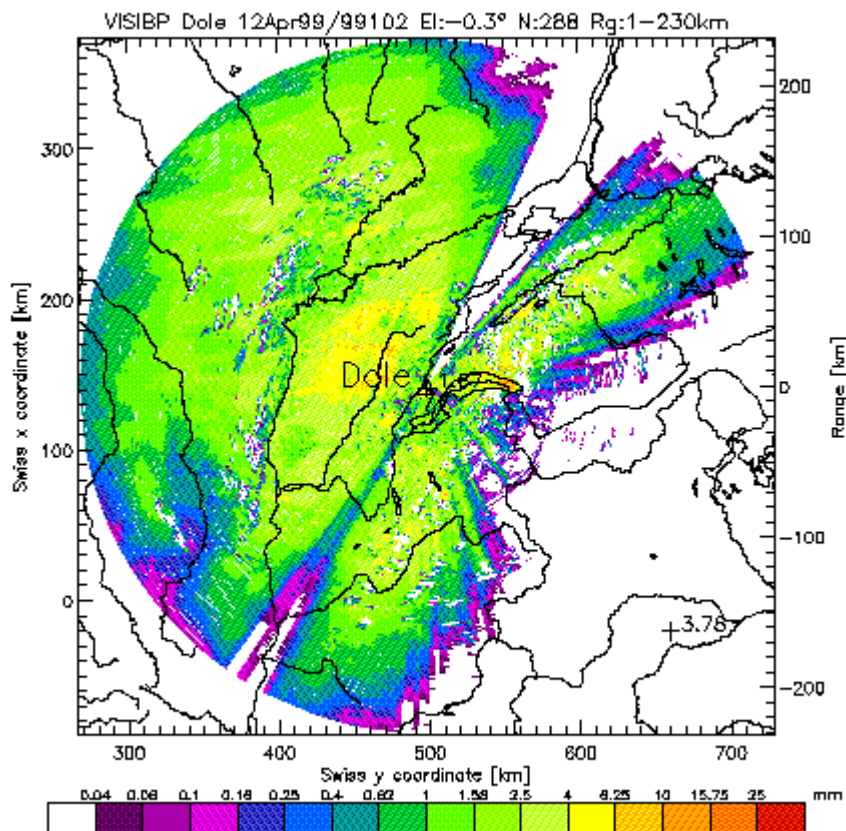
POLAR-Z products (PPIs of reflectivity) do not distinguish between valid zero-intensity and missing values (both having code 0).



The example gives the percentual number of valid measurements over 24 hours (288 scans taken each 5 minutes) for each measured point of the radar station La Dôle on 12 April 1999 (day 102) at the -0.3 degrees elevation tilt of the antenna.

6.1.9. VISIBP: Cumulated Precipitation Quantities

The VISIBP product provides fast access to daily totals, useful to obtain a first image of precipitation events or to calculate long-term accumulations in the full volume. Assuming spatial continuity of precipitation (eg. uniform annual precipitation at a given altitude in a given region of interest) the accumulation can be used to estimate the real visibility of the polar radar volume (Joss and Lee, JAM 1995, pp 2612-2630). In regions of frequent clutter or partial beam shielding, the long-term accumulation will show smaller totals than in the well-visible neighbourhood.



The example gives the accumulated precipitation amount, estimated from the measured reflectivity, during 24 hours (288 scans taken each 5 minutes) for the radar station of La Dôle on 12 April 1999 (day 102) at the -0.3 degrees elevation tilt of the antenna. Note that a blanked sector is present between 27 and 39 degrees azimuth (northeast).

6.1.10. CALIB: Calibration Report

The product CALIB contains the results from the automatically or manually started calibration operations. It is principally used by the maintenance equipe and by the development engineer staff. The example presented here shows an extract taken from the listing of the calibration report for the radar station Monte Lema performed on 18-Aug-1999. The best fit with a straith line is calculated and the intercepts with the signal power axis at -99.0 dBm (RN) and with the saturation line placed at 3677 adu (units of the analog to digital converter) denoted by RS as well as the rms value of the residuals of the fit (which is taken as a goodness factor of the calibration) are given.

```
IDL> show_rad, '/srm/data_rad3/CVL/CVL99230*'
===== Calibration for CVL9923000157L =====
Generator frequency:      5438942 [kHz]
Delay of pulse:          775000 [ns]
Width of pulse:         25000 [ns]
Quality code:           13
Tolerance for calibration: 30 [adu]

Start of calibration: 18-Aug-1999 00:01:32
End   of calibration: 18-Aug-1999 00:14:04

Date of current calibration: 992300010
Radar Calibration table dbm_to_adu(0..120) :

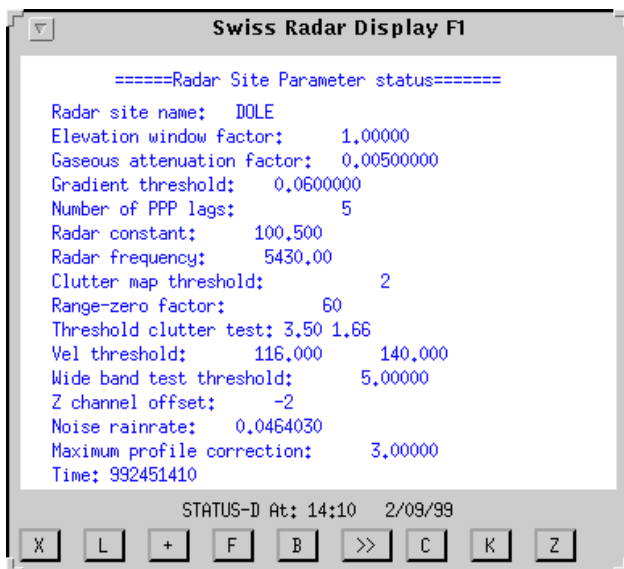
dBm   0   9   8   7   6   5   4   3   2   1
-110  457 462 459 463 466 470 469 479 485 495
-100  511 518 540 560 579 603 631 659 688 727
-90   755 809 840 875 906 938 970 1004 1038 1075
-80  1107 1149 1179 1215 1246 1279 1308 1339 1372 1407
-70  1436 1491 1525 1560 1588 1620 1650 1683 1714 1747
-60  1779 1823 1857 1892 1923 1954 1988 2020 2053 2083
-50  2113 2164 2193 2232 2268 2303 2334 2366 2397 2432
-40  2462 2501 2536 2575 2605 2637 2669 2701 2730 2766
-30  2794 2853 2887 2926 2962 2995 3028 3060 3087 3123
-20  3153 3198 3234 3273 3305 3334 3362 3393 3424 3457
-10  3489 3541 3570 3601 3621 3642 3655 3666 3675 3679
  0   3682 3683 3684 3684 3684 3683 3683 3682 3680 3679 3677

dBm   0   1   2   3   4   5   6   7   8   9  10
RN<adu= 457>= -99,0dBm, RS<adu=3677>= -4,6dBm, rms= 7,43adu (-80/-20dBm)
```

6.1.11. STATUS: Status Report

The product STATUS contains a summary of the currently active parameters of the radar station. It mainly serves for supervision purposes by the operating staff, the maintenance equipe and the developping engineers. The user can also in part inspect the content of this product using the display program of Lassen Research as show in Figure 5.6bis.

Figure 5.6bis: STATUS La Dôle
2. September 1999 at 14:10 utc.

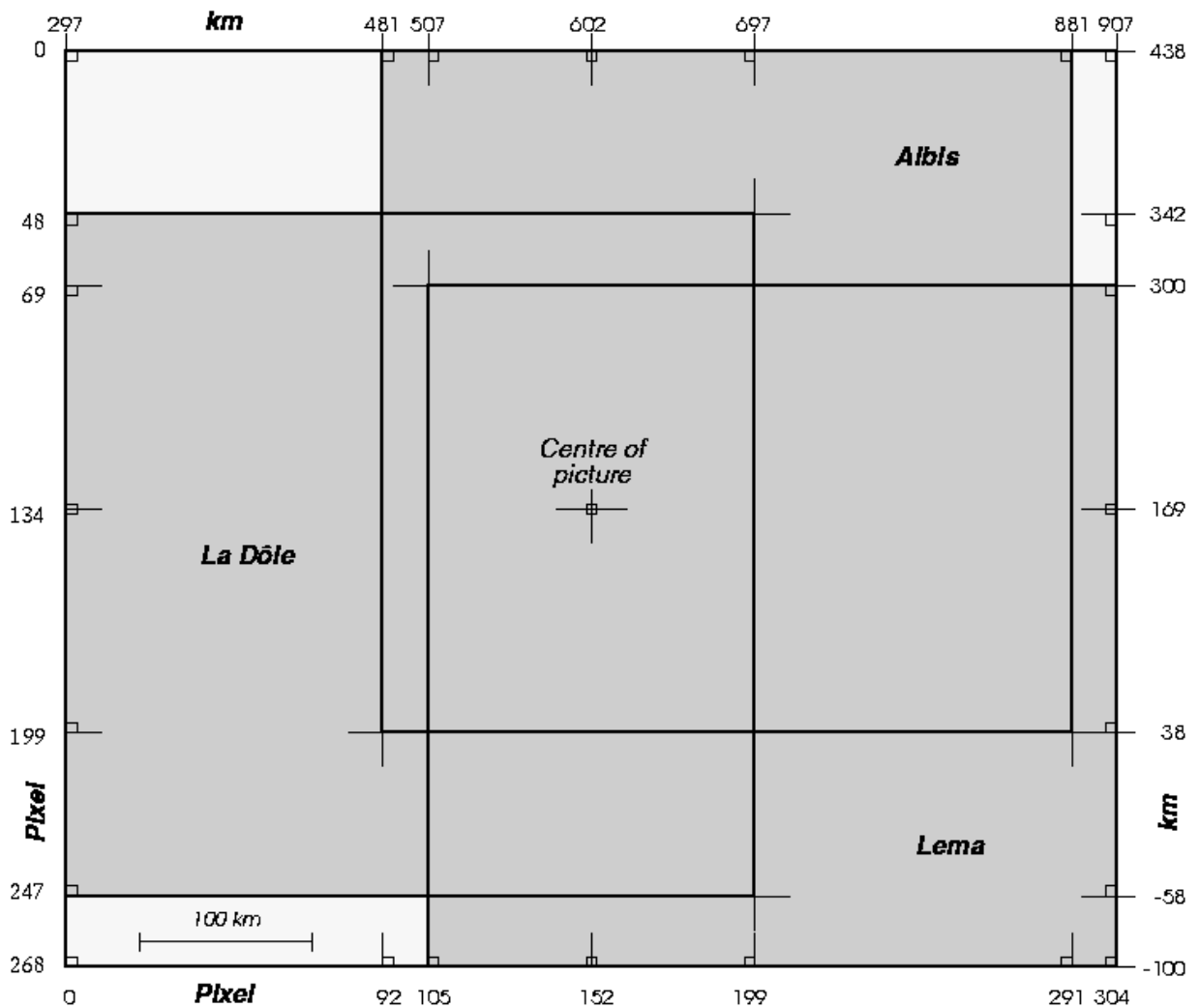


6.2. Formats of Composite Products

6.2.1. OVERVIEW(OYC) RAPID(RLC) and RAIN(PLC) Composite

Figure 5.7: Composite format for OVERVIEW, RAPID and RAIN.

The coordinates are indicated in pixels on the bottom and left side of the picture (pixel: 2-km x 2-km) and in Swiss National coordinates on the top and right side. The boundaries of the radar-site products for the 3 radars are shown (squares of 400km x 400km).



Description of product OVERVIEW:

- 1 - Product identifier: OyC with $y = \{1,2,3,4,5,6,7,8,9,A,B,C,M\}$
- 2 - Physical data: reflectivity on an horizontal plane of 1 km thickness, centered at height "y"
(1 to 12km for $y=1$ to C, maximum over all 12 planes for $y=M$)
- 3 - Image format on file: 269 lines each of 305 samples, with 8bit/sample
- 4 - Byte order: lines from North to South, samples from West to East
- 5 - Update interval: 5 minutes
- 6 - Pixel coding: values in range [0-15] corresponding to 16 rain rates

Description of product RAPID (same as for OYC except the following):

- 1 - Product identifier: RLC
- 2 - Physical data: maximum reflectivity along a vertical to the surface, updated each 2.5 minutes.

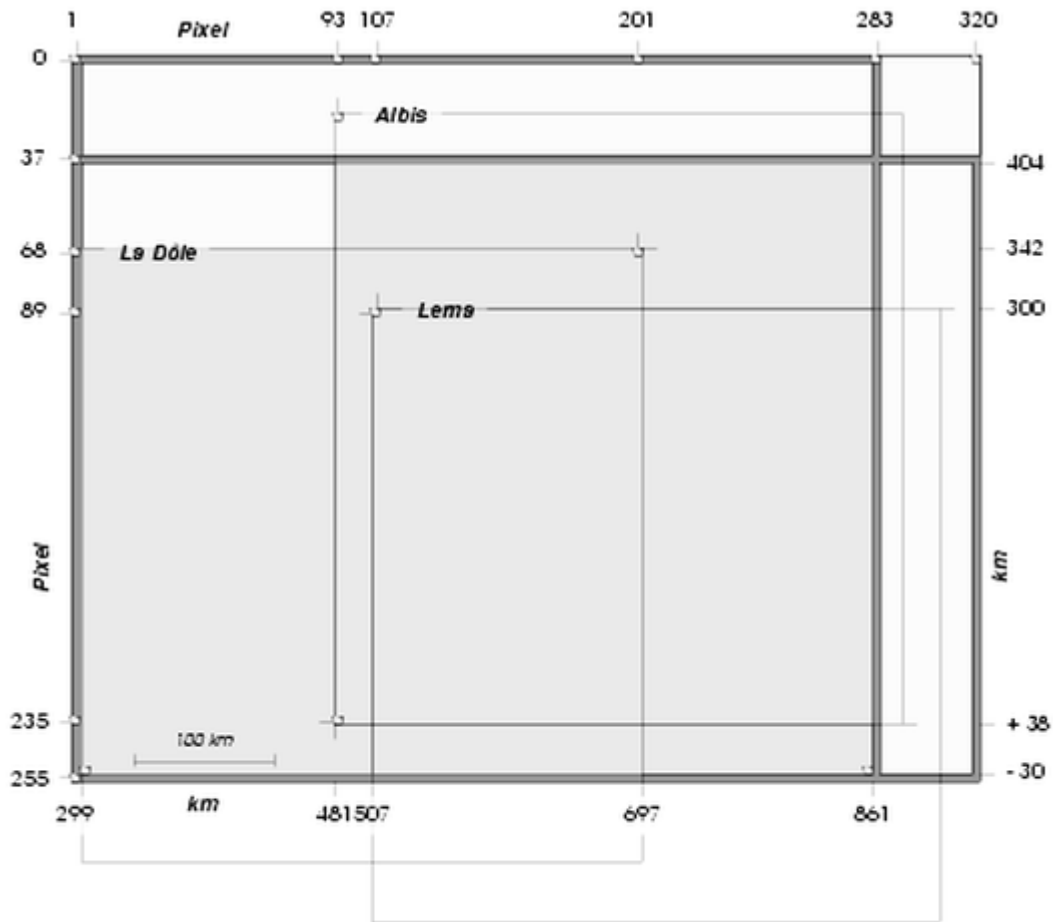
Description of product RAIN (same as for OYC except the following):

- 1 - Product identifier: PLC
- 2 - Physical data: best estimate of averaged precipitation rate at ground-level, mean value representative for the last 30 minutes

6.2.2. TODAY(TGC) Composite

Composite format with side-views, 320x256 pixels.

The layout of the composite image for product TODAY is indicated in pixels on the top and left sides of the figure (1 pixel is 2-km x 2-km); the geographic position on the bottom and right sides is given in Swiss national coordinates. The boundaries of the radar-site products for the 3 radars are also drawn.



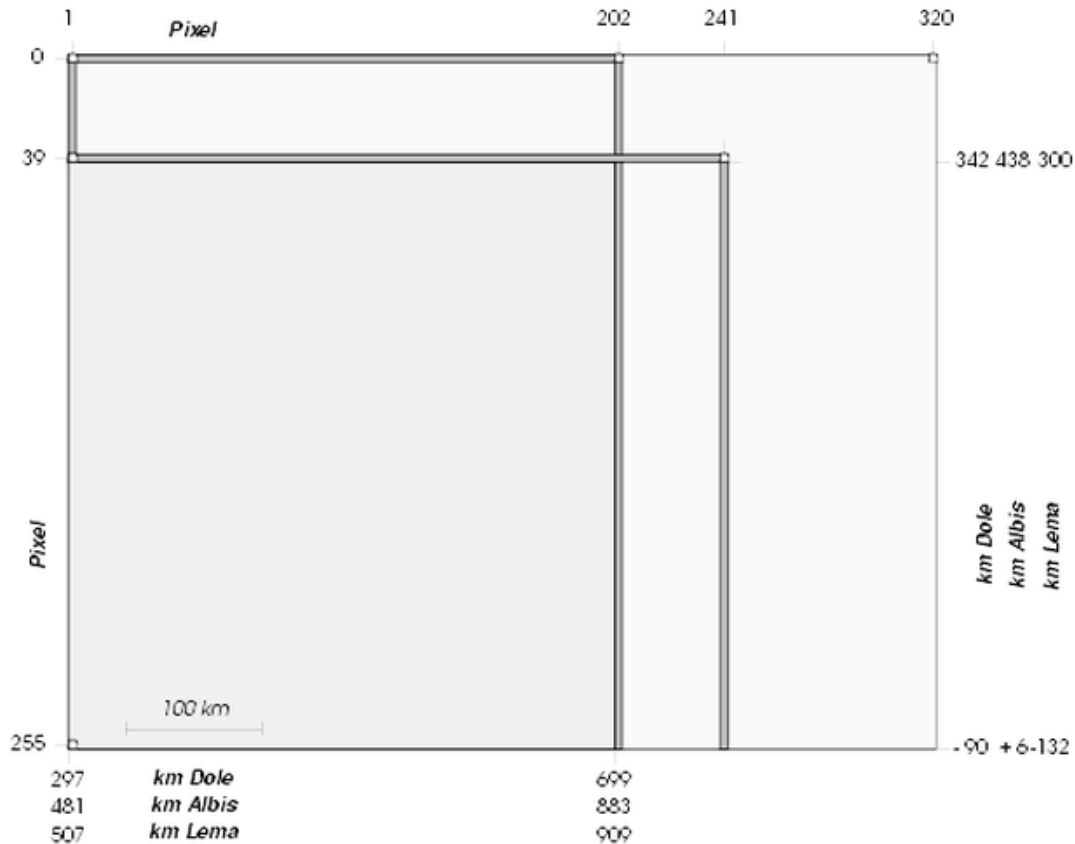
Description of product TODAY-COMPOSITE:

- 1 - Product identifier: TGC
- 2 - Physical data: reflectivity, maximum projection in 3 planes:
ground-view (281x217 pixels), front-view (281x36 pixels) and side-view (36x217 pixels)
N.B. the overlay borders (see figure) are excluded!
- 3 - Image format on file: 256 lines of 320 samples each, with 4bit/sample
- 4 - Byte order: lines from North to South, samples from West to East
- 5 - Update interval: 5 minutes
- 6 - Pixel coding: values in range [0-7] corresponding to 7 rain rates + 1 value for graphics

6.2.3. TODAY(TGA,TGD,TGL) Single site

Single site format with side-views, 320x256 pixels.

The layout of the single site image for product TODAY is indicated in pixels on the top and left sides of the figure (1 pixel is 2-km x 2-km); the geographic position on the bottom and right sides is given in Swiss national coordinates.



Description of product TODAY-SINGLE SITE:

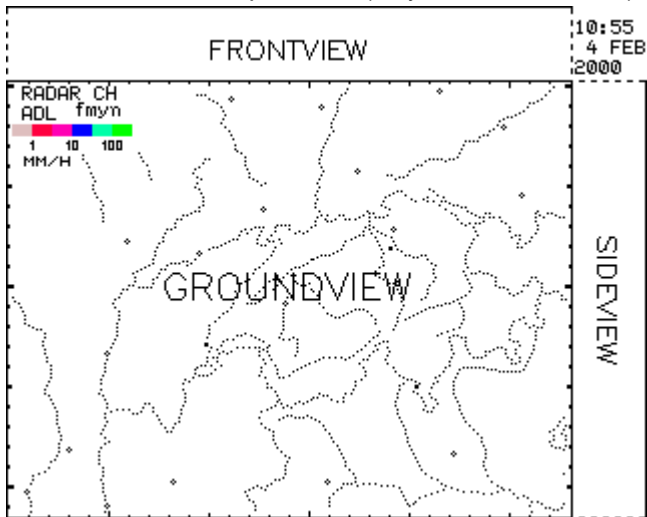
- 1 - Product identifier: TGA, TGD, TGL
- 2 - Physical data: reflectivity, maximum projection in 3 planes:
 ground-view (201x216 pixels), front-view (201x38 pixels) and side-view (216x38 pixels)
 N.B. the overlay borders (see figure) are excluded!
- 3 - Image format on file: 256 lines of 320 samples each, with 4bit/sample
- 4 - Byte order: lines from North to South, samples from West to East
- 5 - Update interval: 5 minutes

6 - Pixel coding: values in range [0-7] corresponding to 7 rain rates + 1 value for graphics

6.2.4. Frames of TODAY products

Following frames are defined inside the TODAY (COMPOSITE and SINGLE SITE) products :

- groundview
- frontview
- sideview
- colorbar
- date
- composite_id (only for COMPOSITE)



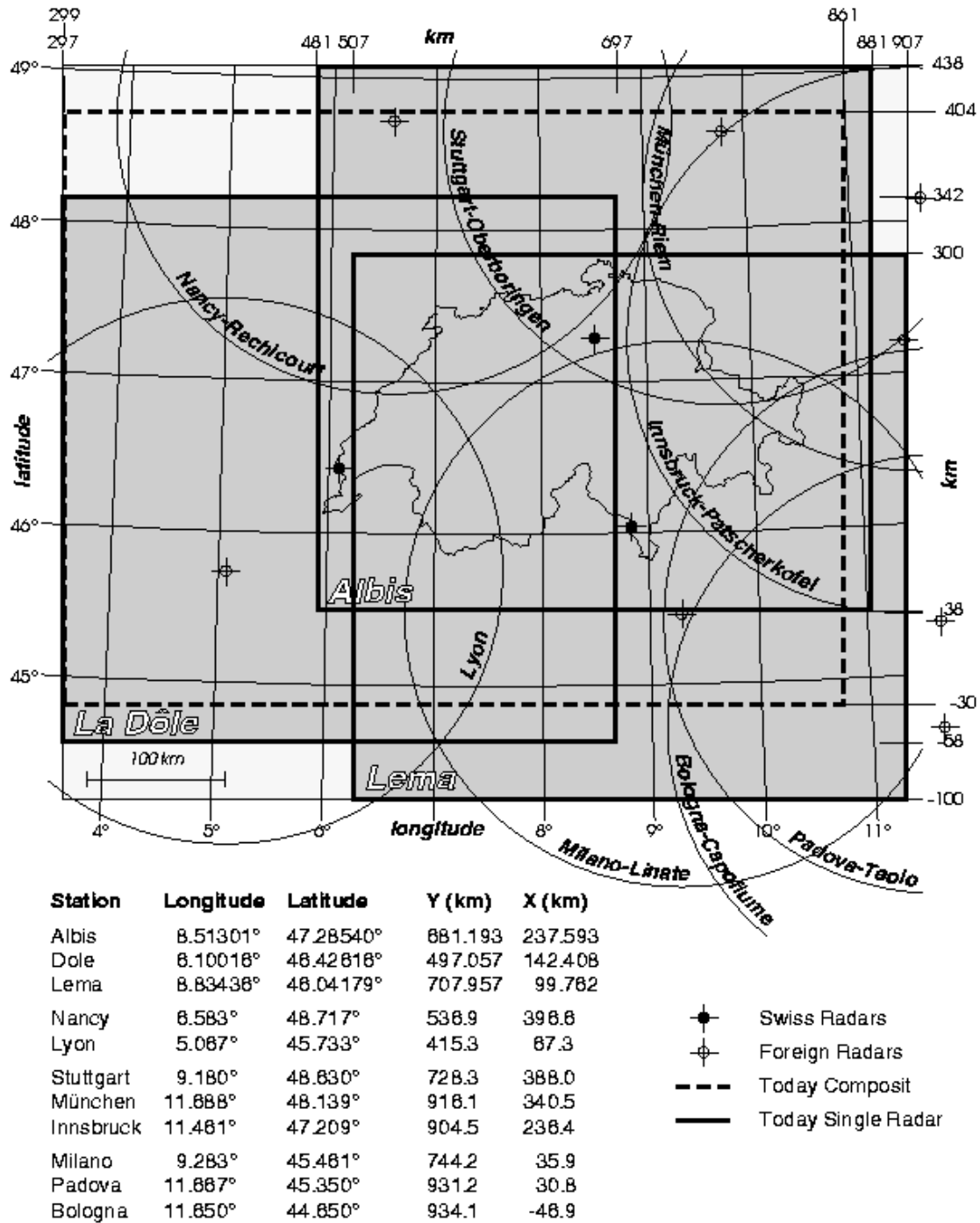
When numbering the columns from West to East with indices 0 to 319 and the rows from South to North with indices 0 to 255 the frames placements are given in the table below by the columns and rows indices of the lowest-left and upper-right corners :

TGC and TGX Frames	LLH-col	LLH-row	URH-col	URH-row
ground view-composite	0	0	282	218
frontview-composite	0	218	282	255
sideview-composite	282	0	319	218
colorbar-composite	3	191	62	196
date-composite	283	219	319	251
composite_id	6	197	70	208
groundview-single_site	0	0	201	216
frontview-single_site	0	216	203	255
sideview-single_site	201	0	240	218
colorbar-single_site	269	0	285	112
date-single site	241	197	319	227

6.3. Coverage and coordinates of radars

Figure 5.9: Swiss composite and neighbouring foreign radars.

Prospect on foreign and Swiss radar coverage and coordinate systems. Longitude/latitude, the Swiss coordinate system and pixel numbers are given as well as the 200km range rings for foreign radars. The range of Swiss radars is indicated in rectangles (400km x 400km).



Prospect on foreign and Swiss radar coverage and coordinate systems. Longitude/latitude, the Swiss coordinate system and pixel numbers are given as well as the 200km range rings for foreign radars. The range of Swiss radars is indicated in rectangles (400km x 400km).

6.3.1. Swiss coordinate system

The Swiss National Coordinates result from a conformal mapping (true angles) of the earth surface to a cylindrical surface. The earth surface (approximated by a Bessel's

Operational Use of Radar for Precipitation Measurements in Switzerland

rotation ellipsoid) is first projected onto a sphere with radius the earth radius in Bern (i.e. the distance between Bern and the ellipsoid's rotation centre) having as centre the ellipsoid's rotation centre. The sphere surface is then projected to a cylindrical surface, tangential in Bern, having the cross section correspondent to the great circle of the sphere perpendicular to the earth meridian passing across Bern (LAT = 46.952, LON = 7.440).

Radar products OVERVIEW, RAIN, RAPID and TODAY are referenced with respect to the Swiss National Coordinates system. The following formulas are useful to transform the Swiss National (Y, X) [km] to geographic coordinates (LAT, LON) [dec.degree] :

$$\text{LAT} = 46.9522 + (X-200) * 8.9956E-3 - (Y-600)^2 * [7.5338E-7 + (X-200) * 1.386E-10]$$

$$\text{LON} = 7.4394 + [(Y-600) * \{8.97044E-3 - (X-200)^2 * 8.550904E-11\}] / \cos(\text{LAT})$$

Geographic (LAT, LON) to Swiss National (Y, X) coordinate conversion is :

$$Y = 600.050 + (\text{LON}-7.44) [76.01781 - (\text{LAT}-47) * 1.418712]$$

$$X = 205.319 + (\text{LAT}-47) * 111.16601 + (\text{LON}-7.44)^2 * [0.48422 - (\text{LAT}-47) * 8.0711E-3]$$

The precision obtained is 50m within the Swiss Composite area indicated in TABLE 5.6.

TABLE 5.6: Coordinates of Swiss Composite products

PRODUCT	Side	Longitude [degrees]	Latitude [degrees]	CH-coord W/E [km]	CH-coord S/N [km]
OVERVIEW,RAIN,RAPID	Top left	3.297	49.021	297	438
OVERVIEW,RAIN,RAPID	Top right	11.636	49.019	907	438
OVERVIEW,RAIN,RAPID	Bottom left	3.652	44.188	297	-100
OVERVIEW,RAIN,RAPID	Bottom right	11.277	44.186	907	-100
TODAY	Top left	3.335	48.725	298	405
TODAY	Top right	11.002	48.743	862	405
TODAY	Bottom left	3.623	44.808	298	-31
TODAY	Bottom right	10.752	44.825	862	-31

TABLE 5.6 indicates for product RAIN (the same is valid also for products OVERVIEW and RAPID) the total covered area, while for the TODAY-product the coordinates are given for the center of the corners in the ground-view area.

6.3.2. Conversion of pixels into Swiss coordinates for Cartesian products

Conversion formulas are used to calculate the geographic position (Swiss National Coordinates) of a given point defined by the row and column indices of the data array containing the radar image.

We define a Cartesian image as a sequence of rows (all with the same length) which are formed by a sequence of points (image pixels) having the extension of $k \times k$ [km]. The number of points per row being denoted by "n" (image width) and the number of rows per image by "m" (image height) it follows that rows will be numbered from 0 to $m-1$ (lin_nr) going from North to South, points from 0 to $n-1$ (col_nr) going from West to East.

The Swiss National Coordinates, expressed in km, are called "Y" for the West to East direction and "X" for the South to North direction. The reference point for the Swiss National projection is Bern, with coordinates $Y=600$ [km], $X=200$ [km] (latitude: 46.952 , longitude: 7.440 degrees).

When the center coordinates (YW, XS) of the most SW image pixel, the image size ($n \times m$) and the pixel size are known, following formulas give the coordinates of the center of the pixel located in the image through the indices col_nr and lin_nr :

$$Y = YW + k \cdot \text{col_nr}$$

$$X = XS + m - k \cdot \text{lin_nr}$$

Examples:

1) Product RAIN, high resolution (1km x 1km), from the Radar-site:

Validity range => lin_nr: {0,268}, col_nr: {0,304}

Albis	La Dôle	Lema
$Y = 529.5 + \text{col_nr}$	$Y = 345.5 + \text{col_nr}$	$Y = 555.5 + \text{col_nr}$
$X = 371.5 - \text{lin_nr}$	$X = 276.5 - \text{lin_nr}$	$X = 233.5 - \text{lin_nr}$

2) Product TODAY Composite (2km x 2km):

Validity range => lin_nr: {38,254}, col_nr: {1,281} (only the ground-view part)

$$Y = 298 + 2 \cdot \text{col_nr}$$

$$X = 479 - 2 \cdot \text{lin_nr}$$

TABLE 5.7: Locations of weather radars in Switzerland

Radars	Height	Longitude	Latitude	CH-coord W/E	CH-coord S/N
Albis	928 m	8.513E	47.285N	681'193 m	237'593 m
La Dôle	1680 m	6.100E	46.426N	497'057 m	142'408 m
Lema	1625 m	8.834E	46.042N	707'957 m	99'762 m

Operational Use of Radar for Precipitation Measurements in Switzerland

TABLE 5.7 gives the altitude of the center of the antenna and the geographic location of the three radar stations in geographic and in Swiss National Coordinates.

7. Archive (Galli)

Operational Radar systems produce an huge amount of data. They must be saved on archival media to allow an easy access to satisfy the many requests, spanning a large spectrum of interests (from scientific to technical/commercial).

At the Swiss Meteorological Institute a home-made archive/retrieve package has been developed which fulfills the needs of the users and considers the special features of the radar products.

The operational archival procedures are executed by the two radar servers of the compositing computer system in Zôrich, where products are saved daily. Users may operate their own archive (e.g. for special products - not processed by the central system).

The data retrieval operations can be performed by each user. The adopted approach is to retrieve data of one full day for specified products. The requestor is informed via electronic-mail when the task is completed. He just has to specify the day, the product(s) and the directory where to store the retrieved data.

7.1. Concept for Archiving

7.1.1. *Archive/retrieve*

The data management systems have to compromise between equipment cost and risk of missing important data. The cost depends from the amount of data and the selected storage media; it is also associated to the desired response time and to the software quality/functionality of the processing system.

There are two extreme positions to decide which data should be archived. One is to save just the raw, polar data (plus radar parameters) and rebuild the user's products on demand. The other is to save all available products, thus avoiding to have to recalculate them from the saved raw data but, as a consequence, having to archive somewhat redundant information. We have decided to operationally archive the most useful products for one category of users (the meteorologists), as well as the polar products, from where other users can recalculate additional products.

7.1.2. *Information content in products*

To help users define their personal archive, the information content and data amount of radar products are illustrated in two tables.

TABLE 6.1 on page 67 indicates the main parameters of the data formats associated to the radar products. The time interval between successive product generations and the size of each product (when resident in memory in non-compressed form) are shown; the structure of image products is

Operational Use of Radar for Precipitation Measurements in Switzerland

given by the number of elements for arrays, two-dimensional and three-dimensional data and by the geometry and spatial extension of the elements.

TABLE 6.2 on page 67 shows the number of products generated per day and the amount of storage required by the various products on a daily and monthly basis. Site product indications are for single stations and for all three Swiss radars together. Where a composite product is available, the space needed is also given.

All products available (early 1997) require an total amount of 1.3 GByte per day. This corresponds to over 39 GBytes per month and about 0.5 TBytes per year of uncompressed data.

The amount of space currently used in the archive media is between 2 and 20 times smaller, depending from type of product and from the weather situation, thanks the applied data-compression. Only loss-less encoding techniques are used because quantitative information are to be retained in the saved data. However interesting weather situations cannot be compressed as much as during fine weather days.

TABLE 6.1 : Information of radar products and generation interval

Product	Pixel resolution	Interval	N _o of pixels	Total size ^(a)
RAIN	1x1x1 [km ³]	5 [min]	305x269	41'070
OVERVIEW	2x2x1 [km ³]	5 [min]	12x200x200	240'000
OVERV-C ^(b)	2x2x1 [km ³]	5 [min]	12x305x269	492'270
WIND	107-m to 7-km	2.5 [min]	100 heights	2'000
POLARZ ^(c)	1 ⁰ _x 1 ⁰ _x 1-km	5 [min]	20 x 360 ⁰ _x δ [km]	348'660
VISIBP ^(c)	1 ⁰ _x 1 ⁰ _x 1-km	24 [hours]	20 x 360 ⁰ _x δ [km]	1'394'640
COUNTP ^(c)	1 ⁰ _x 1 ⁰ _x 1-km	24 [hours]	20 x 360 ⁰ _x δ [km]	1'394'640
STATUS	-	5 [min]	-	1244
TODAY	2x2x1 [km ³]	5 [min]	281x217	30'720 ^(d)
POLARU ^(e)	1 ⁰ _x 1 ⁰ _x 1-km	5 [min]	20 x 360 ⁰ _x δ [km]	549'720

^(a)Size in [Bytes] before compression (product information content)

^(b)OVERV-C is the composite made out of the CH-Radars (OVERVIEW)

^(c)Number of 1-km range elements: δ (230 for the lowest, 18 for the highest elevations, Sec. 5.1.5)

^(d)The whole picture (including side-views and added information) is 320x256 pixels

^(e)Number of 1-km range elements: δ (130 for the lowest, 18 for the highest elevations, Sec. 5.1.6)

TABLE 6.2 : Content of products in MByte (uncompressed)

Product	N/day ^(a)	One day ^(b)	One month ^(c)	Three radars ^(d)	Composite ^(e)
RAIN	288	11.828	354.845	1'064.530	354.845
OVERVIEW	288	69.120	2'073.600	6'220.800	-
OVERV-C ^(f)	288	-	-	-	4'253.210
WIND	2x288	1.152	34.560	103.680	-
POLARZ	288	100.414	3'012.420	9'037.260	-
VISIBP	1	1.395	41.839	125.517	-
COUNTP	1	1.395	41.839	125.517	-
STATUS	288	0.358	10.748	24.364	-
TODAY	288	8.847	265.420	796.262	265.420
POLARU	288	158.319	4'749.570	14'248.709	-
Total	2'018	352'828	10'584.841	31'746.639	4'873.475
Great- Total^(g)					36'620.114

^(a)Number of products transmitted from one radar station per day

^(b)All products of one radar station and per day

^(c)One month of data of one radar station

^(d)Information content of all products transmitted during one month from all three radar stations

^(e)Product information generated by the composite computer during one month.

^(f)OVERV-C is the composite made out of the CH-Radars (OVERVIEW)

^(g)Total Swiss radar information (three radars and composite products) for one month

7.1.3. On-line products

When defining the set of products directly available on disk (on-line data), care was taken to satisfy a large amount of requests. The compromise between an acceptable interval between products, the length of time series (retention time) and the total occupied space is reflected in the TABLE 6.3.

TABLE 6.3 : On-line Radar Data Products

Product palette	Retention time	Data size [MB] ^(a) (non-compressed)
All products, all Radars including Composite (5 min) ^(b)	48 hours	2'447
TODAY-Composite (5 min) + RAIN all Radar stations (5 min)	14 days	621
RAIN-Composite (each 30 min) + VISIB + COUNTP (24 h)	62 days	641
TODAY-Composite (30 min) + STATUS all Radar stations (5 min) + Archive Index files ^(c)	unrestricted	per year: 823
Total		3'709 + 823/year

^(a)Total occupied space

^(b)Interval between successive products

^(c)About 250 kBytes per year for 24 products and 365 days

In TABLE 6.3 products are ordered by increasing values of time retention; the total amount of space on disk which would be used when the data wouldn't be compressed is also indicated. The Archive Index files are the lists of all archived products, for individual years (see "6.2.1 Program archive").

The radar products are transmitted from the radar-site data systems to the compositing computer system. They are retained on local disks during the retention time indicated in TABLE 6.3.

Currently (Jan. 1997) the products are archived every day, shortly after midnight, for "yesterday's" data. The chosen mass storage device is the DAT tape drive. One record contains all pictures generated during one day for a given product in compact (compressed) format. This facilitates the data handling and optimizes the data access time versus the required storage space. As an acceptable drawback, when retrieving the stored information, the data of at least one day must be replayed (e.g. 288 files for products with 5 minutes generation interval), even if only one single file is desired.

7.2. Software

Two utility programs are available for the saving and restoring of the radar data. Their user's guide can be found in Jiang, C. and G.Galli, 1996.

During the archive operation a list of all saved products for a day is written on a text file together with associated attributes like the total size and some quality advice. This information, called

index, is stored on a disk file accessible to the users: a utility program permits to obtain errors statistics, availability of products for specified periods of time, tape identification, etc.

Two types of archives are used (Jan. 1997):

1. one OPERATIONAL: all products requiring up to two (4 GB) tapes per month
2. one RESEARCH: with ad hoc products (e.g. depending on current projects or special weather situations).

7.2.1. Program archive

Program archive is installed on the radar servers; it is operated by the staff of the informatic service and is run on a predefined interval basis (e.g. once per day). It requires little intervention from the operators and was conceived for an operational environment. The saved product files are in LZW compression format and are written on tape through the UNIX program utility **tar**.

The type of products to be saved on tape and their location on disk are specified by a selection file (in plain text form). The program design allows any product to be added into (or removed from) that list: the list can easily be modified (from day to day).

The products are organized according to the product type and the day; all files of a given type for one day are grouped into one recording unit (one tar writing operation). Within a day, product files are archived in alphanumeric order by name, grouped by radar station.

After interruption of the archival operation the missing information will be automatically archived upon process restart (i.e. non-archived data files of several days may be recovered after system down-time).

7.2.2. Survey on archived data

The index information is collected in one file per archive per year with one entry for each product. Index files are resident on a predefined directory named `/srn/archive/index/`. They contain all indications about the archived data.

The meaning of the record fields are self-explanatory:

/ DATE / PROD / NUMF / SIZE / RECN / QUAL / ARCTIM / TAPE with:

1. DATE: starting date of data in form YYDDD(dd-Mmm) e.g. 95163(12-Jun)
2. PROD: 3 letters product identifier e.g.: TGL (TODAY-GAP-LEMA)
3. NUMF: number of the saved files per day as 6-digits integer
4. SIZE: average size of one of the NUMF files in Bytes as 8-digits integer
5. RECN: sequence number of the records on tape as 6-digits integer
6. QUAL: quality/format number as 4 digits integer. The most left digit is for the compression code, the right 3 digits represent the daily mean quality factor of the product
7. ARCTIM: time of archival as 9 digits integer in form YYDDDHHMM
8. TAPE: name of the tape identification as 15-characters string

Each line in the index file provides information for each single tape record. It contains 71 characters including one line-feed at the end with 8 items separated by one space. For example:

96202(20Jul) SVC 000288 00295345 000017 1700 962032049 aaaa19962032029

indicates that in record number 17 of the tape named aaaa19962032029, 288 files of product SVC (STATUS-COMPOSITE) are available for day 96202 (20-Jul-1996) using a total amount of space of 295.345 kBytes.

The quality/format factor (item 6) in its left-most digit (ranging from 0 to 2), indicates whether the data is uncompressed (0), has LZW- (1), or GIF-format (2). The three right-most digits represent the mean quality factor multiplied by 100. For example, the quality/format factor 1700 means: the average quality factor is 7.00 and the data format is LZW. The quality factor is the averaged value of all available files of one day: 1 is for the lowest and 7 for the highest data quality. It takes into account the completeness of the volume scan (the number of the used elevations), the condition of the transmitter (i.e. the radiated power) and of the receiver (i.e. the current estimate of the receiver noise figure). The format code value is used by program **retrieve** to estimate the data amount after the format conversion.

The record time (item 7) provides a time stamp of when the product was archived: it is an useful indicator for the archive manager, showing for example time delays between different days.

7.2.3. Access to the index file

Two figures illustrate the information contained in the index file as displayed by program **retrieve**; in this example they reflect an archive used for research activities.

Figure 6.1 : Number of archived days.

General information taken from the index file of a tape produced during month October 1995. The number of days for each archived product type, radar station and composite products are showed; other items can be selected through the buttons at the bottom of the windows. This picture is produced with the program **retrieve**. Clicking on a desired number (e.g. product PH for radar Lema) will produce results in form of plots.

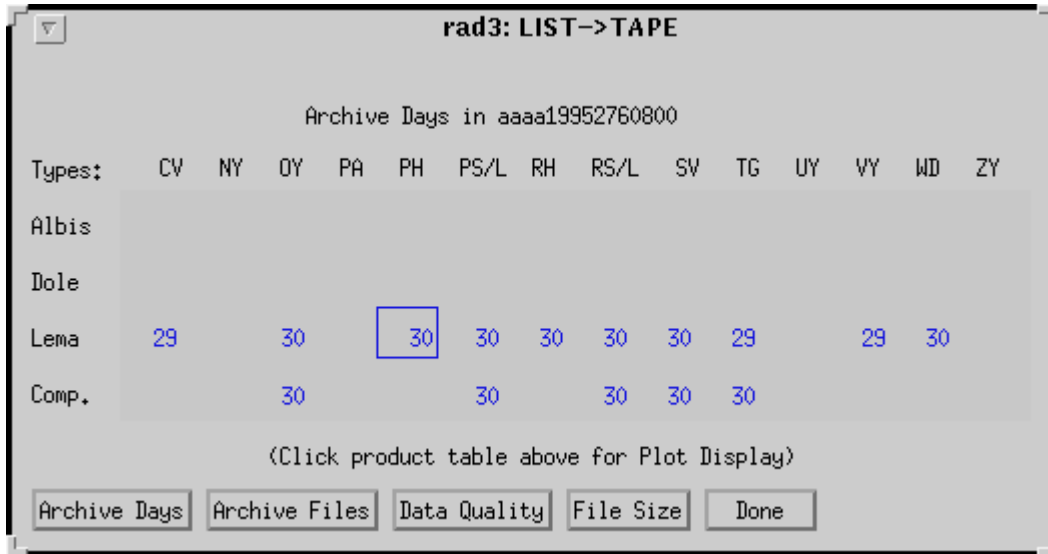


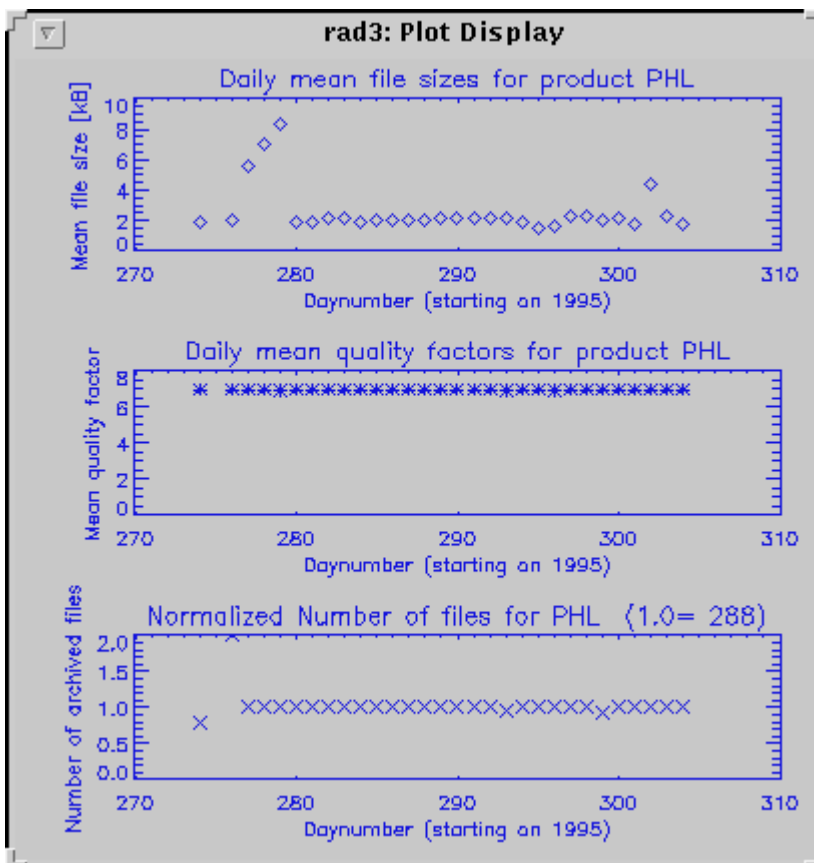
Figure 6.1 displays the number of days with archived products for one tape with data of October 1995, classified by station and product type. Products from the radar stations Albis and La D'Yle are missing here, so are certain products on single days. Other statistical reports can be generated either in numeric representation or in plot form.

Figure 6.2 gives three plots for product PHL (RAIN-LEMA) during the month of October 1995 (day 274 is Oct 01 and day 304 is Oct 31). Note that day 275 is missing, so we have a total of 30 days on the tape for this product.

The following quantities are plotted:

1. the daily mean size of the product data files (depending on the precipitation activity during the day);
2. the daily mean quality factor: all days have data with optimal quality here;
3. the number of files per day: nominally there are 288 files per day (each 5 minutes); on days 274, 293, 299 some files are missing and on day 275 the data was saved twice so we have the normalized number of files = 2.0.

Figure 6.2 : Availability, quality and size of one single product.
Product information, taken from the tape index file of month October 1995, for product PHL. Note that the data is in compressed form, thus in absence of precipitation the file size is small: during days 277 to 279 and 302 there was some precipitation activity.



7.2.4. Program retrieve

Program **retrieve** is run by operators or single users on request. It was conceived for comfortable use through a graphic user's interface. It is available to access data from a source-device and writes the data in a selectable format on a destination-device. Source and destination-devices can be either a tape or a hard disk.

Operational Use of Radar for Precipitation Measurements in Switzerland

The product files, read from the source-device, are written to the destination-device with optional conversion from compressed LZW to uncompressed or GIF formats.

The graphics interface of **retrieve** guides the user in the step by step definition of the data transfer operation parameters. The window appearing after starting the program is shown in Figure 6.3.

The parameters for the requested data transfer operation are given in steps 1 to 7. The interface is context dependent: for example, once the source device and the date have been specified, the program **retrieve** knows the list of all available products and displays them in a graphic table.

The button "List..." permits the display of statistical information about the data present in the source-device (see Figure 6.1 and Figure 6.2).

The retrieve process supports the following 4 types of data transfers:

1. the DISK_to_TAPE operation which may be used to store real-time data on a user's tape,
2. the TAPE_to_DISK operation usually applied to access old (archived) data: the user specifies its own place on disk for storing the retrieved data,
3. the DISK_to_DISK operation typically used to store real-time data on a user's specified location on disk or to change the product format and
4. the TAPE_to_TAPE operation which can be started by the user to make a copy of old (archived) data on its own tape.

The input data format is always LZW; the user may select the desired output format:

1. Uncompressed,
2. LZW,
3. GIF.

The data tapes are divided into two groups: public and private. **Retrieve** only reads (can not write) public tapes, while it reads and writes private archive tapes.

The following 40 types of products are known to this program:

CVA, NYA, OYA, PAA, PHA, PSA, SVA, TGA, UYA,VYA, WDA, ZYA, CVD, NYD, OYD, PAD, PHD, PSD, SVD, TGD, UYD, VYD, WDD, ZYD, CVL, NYL, OYL, PAL, PHL, PSL, SVL, TGL, UYL, VYL, WDL, ZYL, OYC, PLC, SVC, TGC.

The user must specify the 3-characters "product type" identification (NAME + SCALE + SOURCE) to select the products through the command interface.

The order indicated above is used by the **archive** and **retrieve** programs to save/restore data: this permits to optimize the access speed during retrieval operations.

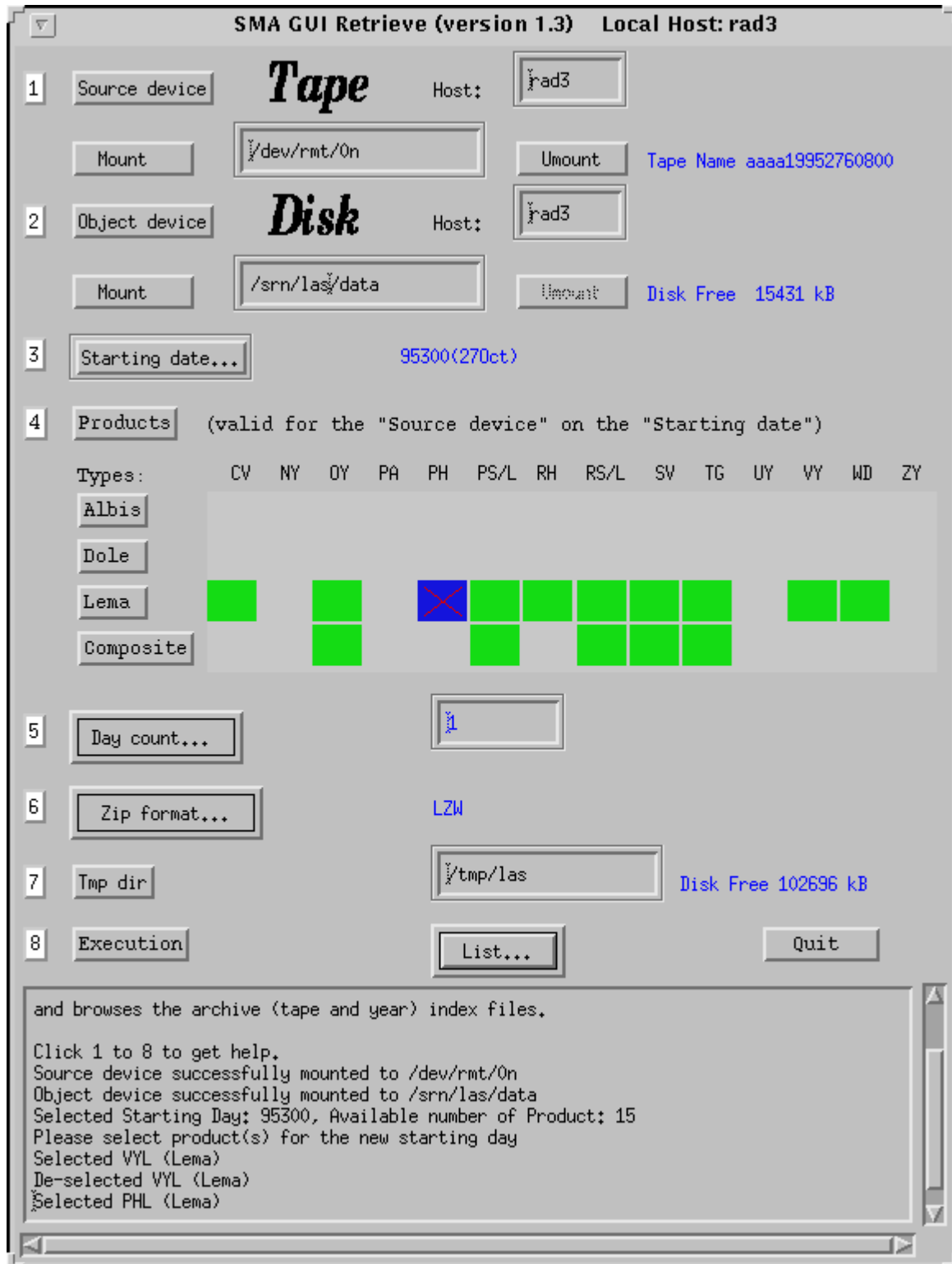
When **retrieve** creates a private tape archive, it updates the tape index file. When the tape is delivered to the users, the associated tape-index-file can be made available. Alternatively, the **archive_index** utility program can regenerate the index file from tape.

Figure 6.3 : Graphical user`s interface of program **retrieve**.

Layout of the graphical user's interface (GUI) for program retrieve. The information to be specified by the user are: 1) the input (source) device (disk or tape), 2) the output (object=destination)

Operational Use of Radar for Precipitation Measurements in Switzerland

device (disk or tape), 3) the date of the first day to be retrieved, 4) the set of products to be considered, 5) the number of successive days to take and 6) the desired format for the retrieved data (LZW-compressed, GIF, uncompressed). The button "List..." permits the inspection of the available information about the input data (directory lists for disks, index files for tapes)



8. Operation (Cavalli, Della Bruna, Boscacci)

8.1. Concept for maintenance

The need for continuous operation of the radars in unattended locations 24 hours a day, 7 days a week and the higher requirements for precise quantitative measurements of precipitation, call for more sophisticated monitoring and maintenance tools and procedures than those found in meteorological radars of earlier generations.

The maintenance of the radar stations is entrusted to swisscontrol, who is also charged with the maintenance of other meteorological equipment of our national and international airports.

In order to remotely monitor the status of each radar, the current operating parameters and alarm conditions are collected by the status system and transmitted to the central compositing site every 5 minutes in a status product. This includes

1. - all relevant power supplies,
2. - transmitter and receiver status (transmitted and reflected power, STALO, COHO, noise levels, receiver calibration parameters, etc.),
3. - servo and antenna status information (azimuth and elevation timing, scan quality, etc.)
4. - data processor hardware status (self-tests results of the boards),
5. - data processing status and clutter test statistics.

This information provides an operation check of each radar and is automatically evaluated by the RADWATCH software tool, described in "7.3 Status monitoring: Radwatch (Della Bruna)". It is used to inform the maintenance crew about anomalous situations, to allow rapid intervention before a failure occurs, i.e. already during performance degradation.

By means of the radar site's data system menu, exhaustive supplementary diagnostics can be run remotely through the radar communication network, thus allowing localization of problems and planning of on-site interventions.

Even software maintenance (updating and debugging of programs, re-booting of the systems) is normally done remotely, to test new or modified algorithms, run them in the desired real situation and to analyze their results efficiently.

Nevertheless, a monthly maintenance visit at the radar stations is needed, mainly for mechanical checks, alignments and level verifications (e.g antenna azimuth and elevation gear oil), cleaning of air filters, change of consumable parts, checks and adjustments of high voltage and/or RF (radio frequency) components, etc.

8.1.1. Calibration and Adjustment

A proper radar calibration requires measurement of the receiver response curve, the system noise power, the transmitter power, the antenna gain and beam-width, and the various system losses.

The antenna parameters and the system losses are not measured automatically, but only at installation and thereafter at rare occasions or when a special event (such as changing a component) suggests the need.

In order to correct rain rates measurements for short-term drifts in the system due to temperature or other effects, the other mentioned parameters are regularly measured during normal radar operation by means of the automatic calibration procedure described hereafter.

8.1.2. Definitions

Receiver Noise: Once per volume scan, the "noise-power-equivalent rain rate" R_N is calculated from the power measured by the receiver when no signal is received, with the transmitter being on. During this noise measurement, there must be no interference from the transmitter pulse, the signal generator, or any reflecting object. This is achieved by making the observation at a high elevation angles (elevations 7-9 and 17-19) and at times corresponding to long ranges (110 to 115 km).

Noise Source: The system BITE (Built In Test Equipment) injects a pulse signal from a noise source with 40-dB excess noise ratio through a 30-dB-coupler to monitor the receiver noise figure; the signal processor independently measures its signal at this point and calculates the "noise source-equivalent rain rate" R_{NS} . Again this is done for each volume scan at elevations 7-9 and 17-19, at times corresponding to a range between 105 to 110 km.

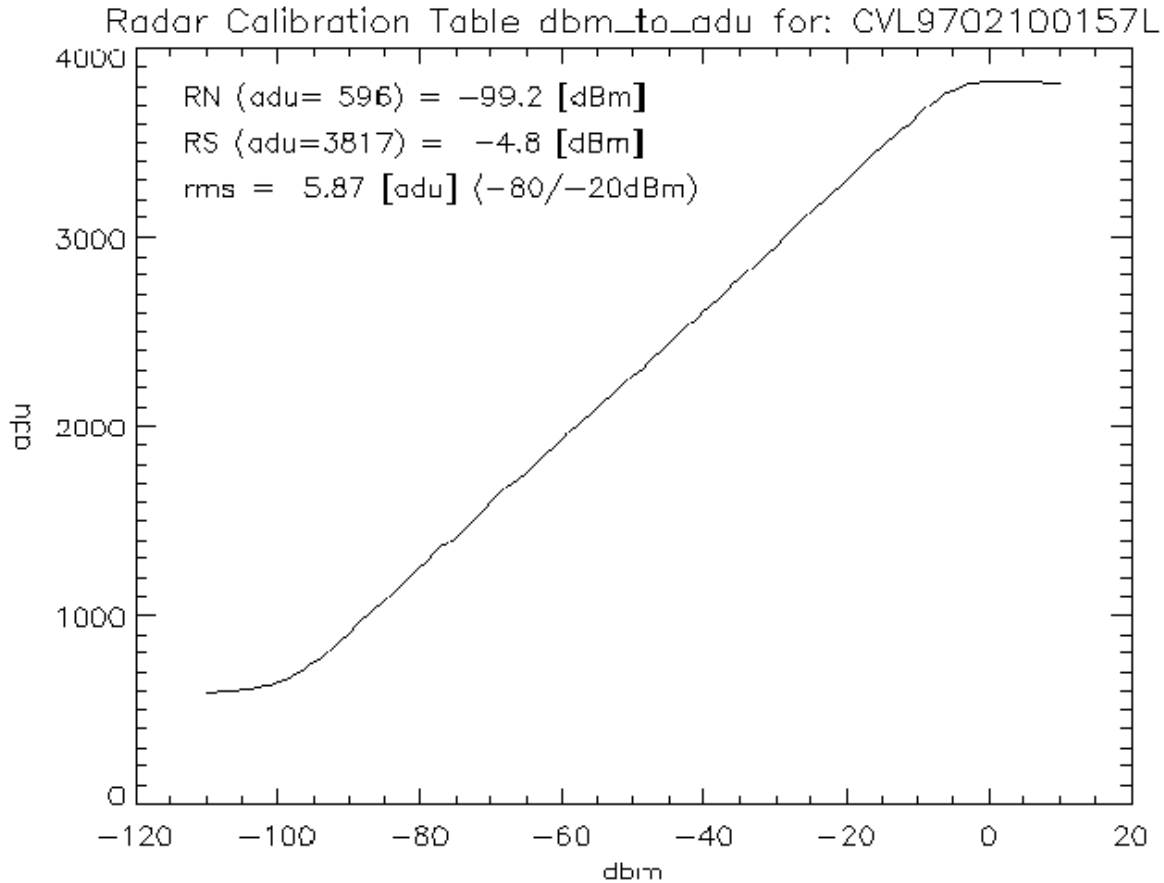
Transmitted power: The system BITE measures the transmitter power on a continuous basis, and reports the current power level to the signal processor, who calculates its "peak power-equivalent rain rate" R_P .

Receiver Response: once per day (usually at midnight, but also at any time on request by the operator) the receiver response curve as a function of signal level is determined using a microwave signal generator, in order to confirm the stability of the receiver sensitivity. The signal generator's pulses are injected at high elevation angles (elevations 7-9 and 17-19) and at times corresponding to a range of 115 to 120 km.

During this calibration the software establishes the log-Z receiver gain curve by stepping the signal generator's level through the entire dynamic range of the system, from -110 -dBm to +10 -dBm in 1-dB steps, thereby determining the response curve of the receiver including the Log-IF amplifier (Figure 7.1). Since the entire response curve of the receiver is established, it is possible to correct for any non-linearity in the receiver, thus extending the effective dynamic range of the system both at the low-signal end (where the thermal noise makes the receiver characteristic nonlinear) and at the high-signal end (where saturation effects make the receiver characteristic nonlinear).

Figure 7.1: A/D-units versus received power.

The output of the log-Z receiver (in A/D-units adu) is plotted as a function of the power (in dBm) injected for calibration purposes with the signal generator into the directional coupler before the receiver.



8.1.3. Automatic correction of errors?

Residual short-term instabilities detected by automatic calibration can be corrected automatically by using:

$$R_i = (R_{NSo}/R_{NS})(R_{P0}/R_P)(\text{range-correction}) \frac{1}{M} \sum_{j=1}^M (R_{ij} - R_N) \quad (7.1)$$

where R_i is the corrected rain rate at range i , R_{ij} are the raw rain rates measurements at range i and azimuth j , M the number of azimuth samples to be averaged for a single 1-degree azimuth sector (nominally $M=33$, see Sec.4.1.4 "Data reduction" on page 45) and R_N is the "noise power-equivalent rain rate" (assuming uniform noise power over the range interval).

R_{NS} is the measured "noise source-equivalent rain rate" and R_{NSo} the nominal noise source-equivalent rain rate (calculated from the nominal value of the noise source)

R_P is the "peak power-equivalent rain rate" of the measured peak power P and R_{P0} the "peak power-equivalent rain rate" calculated from the nominal peak power P_0 of the transmitter. "range-correction" implements the range-correction, adjusted for the Z-R relationship assumed. Note that all calculations are performed in rain rate terms, rather than in reflectivity units, to avoid bias errors caused by the variability of the weather in the sample to be averaged. Experience has demonstrated that bias errors produced by averaging nonlinear variables (such as reflectivity instead of rain rate) can cause important errors (Joss, J. and A. Waldvogel, 1990).

It remains to be seen, to what extent automatic correction is desirable or if an alarm procedure to produce a manual intervention is more appropriate: up to now all equipment was either working well with excellent results or had to be replaced. Experience will show whether the test equipment is more stable than the radar itself.

Further details on our concept of calibration and the results of the first years of experience are discussed by (Della Bruna, G., J. Joss and R. Lee, 1995).

8.1.4. Value of instrumental calibration

Calibrating weather radars is as old as their use. The results aimed at in the German and the Swiss Weather Service are described in Joss, J., H. London and J. Weisbarth 1996a. They demonstrate clearly what we have guessed for a long time: instrumental variations can be made by far smaller than uncertainties caused by meteorological influences. In other words, if enough care and effort is dedicated to good equipment and its calibration, the instrumental stability (transmitter, receiver etc.) is so good that errors caused by the equipment can be neglected compared to variations related to the phenomenon weather itself (variations in the vertical profile of reflectivity, errors caused by limited resolution of the beam, Z-R relationship, attenuation, etc.).

8.1.5. Absolute and relative calibration - adjustment with gauges

Calibration has to show the state of the equipment and help in compensating for short term variations of the radar equipment, i.e. to provide stable conditions for precipitation measurements. It is the basis for long-term adjustments with rain gauges. Calibration may also be needed after component replacement to ensure that no relative change in sensitivity has occurred: this all means that high reproducibility is the aim. To strive for high absolute accuracy, i.e. absolute calibration, is neither the required goal nor may it be possible (at least at good cost/benefit-ratio). Absolute accuracy in this context means that we know the actual transmitted power in Watts, the antenna pattern in detail, the noise power of the receiver in electrical units and the true pointing angles. Relative accuracy defines our ability to reproduce the values we measure today in the future. If parts remain stable, we may adjust our equipment with experience gained in the domain of our variable of interest. E.g. data from rain gauges are integrated over long intervals to improve its representativeness to the point where it is useful for radar data adjustments. These and other aspects concerning absolute and relative calibration are discussed in greater detail in Joss, J., H. London and J. Weisbarth 1996b.

8.1.6. Conclusions and outlook

The excellent stability of hardware (system parameters) is verified for the Swiss radars by automatic calibrations repeated every five minutes. During normal operation of a high quality radar the stability is well within 0.2 dBZ (3% of rain rate), as needed for estimates of rain amount and flood warning.

Much care has been taken to ensure redundancy in determining relevant system parameters. This is of great importance for remote mis-function monitoring and diagnosis. Correlation between calibration points sampled every 5min usually allow defective parts to be identified at an early stage: a very important feature in unmanned, automated equipment used for flood warnings.

The following three steps of data analyses should produce a solid basis for optimum precipitation estimates at ground level:

- 1 -Verify sufficient system stability (*relative* accuracy) through frequent automatic calibration, thereby checking the radar equipment for hardware faults due to aging, thermal and other effects.
- 2 -Use software to correct for: clutter, beam shielding, reflectivity profile and possibly Z-R relationship and attenuation. Doppler analyses is made continuously and at all ranges for best clutter elimination.
- 3 -Achievement of *absolute* accuracy by long-term correlation and adjustment using rain-gauge data.

The equipment being stable, we may concentrate on variations related to meteorological phenomena (influence of the orography on the precipitation process, storms characteristics, etc.). An important future task will be to determine the (local?) Z-R relationship from volumetric radar data. It must be left to future work, however, to quantify how, when and where (at what range) radar can help to satisfy special user needs.

8.2. Status monitoring: Radwatch (Della Bruna)

8.2.1. Motivation and description

In a radar network it is crucial for maintenance and the users to be informed on the state-of-health of each radar. The Radar-Site software reports the status of its radar every 5 minutes, sending the so-called "status product". Before designing RADWATCH, the only way to detect mis-function was to look at the status product manually and check whether the values of all parameters remain inside a chosen range. As can easily be imagined, this procedure, repeated daily, turns out to be rather annoying and expensive. RADWATCH was developed to automate this task: it monitors the status of every radar continuously and raises an alarm when a parameter is outside of a user-definable range.

RADWATCH checks the radar status products to be compliant with the constraints specified in a configuration file. These constraints define the allowed value ranges for the 171 operational parameters (also called "fields") reported by the radar site software in the status products. If a constraint is violated, an alarm is raised and reported to the maintenance staff via electronic mail (Email). A message is also sent when all previously reported alarm conditions have disappeared. All 3 radars are treated independently. All alarms (if any) generated by a single RADWATCH run for all radars, are sent to the operators as Email messages. Current alarms can be recalled anytime (from the last received status product) without filtering.

8.2.2. Priorities and alarm-filtering

Every constraint has an associated priority, which defines the severity of the alarm condition. This priority affects the behavior of the filtering process described in the next

section. The allowed values for priorities are 1, 2 and 3. After the filtering process priority 1 alarms are reported immediately, whereas priority 2 alarms are reported only if they are present for 6 consecutive times, i.e. 1/2 hour. Priority 3 alarms are warnings and are not reported by Email; they are only written to a log file. A missing status product is considered as a priority 2 alarm.

All alarms are logged without any "filtering" to a file common to all 3 radars. In order to avoid an excessive number of alarm messages, some "filters" can suppress them. A first filter has the effect of suppressing repeated messages in case of a persistent alarm condition: then the alarm is reported only once. A second filter is implemented by the priority scheme: priority 2 alarms must persist for at least 1/2 hour before they are reported, whereas priority 3 alarms (warnings) are not reported by Email. A third filter allows to suppress selected alarms, in order to avoid repeated Emails in case of a known, intermittent problem. Selective alarm suppressions is defined by means of 3 files (separately for the 3 radars) containing the names of the fields to be suppressed.

8.2.3. Configuration files, activation and alarm message

Four configuration files contain the constraints (one for each of the 3 radars and 1 common to all). The syntax is as follows:

```
<priority>: <field> <op> <const>
```

where priority is "1", "2" or "3", <field> is a valid field in the status product, <op> is one of the operators "<", "<=", ">", ">=", "=", "!=", "in", "not in", and <const> is an integer, a float, an integer range or a float range. Comments can be inserted into the configuration file by prefixing them with "#".

Here is an example of a configuration file:

```
3: sens_factor = 1.0          # total sens. correction (NS and for_pw)
2: average_I in (1840:2250)  # average I in ADU (nom. 2048)
2: average_Q in (1840:2250) # average Q in ADU (nom. 2048)
1: bite_stat.radar_main = 1  # radar main power, on = 1
2: bite_stat.noise in (10:50) # perf.mon. noise figure > 1 dB
```

Activation of RADWATCH is initiated every 5 minutes on a UNIX workstation by cron (the UNIX clock daemon). Here is an example of an alarm message (Email) generated by RADWATCH:

```
Return-Path: <gdb@otl.sma.ch>
Date: Thu, 21 Mar 96 12:54:08 +0100
From: gdb@otl.sma.ch (Guido Della Bruna)
To: gdb Subject: Radwatch alarms (ALBIS)
ALBIS; 960811150; Priority 2;
radar_site.noise_diode = 0.357617 not in (0.380000:0.470000)
This alarm was generated by the constraint:
2: radar_site.noise_diode in (0.38:0.47)
```

8.2.4. Summary of alarms

Once a day (at 6:00 UTC) a list of all (filtered) alarms for the past 24 hours is sent to the maintenance staff by Email. A copy of the configuration file for the selective suppressions is appended to the Email message, as a reminder to de-activate the suppressions as soon as the problems are solved.

The alarms from the last status product can be recalled at any time with the command "radwatch_active". No filtering is applied, so that, for example, a priority 2 alarm is reported even if it was active for less than 6 times.

8.3. Hard- and software (*Boscacci*)

8.3.1. Radar-Site

On the Radar site, the computer hardware assembled by Lassen Research consists of:

- SparcII board with 16MB (cpuA)
- SparcII board with 64MB (cpuB)
- 8MB VME-Bus Memory
- 12DSP PSP32, digital signal processors
- 16 MB Flash-RAM to store conversion tables.

This equipment (called data-system) is operated in a single 19" rack.

The antenna is controlled by the BITE (Built In Test Equipment), delivered by Gematronik (a dedicated hardware interface accessible by the data-system). The Digital Signal Processors (DSPØs) receive the radar signals and eliminate the ground clutter (See "Elimination of ground clutter" on page 23. and See "Clutter suppression" on page 46.). The cpuA controls the antenna through the BITE and transfers the data from the DSP memory to the cpuB through the VME-Bus memory. The cpuB generates the products (See "Products (Galli)" on page 51.) and sends them to the Compositing-System (See "Product processing" on page 46.). Each cpu monitors the other one, and requests a re - boot of the radar - system when something is not working correctly.

The operator can check the status or change parameters using a menu program running on the Radar-Site; an ethernet link connects the operator to the cpuB. This menu offers additional possibilities to check both cpu's, the DSPØs and the main memory. A partial reset of the Radar-Site software is also possible. Through the same port, the cpuB can receive special commands from the compositing-system, such as messages for time-correction or requests to send logging files of all operations.

VxWorks, installed on both cpu's, is a real time operating system. The source of the programs to ingest the data from the DSPØs (cpuA) and generate the products (cpuB) are mainly written in C; the source-code of the DSPØs programs is written in its own machine-language. All the programs are developed and cross-compiled on a SparcII-workstation under Solaris operating system.

During the development phase a test-chassis (spare 19"rack with the same hardware than above) is used to check, validate and improve algorithms.

8.3.2. Composite-site

The Composite computer hardware consists of Sparc 1000Server with:

2 CPU's
128 MB RAM
12 GB HardDisks

The installed Operating System is Solaris 2.5 (Unix System V Release 4).

The application Software delivered by Lassen Research performs following tasks:

- data ingest from the radar sites
- generation of composite products
- transmission of Radar-Site and composite products to the users
- saving of radar products on disc and on tape

At the compositing center in Zuerich there are two servers linked to the 3 Swiss radars and to a general purpose message switching machine for the acquisition of data from foreign radars. If one server fails the second one overtakes the operation.

The two servers are connected to:

- the SMA-network, allowing only basic services
- a separate router for the connection with the three Swiss radars.

A third server is located in Locarno, linked only with Radar Mte Lema. Its purpose is to develop and test new versions of the compositing algorithms and to assure the support of the test-chassis, without interfering with the operational servers in Zuerich.

8.3.3. Data distribution and transmission

Copies of products (except polar data) are transmitted from the Compositing-System to the userØs servers over the SMA-WAN. All SMA-users can access this data via an on-line archive (See "On-line products" on page 68.). From this archive an IDL-program allows to display the products on SUN workstations using Solaris 2.x. A version for PC is also available to receive and display the TODAY product.

A dedicated telephone line is accessible to external users employing hardware such as the SAteellite-RAdar-terminal called "SARA". Other solutions have been developed for end-users.

An Ethernet network at the Radar-Site is used to connect the two cpuØs (cpuA and cpuB) of the radar site, a local "Terminal Server" and an Ethernet router for exchanging data/commands to the Compositing-System. The Radar-Site- and the Compositing-Systems are connected by an Ethernet cable on a dedicated 64Kbit/s telephone-line. The "Terminal Server" connects the serial ports of both cpu's and the BITE to the outside world. This allows the operator to control the Radar-Site processors for example by requesting boot-operations.

The cpuB compresses the products and sends them to the Compositing-System. For compatibility with the past, it also sends the un-compressed product TODAY through a slow telephone line (2.4kBaud).

At the compositing centre in Z?rich there are two servers: one is doing the work, the other is operated in standby.

Operational Use of Radar for Precipitation Measurements in Switzerland

The Compositing-System receives products from all the three Radar-Sites and creates composite products as described in Sec.4.2 "Compositing" on page 48. A program monitors all activities between the different systems and attempts to re-activate lost connections with the Radar-Sites.

A redundant 64Kbit/s link between Lema and Locarno helps to develop and improve algorithms and new versions of the Radar-Site programs.

9. Influence of the orography (Held, Kappenberger)

9.1. Questions

In a radar image of an Alpine region two different types of additional influences can be detected, compared do images taken in flat landscapes: 1) our principal interest: the direct physical influence of the Alps on the precipitation process and 2) the influence of the Alps on the radar measurement (clutter, shielding). If artifacts originating from the second point are sufficiently reduced, i.e. if instrumental anomalies (intrinsic deficiencies) are corrected for, then it is much easier to detect the real, meteorological influences of orography on precipitation. We suppose that this "natural" influence *can* be quantified in radar pictures. We tried to answer the following questions:

- What corrections should be applied to radar data before making meteorological investigations such as studying the orographic influence on precipitation?

- 1. - Can we quantify the relations between orography and precipitation such as a height dependence of the rain amount (Blumer and Spiess, 1990) or windward and lee side effects? How well do radar data agree (disagree) with the precipitation distribution shown on the precipitation map in the "Niederschlagskarte der Schweiz" by Kirchhofer and Sevruc (1992)? Can we use the radar data to explain distributions of heavy precipitation in Southern Switzerland as presented by Spinedi (1992)?
- 2. - Where are the possibilities and limitations of the radar as an instrument for nowcasting in an orographically complex area?

9.2. Instrumental and meteorological influence

To what extent can we detect the influence of the orography on precipitation in radar data? When we ask this question, we usually think of the physical, meteorological influence of the orography on the precipitation process. The low spatial resolution of the rain gauges often makes it difficult to study this phenomenon. Here the radar with its spatial resolution of 2km (new generation 1km) holds promise. But before investigating meteorological questions, various corrections have to be applied to the radar data. Following Held (1995, page 38) these are: 1) correction for the influence of the vertical profile of reflectivity combined with reduced visibility caused by geometrical shielding by mountains and earth curvature, 2) elimination of clutter echoes (including the interpolation of weather echoes over the residual holes remaining after clutter elimination), 3) reduction of concentric structures around the radar and caused by the bright band and 4) reducing small scale variability by applying spatial smoothing to all data. To optimize these corrections, the correlation coefficient was used as a criterion for the improvement obtained. Here the correlation was determined between radar data over a set of more than 400 rain gauges with the data of the rain gauges, i.e. an independent set of data at ground-level.

In the old radar data the corrections had to be done off-line, afterwards. This is being implemented to be done in real time in the software of the new generation of radars.

9.3. Corrections

To illustrate the corrections applied to the radar data, we look at an event extending over 48 hours during 7/8 July 1990.

9.3.1. Correction for the visibility

The dependence of the radar precipitation estimates from the visibility (combined with the vertical profile of reflectivity) is a serious problem in this experiment, aimed at determining the influence of the orography on the development of precipitation. Two causes may reduce visibility:

- 1.) At low elevations the elimination of clutter echoes (ground targets) can produce blind zones (a loss of information) and
- 2.) the earth's curvature and mountains may make it impossible for the radar beam to propagate close to the ground.

Therefore, reduced visibility occurs in areas behind and even above mountains (caused by ground clutter received via side lobes of the antenna) or in areas far away from the radar (i.e. are only visible above a given height). Since in precipitation the reflectivity is not constant with height, the measurement aloft must be corrected to estimate the rain rate at the ground. A representative vertical profile of reflectivity is therefore needed, which is found by optimizing the correlation between the radar data (corrected with a wide variety of vertical reflectivity profiles) and all available rain gauges. After applying the regression - in our case individually to every rain event -, the profile leading to the lowest residual and fractional standard deviation is defined as the "best" profile. Using this profile and knowing the visibility, we can extrapolate the estimated rain rate to the ground multiplying the radar-based estimate of ground-level precipitation with the corresponding correction factor. Correcting the radar data with the best profile raises the correlation coefficient $c^2_{R,G}$ between radar and gauges from 0.12 to 0.18.

9.3.2. Interpolation

As a second correction, the radar data of pixels seen only above 4500m were interpolated with those neighboring pixels which are visible below 4500 m (i.e. clutter free *and* geometrically visible by at least one radar station). Again, the threshold of 4500m was found by looking for the best correlation between radar and gauges. The interpolation goes from east to west and was only applied if not more than 10 pixels (20km) next to one another had to be interpolated. With this correction the correlation coefficient $c^2_{R,G}$ between radar and gauges rose from 0.18 to 0.21.

9.3.3. Corrections for the bright band

To reduce the influence of the bright band, a correction has been applied to eliminate concentric structures around the radar at Albis. This correction is based on the assumption that in nature there are no natural concentric echo structures around a radar station, "the rain should not know that there is a radar". The rain amount averaged over azimuth is smoothed over distance. With this correction $c^2_{R,G}$ is increased e.g. from 0.21 to 0.27.

9.3.4. Smoothing

As a last step in the correction procedure we investigated the influence of smoothing the rain estimates. Smoothing means to substitute every pixel by the mean value of

surrounding pixels in a box of a certain size. Smoothing reduces the clutter problem (small patches of too little or too much precipitation), eliminates small scale structures (often artifacts) and mitigates errors caused by the horizontal drift of precipitation in the wind. E.g. a drift $d = 6.6\text{km}$ ($d = (hc \cdot u)/vf$) can be expected for a raindrop falling at a speed of $vf = 3\text{m/s}$ through a cloud of depth $hc = 2\text{km}$, wind of speed $u = 10\text{m/s}$.

In our example 7/8 July 1990 we achieved the lowest residual, fractional standard deviation after smoothing radar data over a box of $22 \times 22\text{km}^2$ (11×11 pixels, 1 pixel = $2 \times 2\text{km}^2$). $c^2_{R,G}$ went from 0.27 to 0.32

9.4. Results

The four corrections mentioned above were applied off-line to ten storm-events. The corrections increase the square of the correlation coefficient $c^2_{R,G}$ between rain amounts estimated by the radar and 470 rain gauges from 0.12 to 0.32. *This result is significant and shows the importance of the corrections. The improvement caused by the corrections is bigger for cases with a higher uncorrected correlation. It confirms the trivial rule that a correction is more effective, if the quality of the raw data is intrinsically good.*

To study the influence of the orography on estimated rain amounts a multiple regression was applied to the corrected precipitation estimates R_c (dependent variable): $R_c = k_1 \cdot h + k_2 \cdot vv + k_3 \cdot vvl$, where h is the elevation above sea level, vv the small scale vertical velocity⁽¹⁾ (averaged over $18 \times 18 \text{ km}^2$), vvl the large scale vertical velocity (averaged over $80 \times 80 \text{ km}^2$). The regression allows to quantify the influence of the terrain on the rain rate recorded in radar pictures.

As an order of magnitude (Held, 1995, page 84), of the total variance of the corrected rain rates (100%) in the radar picture we can explain a variance of:

- 1 - 10% due to terrain elevation, with a vertical gradient of 4mm/km ,
- 2 - 14% due to small scale wind exposure, with an increase of 3mm per ms^{-1}
- 3 - vertical wind speed (averaged over $18 \times 18 \text{ km}^2$),
- 4 - 31% due to large scale wind exposure, with a change of 72mm per ms^{-1} vertical wind speed (averaged over $80 \times 80 \text{ km}^2$).

(1) The vertical velocity is defined as the scalar product of the 2-dimensional average wind vector and the vector describing slope orientation and steepness. The vertical velocity is maximal, when the wind blows parallel to the slope orientation (e.g. a southerly wind blowing towards a south-exposed slope), therefore accounting for windward / lee side effects. This formulation reflects the assumption that topography deflects the air streaming over it vertically but without horizontal channelling.

The combination of all three variables together can explain, on the average, 44% of the variance of the accumulated precipitation field. It is reasonable that we cannot explain 100%, because meteorological influences such as the mesoscale situation causing part of the distribution of echoes is not considered at all in this exercise. The 12 case studies considered consisted in

single events, which produced of the order of 100mm of rain per case and had a duration of 24 hours. More details on this first step of trying to understand the influence of the orography are given (in German) in the thesis of Held (1995) and in an earlier, shorter, English version by Held and Joss (1994).

To answer the three questions raised in Sec. 8.1:

1 - Which corrections should be applied: We definitely gain much by applying the corrections described in Sec.8.3 "Corrections" on page 86. Actually we expect even better results, if we eliminate the clutter determining the profile in real-time, in spite of the fact of having additional variability in space and time. An important task will be to find the optimum averaging scales to obtain representative values in a reasonable range in time and space.

2 - Orography and rain amount: The influence of the orography can be quantified, but the phenomena are rather complicated and have received different weights in the ten case-studies analyzed. Certainly not only the absolute altitude of a site or pixel determines its influence on the rain amount but also the slope steepness and the wind in the weather system, accounted for in vv and vvl. When comparing these results to precipitation maps (Kirchhofer W. and B. Sevruk, 1992), we should remember that such maps reflect averages over many years, therefore reflecting a much more representative sample regarding weather situations (with varying wind speed and direction). The results presented in this chapter, in contrast, are restricted to a few case studies. They are a useful first step towards a deeper understanding of fundamental principles influencing precipitation distribution patterns. They could become helpful in the future for a better comprehension of the mechanisms leading to heavy precipitations as discussed by Spinedi (1992), as well as - after appropriate averaging over a large number of different situations - to maps as anticipated by Kirchhofer W. and B. Sevruk, 1992. We should also further investigate the influences of orographic conditions encountered by an air mass on its way to the site under consideration, as well as the water content of the advected air mass.

3 - Nowcasting: A small first step has been made in showing how to use radar data, both for understanding orographic influences and interpreting radar images in real time (Held, E. 1995). But more has to be done, before we can use radar for nowcasting in an optimal way. Using a variational method as described in Kitchen (1994) may further reduce the bias at longer range; to what extent automation for nowcasting used in NIMROD (e.g. Harrison et al., 1995) can be improved by object-oriented procedure as proposed by Collier et al. (1995) for the GANDOLF system, needs more experience.

9.5. Alpine precipitation, past records (*Kappenberger*)

A final aim of the radar work described in this book is to better understand the mechanism of precipitation over and its distribution in the Alpine region. At present, radar is only starting to be quantitative: therefore, maps of the kind presented in Figure 8.1 on page 90 based on radar are still "future music".

Two precipitation maps of Baumgartner et al, 1983 from the East-Alps and the West-Alps (scale 1:500'000) were analyzed and summarized in Figure 8.1. The work of Baumgartner et al. is based on an extensive data base and on many references. A significant advantage of this work lies in the over-all check of the data using the equation of the water balance. This advantage

compensates the fact that the data relies not on the most recent interval, but is based on the period 1931-1960.

Figure 8.1 shows precipitation yearly amounts in cm depth. A thick line indicates 120cm and areas of over 240cm are hatched. The Swiss National Coordinates are indicated on the border of the map.

An effort to compare this map with several existing maps was done based on precipitation profiles across the Alps. Various sources of error influence such a comparison and lead to a rather qualitative comparison. Among them are differences in the time period over which the data were collected, effects of quantization by using isolines of precipitation as well as limitations caused by reading the data from graphical information.

Comparison with four publications referring to the whole Alpine area or part of it:

1 - Niederschlagskarte aus dem Atlas der Schweiz (1901 - 1940) von Uttinger, 1966 (Schweiz und umgrenzende Gebiete). Agreement within 5%.

2 - Niederschlagskarte aus dem Klimaatlas der Schweiz (1931 - 1970) von Defila/Kirchhofer, 1984 (Schweiz ohne umgrenzende Gebiete). Similar to (1), Uttinger shows rather smaller values.

3 - Korrigierte Niederschlagskarte aus dem Hydrologischen Atlas der Schweiz (1951 - 1980) von Sevruck/Kirchhofer, 1992 (Schweiz ohne umgrenzende Gebiete). With increasing altitude this map shows higher values: 10% in the flat part, 25% in the higher Alps.

4 - Karte Frei/SchSr 1997, (gesamter Alpenraum, fYr die Zeitperiode 1971 - 1990). In a profile Lugano-ZYrich it shows ca. 10 to 20% less precipitation.

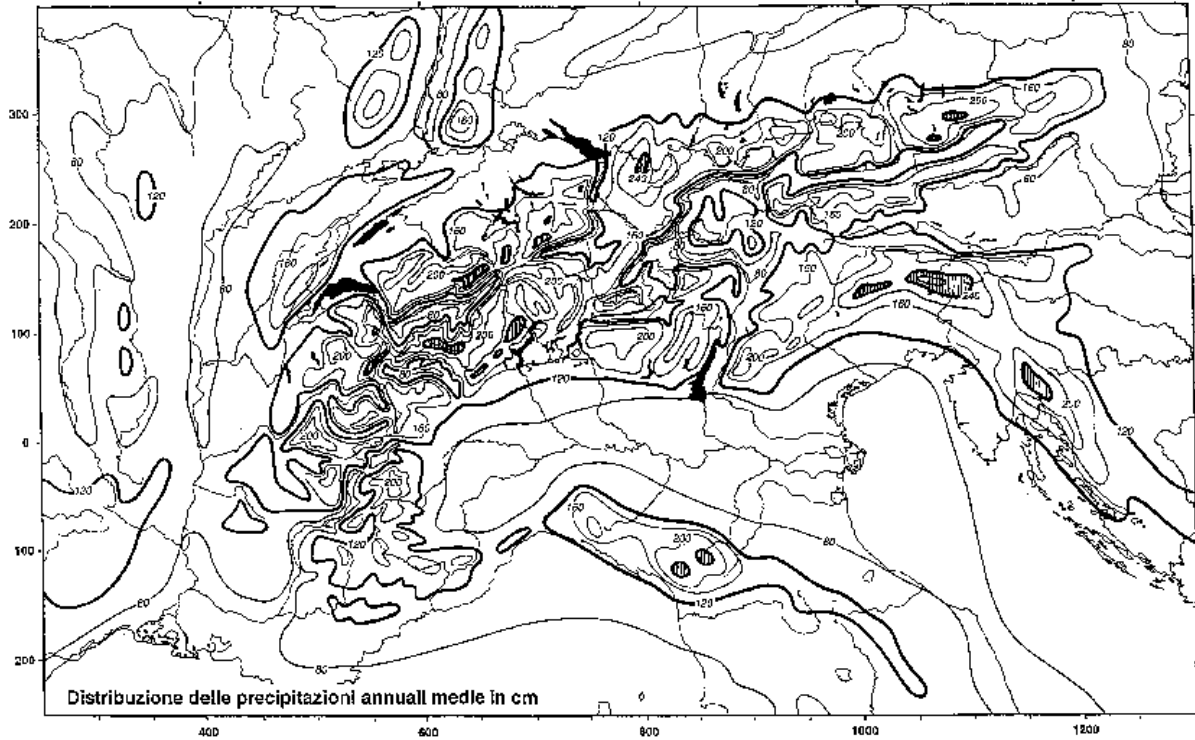
5 - Regionalkarte des Friuli, vom Centro Studi Agricoli (CSA), Cervignago von A. Cicogna, in Bearbeitung (Jahre 1961-1990). This map shows ~5% less precipitation.

6 - Regionalkarte des Piemonte, aus einer Arbeit der Regione Piemonte: "Relazione sullo Stato dell'Ambiente" 1995, (Jahre 1920-1980). This map shows ~10% less precipitation.

7 - Regionalkarte "Ticino e Mesolcina" aus einer Arbeit von Spinedi, 1991 (Jahre 1961-1990). This map shows ~15% less precipitation, especially at Alpine crests.

8 - Niederschlagskarte des hintern Glarnerlands (BeitrSge der Hydrologie der Schweiz Nr. 36) von MYller-Lemans et al. 1997. Rather good agreement.

Figure 8.1: Annual depth of Alpine precipitation in [cm], average: years 1931-1960.



10. Wind induced error of precipitation gauges (Nespor)

10.1. Introduction

Gauges are often used as ground-truth reference for radar precipitation estimates. But how true are they? In this chapter investigations of the wind-induced error of measurements for rain and snow, which were made with Hellmann and ASTA precipitation gauges, used in Switzerland, are discussed.

Measurements by precipitation gauges are subject to systematic errors, the most important sources of which are:

1. the deviation of precipitation particles due to wind field deformation around the gauge (wind-induced error),
2. losses caused by wetting of the inner walls of the gauge,
3. evaporation of water accumulated in the gauge container, and
4. splashing of rain drops or blowing of snow flakes out or into the gauge.

The most important component of the systematic errors is the first mentioned error due to wind field deformations (see e.g. Sevruk, 1989), described hereafter.

The strong effect of turbulence can be explained by the air flow around the gauge. This flow is divided into the internal recirculating flow inside the gauge collector, and the external main flow around the gauge. These two flows are separated by a thin layer above the gauge opening. Due to a blocking effect of the gauge, the external air flow is deviated around the gauge and is accelerated. The strongest production of turbulence above the gauge occurs in the shear layer along the separation between the internal and external flows. In the present computation the major effect of the turbulence on the particle motion is to increase its drag (see e.g. Hinze, 1975). Therefore, particles tend to follow the flow more closely in the turbulent regions above and inside the gauge.

The effort needed to estimate wind-induced error of solid precipitation particles is larger than for water drops, because ice crystals and snow flakes are very variable in size and shape. This variety leads to significantly different drag coefficients and density (terminal velocities of free fall) which, therefore, leads to different partial wind-induced error. In general, the terminal velocities of solid precipitation particles are much smaller than those of water drops, resulting in larger wind-induced errors.

In the present work the influence of turbulence on the particle movement was taken into account (Nespor, 1997). The results for rain- and snowfall (snow flakes) allow the determination of the 'true' precipitation intensity (eq.(9.1)) from the known measured intensity, wind speed and type of particle size distribution. The computational results agree well wind-induced errors estimated from field measurements.

10.2. Assumptions

10.2.1. Concept

All computations discussed in this chapter are based on Nespor (1996). In this approach the computation of wind-induced error is divided into the following three steps:

1 - computation of the turbulent flow field around the precipitation gauge using a commercial software package for fluid dynamics (PHOENICS model),

2 - simulation of precipitation particle movement in the computed flow field (determination of the *partial wind-induced error* as a function of the free-stream wind velocity and particle diameter),

3 - integration of partial wind-induced errors over particle size distribution (determination of the *integral wind-induced error* as a function of the free-stream wind velocity, precipitation intensity and parameters of the particle size distribution).

The computations and the subsequent error estimations are based on the following assumptions:

4 - the motion of particles does not affect the air flow, therefore the air flow and the particle motion can be computed separately,

5 - the moving particles do not influence each other, therefore their trajectories can be simulated individually.

Flow fields and particle trajectories were calculated for the properties of air, summarized in TABLE 9.1, and the density of water $\rho_w = 999.84 \text{ kg m}^{-3}$. The free-stream turbulence was characterized by the turbulent kinematic viscosity, assumed to be equal to the kinematic viscosity of the air. To simulate the influence of a distorted wind field and of turbulence on the trajectories of falling particles the k-e turbulence model was used (see Nespor, 1996).

TABLE 9.1 : Properties of the air used in the present computations

Temperature	Pressure	Relative humidity	Density	Dynamic viscosity	Kinematic viscosity
[-C]	[kPa]	[%]	[kg m^{-3}]	[$\text{kg m}^{-1} \text{ s}^{-1}$]	[$\text{m}^2 \text{ s}^{-1}$]
0	101.325	50	1.292	1.718×10^{-5}	1.329×10^{-5}

10.2.2. Properties of snow crystals and snow flakes

In the case of liquid particles (water drops) the distribution of shape, size and terminal velocities are well known. In the case of solid precipitation, the situation is more complicated. In general, the properties of snow crystals depend on meteorological conditions (e.g. humidity, temperature). There is a large variety of natural snow crystals and their classification can be found in Magono and Lee (1966). One of the most complete

descriptions of snow crystal shape properties, relevant to their trajectories, is given by Heymsfield and Kajikawa (1987).

Muramoto et al. (1996) made an interesting study on the size and fall velocity of snow flakes by image processing technique. Their results are based on measurements of a snowfall event lasting 7.5 hours. Although they reported neither the type of snow flakes, nor the detailed structure of snowfall, they measured the density and size distribution of snow flakes. The last two parameters together with the fall velocity are essential for the determination of the precipitation intensity. Their results are in a good agreement with the results of Barthazy et al. (1996), whose measurements were made in real precipitation with a well developed stratiform structure. In addition, the measured data of Muramoto et al. (1996) agree well with the typical range of terminal velocities and densities of snow particles (e.g. Locatelli and Hobbs, 1974; Hobbs, 1974; Goodison and Metcalfe, 1981; Sevruk, 1985). Therefore, the terminal velocities and particle size distribution of Muramoto et al. (1996) seem to be quite representative for an average snowfall.

The summary of measured properties of selected planar crystals, graupel and snow flakes are presented in TABLE 9.2. These data together with empirical relations between the particle mass, particle terminal velocity and particle diameter were used to evaluate partial wind-induced errors in Nespor, 1997.

TABLE 9.2 : Summary of measured particle data according to Heymsfield and Kajikawa (1987) (ice crystals) and Muramoto et al. (1996) (snow flakes). In the table the particle description code is according to Magono and Lee (1966), T is the air temperature, D is the particle diameter, m is the particle mass, wT is the particle terminal velocity, and ρ_p is the particle density.

Description	T	D	m	wT	ρ_p
	[-C]	x10-3[m]	x10-6[kg]	[m s ⁻¹]	[kg m ⁻³]
Dendrite	---	0.6 - 5.3	0.0007 - 0.108	0.13 - 0.43	20 - 100
rimmed stellar	---	0.7 - 5.3	0.0020 - 0.539	0.19 - 0.72	50 - 150
densely rimmed stellar	---	1.1 - 4.7	0.0310 - 0.905	0.43 - 1.43	100 - 130
lump graupel	≥ 0.5	0.5 - 4.7	0.0390 - 17.200	0.70 - 4.40	210 - 630
	< 0.5	0.5 - 9.0	0.0140 - 68.000	0.47 - 4.65	89 - 350
conical graupel	≥ 0.5	1.1 - 7.5	0.1650 - 110.000	1.07 - 5.70	210 - 630
	< 0.5	0.8 - 8.6	0.0580 - 53.700	0.64 - 4.08	89 - 350
snow flakes	---	0.5 - 15.0	0.0019 - 12.740	0.43 - 1.51	48 - 190

10.2.3. Particle size distribution

The particle size distribution is very important to determine snowfall intensity and estimate the integral wind-induced error. Because of the large variety of solid precipitation particle types occurring in real precipitation events, and because of difficulties with measurements, the information about solid particle size distributions in literature is rare. Our calculations are based on the particle size distribution of snow flakes presented in Muramoto et al. (1996), whose measurements were made during a snowfall event lasting 7.5 hours. Their size distribution was fitted by the gamma

distribution, and the result was used to find wind-induced errors for the Hellmann and ASTA gauges in the present study.

10.3. Results

10.3.1. Liquid precipitation particles

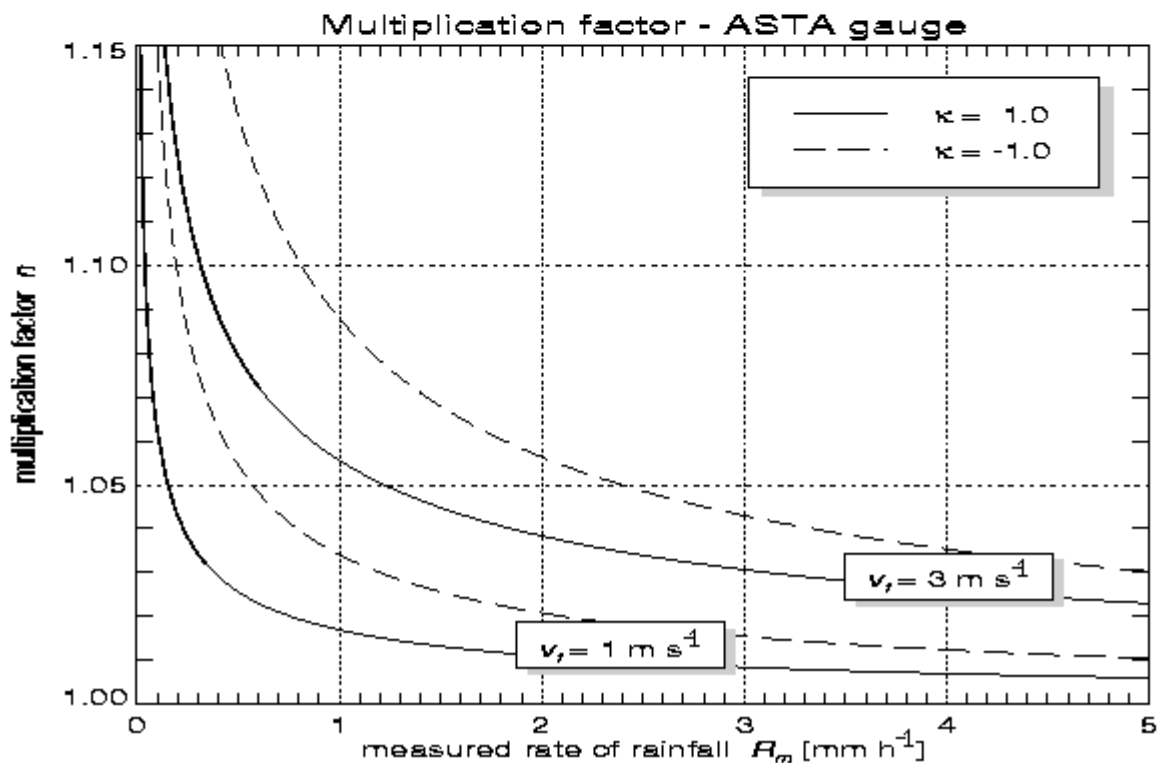
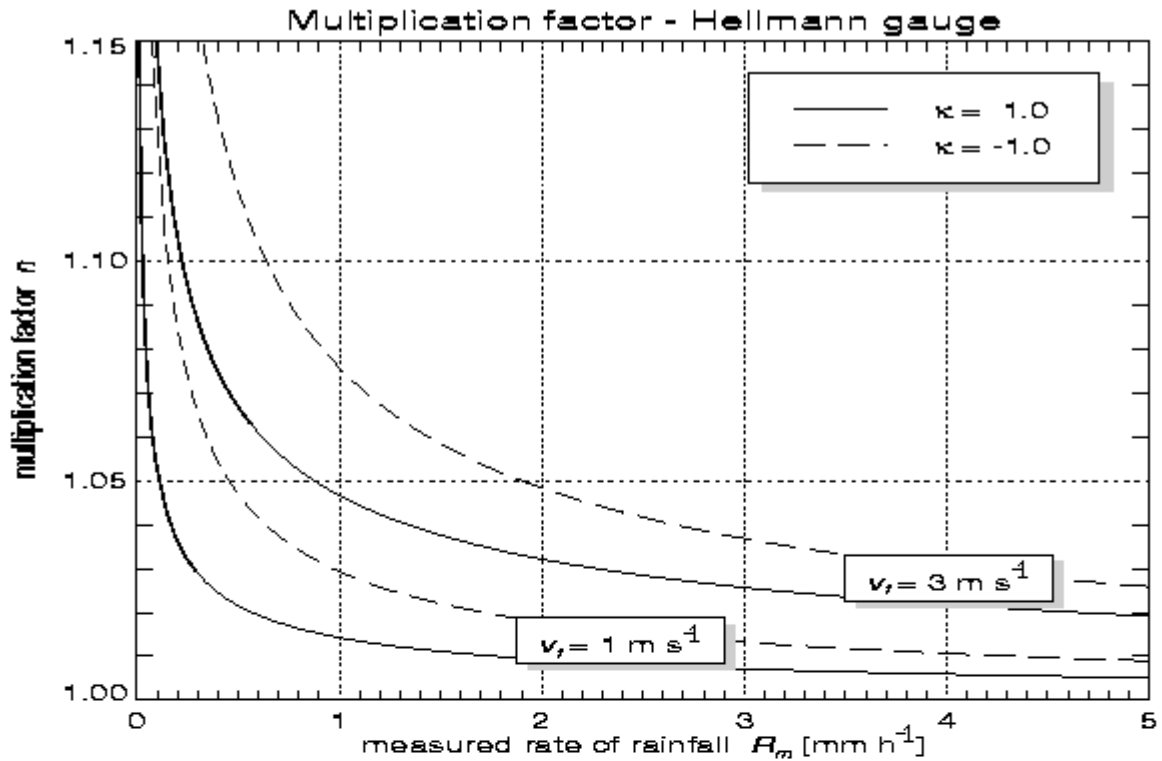
For Hellmann and ASTA precipitation gauges flow fields were computed for the free-stream velocities ranging between $v_f = 0.5$ and 12 m s^{-1} . In the case of rain drops minor modifications were made in the source code for particle trajectory computation (model PHOENICS, see "9.2 Assumptions") in order to include the influence of turbulence on the particle motion. Computations of partial wind-induced errors and the subsequent integration over the drop size distribution resulted in the integral wind-induced error as a function of rainfall intensity R , the free-stream wind speed and the parameter k in the Ulbrich drop size distribution (Ulbrich, 1983, eq.(9.2)). The results showed that the error increases with increasing wind speed. Moreover, smaller rain rates and cases with lower parameters k have a larger contribution from small drops to the precipitation amount and, therefore, larger wind-induced errors (see Nespor, 1996, 1997).

For practical use it is convenient to express the rainfall rate as

$$R = n \cdot R_m \quad (9.1)$$

where R_m is the rate of rainfall measured by the gauge, n is the multiplication factor and R is the true rain rate, intended as the desired precipitation flux across a large area, i.e. without boundary effects caused by the instrument. The integral wind-induced errors are presented in Figure 9.1. It can be used to correct the measured rain rates (amounts) if k and v_f are known.

Comparing the multiplication factors of the two gauge types (Figure 9.1) shows slightly larger values for the ASTA gauge, indicating a lower efficiency of the ASTA compared to the Hellmann gauge. This is probably caused by the different constructions: although the Hellmann and ASTA gauges have the same orifice area, the body of the ASTA gauge has a larger outer diameter because of the heating and, therefore, introduces the larger disturbance to the air flow.



: The multiplication factor n in eq.(9.1) of the Hellmann (top) and ASTA (bottom) precipitation gauges is plotted as a function of the measured rate R_m . The multiplication factors were derived from the computed integral wind-induced errors. The drop size parameter $k = -1$ in eq.(9.2) is

typical for orographic rain (with a larger fraction of smaller drops), and $k = 1$ for a thunderstorm rain (with a larger fraction of larger drops, parametrization described by Ulbrich, 1983).

10.3.2. Results for solid precipitation particles

In contrast to water drops, ice crystals and snow flakes have a larger variety of forms and densities. Therefore, large modifications in the calculation of trajectories (see "9.2.1 Concept") were necessary. In the first step the partial wind-induced errors were evaluated. Again, the computations were concentrated on the Hellmann and ASTA precipitation gauges, and on those solid particles for which information about the particle shape, density (or mass), and terminal velocity was completely available (Heymsfield and Kajikawa, 1987; Muramoto et al., 1996).

The results for various ice crystals produced larger multiplication factors than rain drops. Generally, for lower terminal velocities, the partial wind-induced error is also larger. Lighter dendrites cause higher errors: less than 20% of the particles were caught by gauges for $v_f = 1.0$ m s⁻¹, while the heavier lump graupels produced much smaller errors (Nespor, 1997).

A snowfall event can contain a variety of different types of ice crystals and snow flakes, determined to a great extent by the prevailing conditions at the location of particle generation, and by the layers of the atmosphere through which the particles pass on their way to the ground. This extreme variability introduces large insecurities, both to measurements of snowfall and to modelling studies, as has already been mentioned above ("9.2.2 Properties of snow crystals and snow flakes"). The results presented here for snow are therefore less reliable than those in the previous section for rain.

The partial wind induced error for different diameters of snow flakes (Muramoto et al., 1996) was evaluated for wind velocities $v_f = 0.5, 1.0, 1.5, 2.0$ and 3.0 m s⁻¹. The computed values of partial wind-induced error were fitted to a gamma probability density function (see Nespor, 1996).

In the Ulbrich drop size distribution (eq.(9.2)) parameter k determines the type of rain. The only parameter that depends on the rate of rainfall is L (Ulbrich, 1983).

$$N(D) = N_0 \cdot D^k \cdot \exp(-\Lambda D) \quad (9.2)$$

In the present computations we assumed that this type of distribution found in rain is valid also for the size distribution of snow flakes and that the values of L varied between 350 and 1400[m⁻¹]. This corresponds to R between approximately 8.6 and 0.03 mm h⁻¹.

Similarly to water drops the integral wind-induced error for snow flakes increases with increasing wind velocity and decreasing snowfall intensity, but for R between 1 and 5 mm h⁻¹ the increase of the error is lower compared to water drops. In general, the errors for snow flakes are 5 to 10 times larger than the errors for water drops (Nespor, 1997). Figure 9.2 shows the multiplication factor n as a function of the measured rate of snowfall R_m and wind velocity v_f . The true rate of snowfall R is then obtained from the eq.(9.1). Similarly to rain the ASTA gauge have a larger wind-induced error (larger n values) than the Hellmann gauge.

10.4. Comparison with measurements

10.4.1. Rainfall

The comparison of computational results and field measurements of wind-induced error of rainfall in Figure 9.3 is based on the study of Sevruk (1989). In this study the wind-induced error is estimated from paired measurements: comparison of the results of a Hellmann gauge elevated to 1.5 m above the ground with those of a Hellmann gauge at ground level. The estimates were based on the 10-year data recorded in Les Avants (Switzerland). Precipitation data were divided into classes according to rain rate and wind speed at the gauge orifice (see Sevruk, 1989). The error is expressed as the difference between the gauge amounts at ground level minus the elevated one divided by the ground level amount. Figure 9.3 shows computed and measured wind-induced errors for average wind speeds of 2.5 and 3.5 m s⁻¹. The curves in each figure indicate the expected boundaries for the measurements. They were computed for the parameter $k = -1$ and a free-stream velocity (v_f) which is 0.5 m s⁻¹ larger than the corresponding wind speed class average, and for the parameter $k = 1$ and a free-stream velocity 0.5 m s⁻¹ smaller than the corresponding wind speed class average. Although the measured data are based on averages and a closer information about the type of precipitation (drop size distributions) was not available, they agree quite well with values derived from computations.

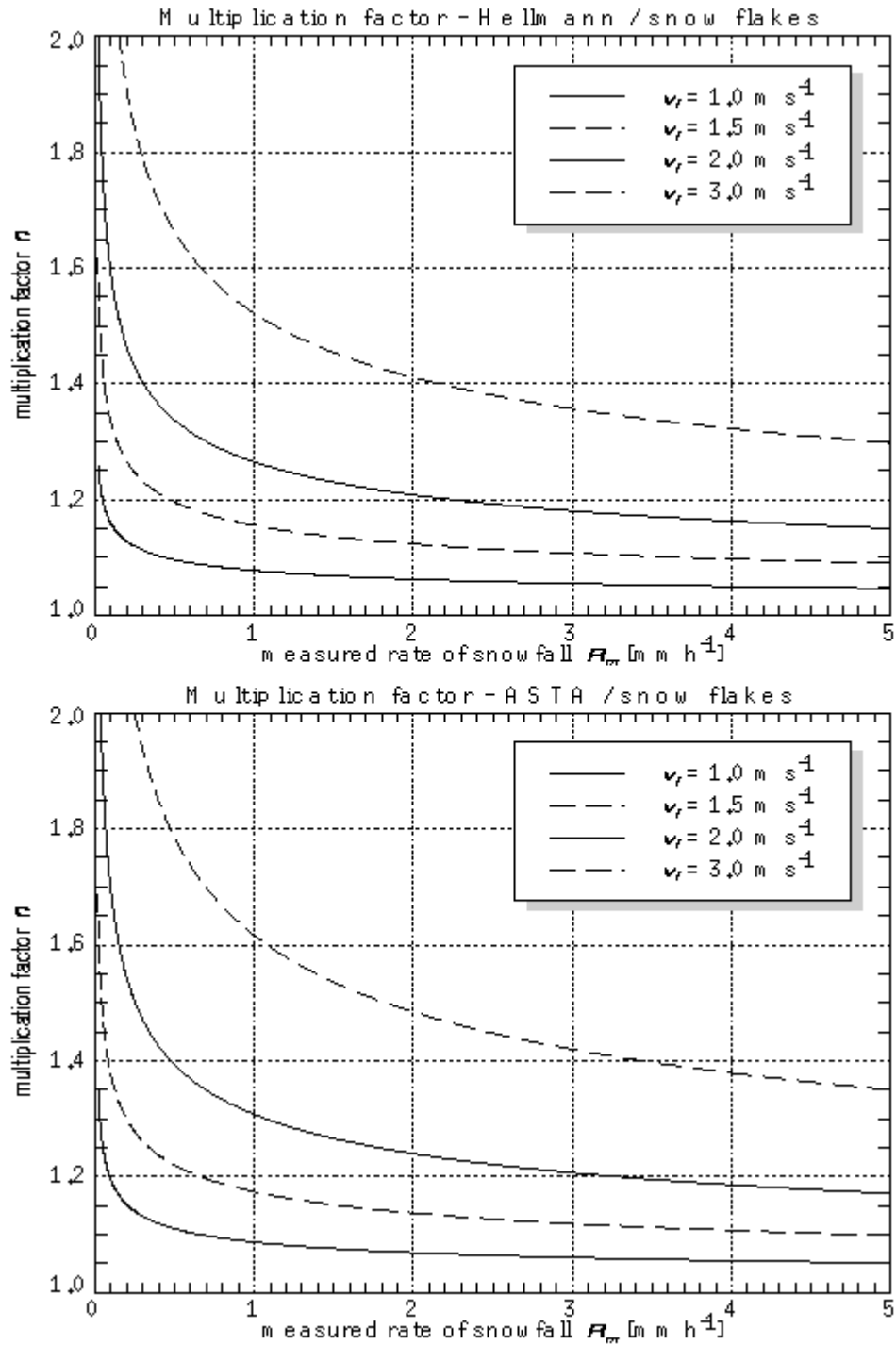


Figure 9.2: The multiplication factor n in eq.(9.1) of the Hellmann (top) and ASTA (bottom) precipitation gauges is plotted as a function of the measured rate of snowfall R_m the multiplication factors were derived from the computed integral wind-induced errors.

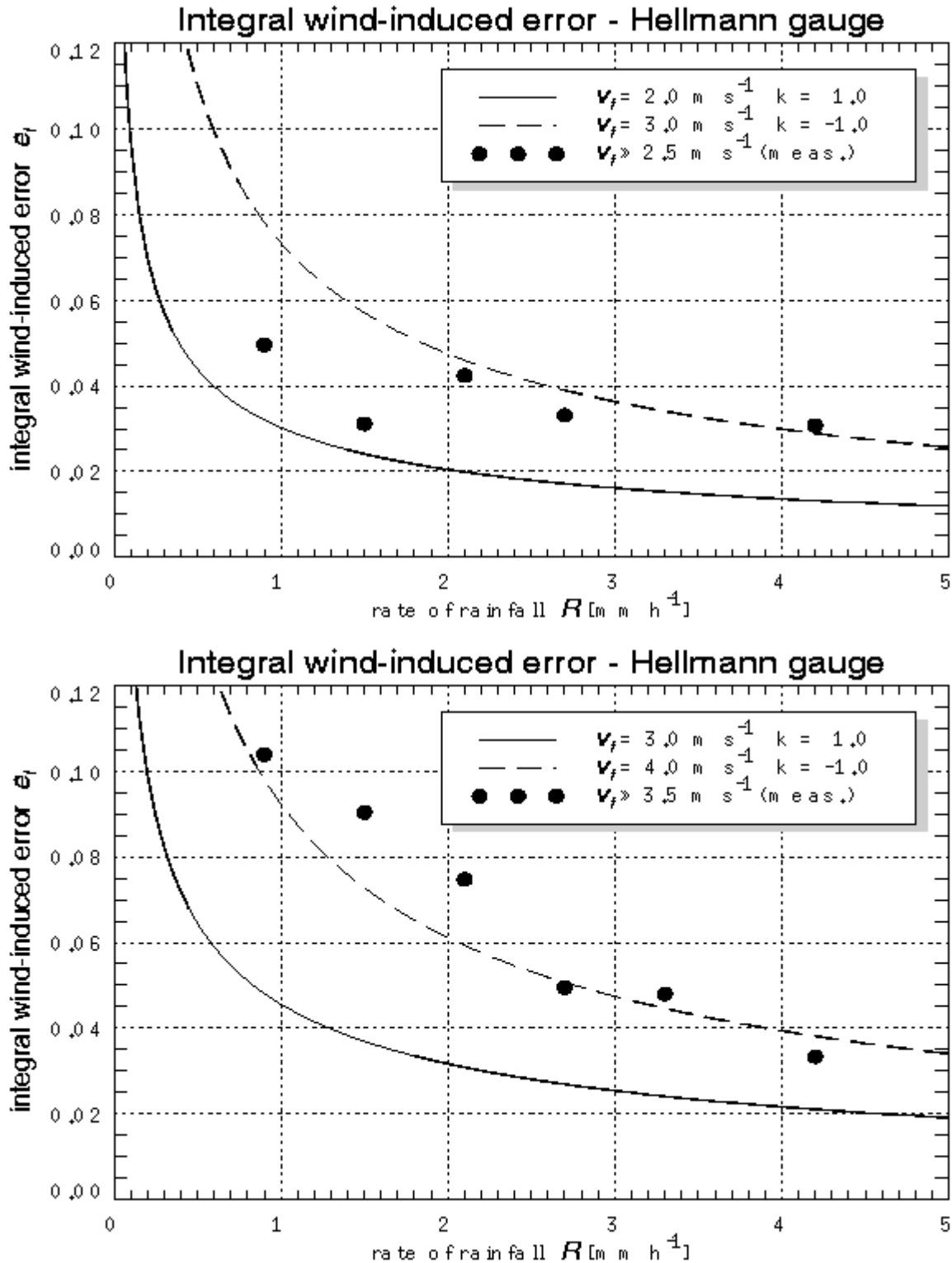


Figure 9.3: Computed integral wind-induced error of rainfall and values estimated from measurements (Sevruk, 1989). The measured values (points) are class averages of several rainfall events for the free-stream velocity of $v_f = 2.5$ m s⁻¹ (top) and $v_f = 3.5$ m s⁻¹ (bottom). The curves represent approximate boundaries for the parameter $k = -1$ and the free-stream

velocity 0.5 m s⁻¹ larger than the measured class average (dashed line), and for the parameter $k = 1$ and the free-stream velocity 0.5 m s⁻¹ smaller than the measured class average (solid line)

10.4.2. Snowfall

In the case of snowfall the present comparison of computed errors and field measurements is based on the study of Guenther (1993), a part of the WMO solid precipitation intercomparison project (e.g. WMO/CIMO, 1996). The wind-induced error was obtained from the difference between the Hellmann precipitation gauge elevated 1.0 m above the ground, and the reference measurement by the Double Fence Intercomparison Reference (DFIR) (see e.g. Yang et al., 1994). The original snowfall data measured in the period 1986-1993 in Herzgerode (Germany) were subdivided according to air temperature and fitted by lines. The solid line in Figure 9.4 represents the resulting fit for the air temperature of 0- C. The points are computed integral errors for the snowfall intensity of 0.5 and 1.0 mm h⁻¹, respectively. Although snowfall intensities of measurements were not published, it can be expected that they were mostly between 0.5 and 1.0 mm h⁻¹. For example, Maurer (1993) reported the mean snowfall intensity of approximately 0.8 mm h⁻¹ for 56 precipitation events in the period of two years. Therefore, the intercomparison in Figure 9.4 shows good agreement between computations and field measurements.

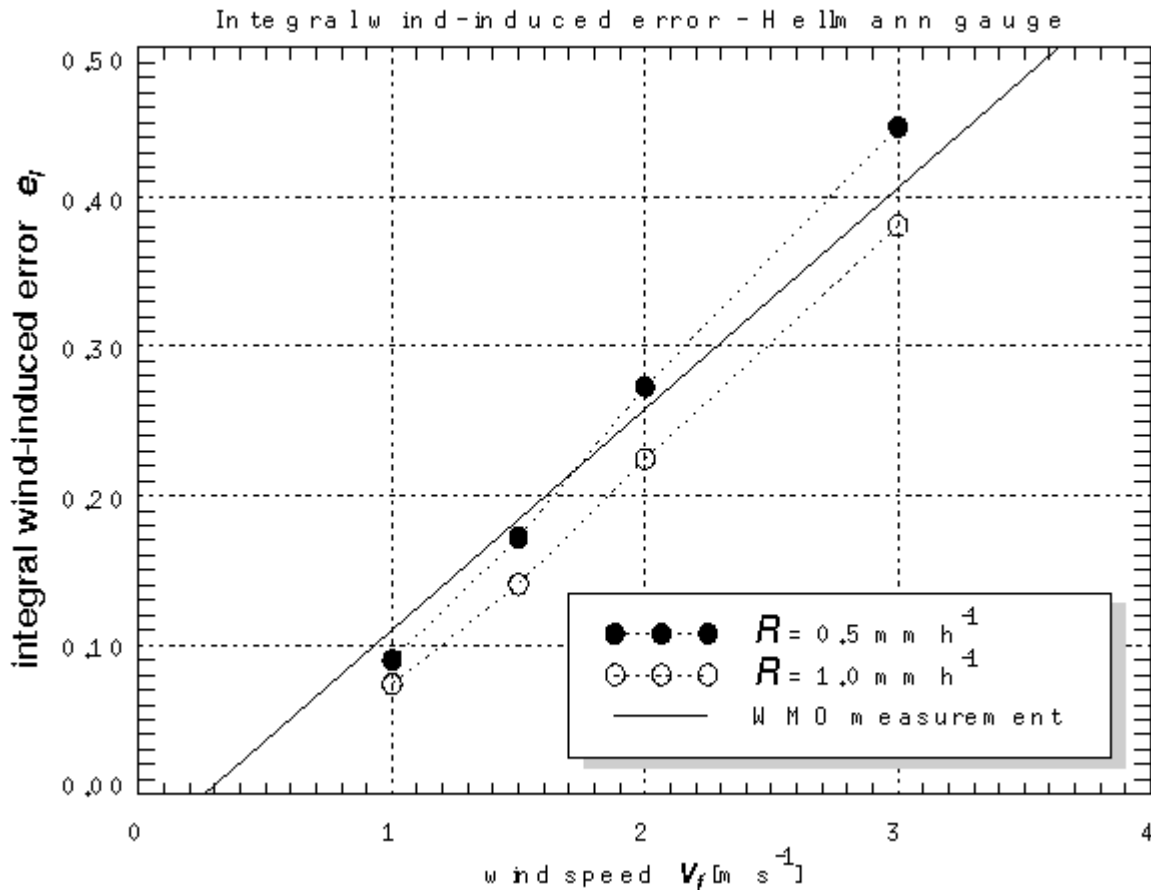


Figure 9.4: Comparison of the computed wind-induced error of snowfall and results based on

measurements (WMO, Guenther, 1993). The solid line approximates the measured data for the air temperature of 0- C, the points represent computed values of integral wind-induced error for the snowfall intensity of 0.5 mm h-1 (filled points) and 1.0 mm h-1 (empty points).

10.5. Conclusions

The present study uses a further numerical simulation to find the wind-induced error of precipitation measurements. The comparison of computed results with error estimates based on field measurements shows good agreement. The computational results can be used to correct measured precipitation amounts if the input parameters are known. The results are presented in the form of a multiplication factor as a function of the measured rate of precipitation and wind speed (Figure 9.1 and Figure 9.2). The computations of the wind-induced errors in snow were based on one well documented precipitation event. As discussed in Sec.9.3.2 "Results for solid precipitation particles" on page 96, the measured parameters (the range of densities and terminal velocities of the snow flakes, and the particle size distribution) are quite representative for an average snowfall. Therefore, the diagrams can be used more generally.

The numerical simulation confirmed that there are differences between precipitation gauges. In general, the ASTA precipitation gauge shows slightly higher wind-induced errors than the Hellmann gauge (higher multiplication factors n in eq.(9.1)). This is caused by the larger flow disturbance introduced by the ASTA gauge body containing the heating elements. Furthermore, the computations confirmed that the wind-induced errors depend strongly on the free-stream velocity at the level of the gauge orifice, and on the weight and shape of precipitation particles. For the same free-stream velocity the lighter snow flakes show an integral wind-induced error 5 to 10 times larger than water drops. There are also differences between various snow crystals, the lighter crystals exhibit a higher wind-induced error.

Limitations of the presented procedure are caused by the fact that the input parameters such as the wind speed at the gauge orifice, the precipitation rate and particle sizes are not known. There would be a possibility to eliminate this uncertainty partially by replacing the input parameters by some representative averages. But to do that, further investigations on real precipitation events are needed. Little is known yet about the size distribution of particles and its variation with time, especially in the case of snowfall.

The presented procedure to estimate errors can also be used to check the performance of existing precipitation gauges, to improve the shape of precipitation gauges, to investigate the influence of different wind shields, and to develop and verify new correction procedures. Last but not least, the results are essential for the interpretation of radar-gauge comparisons.

11. References

11.1. General References

Andrieu H., G. Delrieu and J.D. Creutin 1995: Identification of vertical profiles of radar reflectivities for hydrological applications using an inverse method: part 1 and 2 - Sensitivity analyses and case study. *J. Appl. Meteor.* 1/95, 225-259.

Atlas D., F. Marks, C. Ulbrich, P. Willies, R. Black and C. Samsury, 1996 : Tropical rain, microphysics and radar properties. submitted to *J. Appl. Meteor.* in April 1996.

Barthazy, E., W. Henrich and A. Waldvogel 1996 : Size distribution of hydrometeors through the melting layer. In: 12th International Conference on Clouds and Precipitation, volume 1, pages 162-165, Zurich, Switzerland.

Baumgartner, A., E.Reichel, E.Weber and G.Weber. 1983: *Der Wasserhaushalt der Alpen*. Verlag Oldenburg, 343 pages.

Blumer F. and R. Spiess, 1990 : Investigation on altitudinal dependence of precipitation in the Swiss Alps, in: *Tagungsbericht zur 21. Internationalen Tagung f'r Alpine Meteorologie*, Engelberg, September 1990, pp 415-418

B.,sch, R. 1993 : *Modellierung von Niederschlagsverlagerungen mit Radardaten*. Geoprocessing Serie of the Geographical Institute of the University Zurich, Vol. 21, Zurich, Switzerland, 134pp.

B'rgi, Th. and B. Sch.,dler 1996 : *GENIRA: Gebietsniederschlag mit Radar*. Technischer Bericht 1996/ 1-60, Bundesamt f'r Umwelt, Wald und Landschaft, 60 Seiten.

Collier, C.G., P.J.Hardaker and C.E.Pierce 1995 : *The GANDOLF System: an automated system for forecasting precipitation*. Preprints 27th Int. Conf. Radar Met. 9-13 October 1995, Vail, Colorado, Amer.Meteor.Soc. pp 606-608.

Collier, C.G., 1996 : *Applications of weather radar systems. A Guide to users of radar data in meteorology and hydrology*. Ellis Horwood Limited Publisher, Chinchester. pp 390, second edition.

Della Bruna, G., J. Joss and R. Lee, 1995 : Automatic calibration and verification of the accuracy of radar for precipitation estimates. Preprints 27th Int. Conf. Radar Met. 9-13 October 1995, Vail, Colorado, Amer. Meteor. Soc., pp 653-655, also COST WD/75/75A.

Delrieu G., S. Caoudal and J.D. Creutin, 1997 : Feasibility of using mountain return for the correction of ground-based X-band weather radar data. Accepted for publication in *J. Appl. Ocean. Techn.*, 30.10.96.

Diviak M., and J. Rakovec, 1995 : *Radar measurements of precipitation: the use of vertical reflectivity profiles*. Final rep. COST 75 /WD/69, ERBCIPECTT-926082, 47 pp.

Doelling I.G., J. Joss and J. Riedl 1996 : Systematic variations of raindrop size distributions measured in northern Germany during 7 years, 12th International Conference on Clouds and Precipitation, Z'rich, Switzerland, 19-23 Aug. 1996 pp. 1310-1313, accepted by the Journal of Atmospheric Research, May.1997.

Fabry, F., and I. Zawadzki, 1995 : Long term radar observations of the melting layer of precipitation and their interpretation. J. Atmos. Sci., 52, 838-851.

Geotis, S.G. and W.M. Silver, 1976 : An evaluation of techniques for automatic ground-echo rejection. Preprints 17th Radar Meteorology Conference, Seattle, Washington, Amer. Meteor. Soc., pp 448-452.

Goodison, B. E. and J. R. Metcalfe 1981 : An experiment to measure fresh snowfall water equivalent at Canadian climate stations. In: Proc. 38th Eastern Snow Conference, pages 110-112, Syracuse, NY, USA.

Guenther, T. 1993 : German precipitation in the WMO Solid Precipitation Intercomparison: Final results. In: B. Sevruk and M. Lapin (Eds.), Precipitation Measurement & Quality Control, Proceedings of the International Symposium on Precipitation and Evaporation, volume 1, pages 93-102, Bratislava.

Harrison D.L., P.D.Newcomb and D.J.Stone 1995 :

NIMROD: a fully automated system for analyzing and forecasting precipitation. Preprints 27th Int. Conf. Radar Met. 9-13 October 1995, Vail, Colorado, Amer.Meteor.Soc. pp 600-602.

Held, E. and J. Joss 1994 : The influence of the orography on precipitation seen by the Swiss radars. COST 75 Seminar on Advanced Radar Systems. Brussels, 20.-23.9.1994.

Held, E. 1995 : Radarmessung im Niederschlag und Einflu^o der Orographie. Dissertation, Eidgen.,ssische Technische Hochschule Z'rich.

Henrich W. J. Joss and A. Waldvogel, 1996 : Influence of snow riming on the bright band and the raindrop size distribution. 12th International Conference on Clouds and Precipitation, Z'rich, Switzerland, 19-23 Aug. 1996, 3 pp.

Heymsfield, A. J. and M. Kajikawa, 1987 : An improved approach to calculating terminal velocities of plate-like crystals and graupel. J. Atmosph. Sci., 44(7), 1088-1099.

Hinze, J. O. 1975 : Turbulence. McGraw-Hill, New York.

Hitchfeld, W. and J. Bordan, 1954 : Errors inherent in the radar measurement of rainfall at attenuating wavelengths. J. Meteor., 11, 58-67.

Hobbs, P. V. 1974 : Ice Physics. Clarendon Press, Oxford, UK.

Jensen, H., 1989:R.,umliche Interpolation der Stundenwerte von Niederschlag, Temperatur und Schneeh.,he. Z'rcher Geographische Schriften, No. 35, 70 pages, Department of Geography, Swiss Federal Institute of Technology (ETH), Zurich.

Joss, J. and E.G. Gori, 1978 : Shapes of raindrop size distributions. J.Appl. Meteor., 17, pp 1054-1061.

Joss, J. and A. Waldvogel, 1990 : Precipitation measurements and hydrology, a review, in "Radar in Meteorology" (David Atlas, Editor), Amer. Meteor. Soc., Boston Mass, pp 577-606.

Joss J. and A. Pittini, 1991 : Real-time estimation of the vertical profile of radar reflectivity to improve the measurement of precipitation in an Alpine region, J. Meteor. Atm. Phys. 47, pp 61-72.

Joss, J. and R. Lee., 1993 : Scan strategy, clutter suppression, calibration and vertical profile corrections. Int. Conference on Radar Meteorology 24-28.5.93, Norman, Okla. USA pp 390-392 (also COST 75/WD/9.

Joss J., G. Galli, A. Pittini, G. Della Bruna and R. Lee, 1995 : Seven years of (dis-)agreement between radar, rain gauges and river flow: possible improvements? Preprints 27th Int. Conf. Radar Met. 9-13 October 1995, Vail, Colorado, Amer.Meteor.Soc. Also COST WD/75/73A.

Joss J., and Lee R., 1995 : The application of radar-gauge comparisons to operational precipitation profile corrections. J. Appl. Meteor., Vol. 34, pp 2612-2630.

Joss. J., H. London and J. Weisbarth 1996a : Need and verification of the accuracy for hydrological radar applications. 20th Nordic Meteorology Conference 28.Aug-1.Sept 1996 in Sweden.

Joss J., H. London and J. Weisbarth 1996b : To what extent do we need absolute calibration, when is reproducibility sufficient? 20th Nordic Meteorology Conference 28.Aug-1.Sept 1996 in Sweden.

Joss J., 1996 : Radome: Attenuation and Phase shift. COST 75 /WD/96 3 pp.

Joss J. and I. Zawadzki, 1997 : Raindrop size distributions again? Proceedings of the 28th Conference on radar meteorology, Austin Texas.

Kirchhofer W. and B. Sevruck, 1992 : Mittlere j hrliche korrigierte Niederschlagsh hen 1951 - 1980. Hydrologischer Atlas der Schweiz, Tafel 2.2.

Kitchen, M., 1994 : Estimation of surface precipitation rate from radar using a variational method. COST 75 Seminar on Advanced Radar Systems. Brussels, 20.-23.9.1994, pp 228-238.

Koistinen, J., 1986 : The effect of some measurement errors on radar-derived Z-R relationships. Preprints 23rd Conference on Radar Meteorology, Vol. 3, pp JP50-53, AMS, Boston.

Laroche, S and I. Zawadzki, 1995 : A single-Doppler radar data assimilation cycle. Preprints 27th Int. Conf. Radar Met. 9-13 Oct. 1995, Vail, Colorado, Amer. Meteor. Soc., pp 255-257.

Lee R., G. Della Bruna and J. Joss. 1995 : Intensity of ground clutter and of echoes of anomalous propagation and its elimination. Preprints 27th Int. Conf. Radar Met. 9-13 Oct. 1995, Vail, Colorado, Amer. Meteor. Soc., pp 651,652., also COST WD/75/74A.

Li L., W. Schmid and J. Joss, 1995 : Nowcasting of motion and growth of precipitation with radar over a complex orography. J. Appl. Meteor., Vol. 34, 6.6.95, pp 1286-1300.

Locatelli, J. D. and P. V. Hobbs, 1974 : Fall speeds and masses of solid precipitation particles. J. Geophys. Res., 79(15), 2185-2197.

Magono, C. and C. W. Lee, 1966 : Meteorological classification of natural snow crystals. Journal of Faculty of Science, Hokkaido Univ., Ser. VII(2), 322-335.

Maurer, C. 1993 : Untersuchung des Winterniederschlages auf dem Gamser Rugg. Diplomarbeit, Geographisches Institut, Eidgen.,ssische Technische Hochschule, Zurich.

Muramoto, K., T. Harimaya, and T. Shiina, 1996 : Snowfall rate determined by image processing data. In: 12th International Conference on Clouds and Precipitation, Vol. 1, pp 470-473, Zurich, Switzerland.

Nespor, V. 1996 : Investigation of wind-induced error of precipitation measurements using a three-dimensional numerical simulation. Z'rcher Geographische Schriften, No. 63, Swiss Federal Institute of Technology (ETH), Zurich.

Nespor, V. 1997 : Investigation of wind-induced error of rain and snow measurements using numerical simulation. Internal report, Department of Geography, ETH Zurich, Zurich.

Press, W. H., B. P. Flannery, S. A Teukolsky., and W. T. Vetterling, 1986 : Numerical recipes. Cambridge University Press.

Sauvageot, H. 1992 : "Radar Meteorology". Artech House, INC. Boston, 366 pp.

Schiesser, H.H., A. Waldvogel, W. Schmid und S. Willemse, 1997 : Klimatologie der St'rme und Sturmsysteme anhand von Radar und Schadendaten. VDF Hochschulverlag AG an der ETH Z'rich, 132 pages.

Sevruk, B., 1985 : Conversion of snowfall depths to water equivalents in the Swiss Alps. In: B. Sevruk (Ed.), Correction of precipitation measurements, WMO/IAHS/ETH Workshop, Z'rcher Geographische Schriften, No. 23, pp 81-88, Department of Geography, Swiss Federal Institute of Technology (ETH), Zurich.

Sevruk, B., 1989 : Reliability of precipitation measurements. In: B. Sevruk (Ed.), Precipitation Measurements, WMO/IAHS/ETH Workshop, pp 13-19, Department of Geography, Swiss Federal Institute of Technology (ETH), Zurich.

Smith P.L., Z. Liu and J. Joss, 1993 : A study of sampling variability in raindrop size observations. J. Appl. Meteorol., Vol. 32, No.7, July 1993, pp 1259-1269.

Smith, P.L. and J.Joss, 1997: Use of a fixed exponent in an "adjustable" Z-R-relationship. Proceedings of the 28th Conference on radar meteorology, Austin Texas.

Spinedi F.,1992 : Synoptical analysis of the events of heavy precipitation on the southern slope of the Swiss Alps, 1961-1990, ICS/ICTP/WMO International Workshop on Mediterranean Cyclones Studies, Trieste, Italy, May 1992.

Streit, U., 1981 : Kriging - eine geostatistische Methode zur räumlichen Interpolation hydrologischer Informationen. Wasserwirtschaft 71, pp219-223.

Ulbrich, C. W., 1983 : Natural variation in the analytical form of the raindrop size distribution. Journal of Climate and Applied Meteorology, 22, 1764-1775.

WMO/CIMO, 1996 : International Organizing Committee for the WMO Solid Precipitation Measurement Intercomparison. Final Report (Draft), WMO Geneva, Toronto, Canada.

Yang, D., B. Sevruk, E. Elomaa, V. Golubev, B. Goodison, and T. Guenther, 1994 : Wind-induced error on snow measurement: WMO Intercomparison Results. In: 23. Internationale Tagung f'r Alpine Meteorologie, Annalen der Meteorologie Nr.30, pages 61-64, Lindau. Selbstverlag des Deutschen Wetterdienstes.

Zimmermann, M. GEO7, 1997 : Beurteilung der Murganggefördung mit Hilfe eines geographischen Informationssystems. Analyse der räumlichen Entwicklung infolge von Klimaänderungen. VDF Hochschulverlag AG an der ETH Z'rich.

11.2. Special references to Swiss radars (being updated)

Galli, G. and J.Joss, 1995 : RADAR PRODUCTS - a description for the users.
[/proj/OTL/WOL/RADAR/DOC/MANUALS/US_PROD/](#)

Jiang, C. and G.Galli, 1996 : SRN Archive/Retrieve Package user's guide
[/proj/OTL/WOL/RADAR/DOC/MANUALS/ARCHIVE/](#)

Haug, M., J.Joss, H.M'ller, B.Hoegger, E.Signer and R.Meyer, 1997:Schlussbericht Ablöschung Wetterradaranlagen, Projektschlussbeurteilung.
[/proj/OTL/WOL/RADAR/DOC/PAPERS/Schlussb.4.3.97](#)

Lassen Research 1995 : Composite System Architecture Document
[/proj/OTL/WOL/RADAR/DOC/MANUALS/CS_ARCH/](#)

Lassen Research 1994 : Radar-site Data System Architecture Document
[/proj/OTL/WOL/RADAR/DOC/MANUALS/RS_ARCH/](#)

12. Format of product data (Galli)

12.1. Introduction

The set of the Swiss Weather Radar products is composed by **images** and **other structured types** of data (e.g. list of the operational radar site parameters).

Image data are distributed outside the Swiss Radar Network (SRN) mainly as GIF coded files, the **other types** of data being coded as ASCII files.

This document explains how to access the data of the various radar site products.

For a description and meaning of the product content (also for composite products) see the section on Product processing.

12.2. Datafile Structure

Images:

Product_file := Header(32Bytes) + Optional_Prefix + Image[rows*cols(Bytes)]

- Currently only product RAIN has a prefix of 48 Bytes, all other products have no prefix.
- The header contains an identification part which permits to recognize the product.

Other types:

Products CALIB , STATUS , WIND are formatted in plain text (ASCII).

Calibration and Status data are mainly given in form of "keyword" : "value" pairs (see example).

For Wind Profiles data are given in form of a structured table .

12.3. Decoder program

Purpose:

Program ***gif_decode*** is used for decoding the GIF-coded SRN product files.

How to use it:

Run program ***gif_decode***, specifying the name of the GIF-coded file as the first argument.

The result of the decoding operation is written to an output file,

taking its name from the input file and setting the last-4th character to "U".

The size of the decoded image will appear in a message.

Example of run:

(execution on a Unix platform)

```
% gif_decode coded.dat
```

the decoded file is : *codeU.dat*

image width x height: 400 x 400 [bytes]

Access to the data:

The binary array of the image data can be extracted from the decoded file after reading and interpreting (or skipping) the header information.

Program download: to download the package and read file *gif_decode.txt* after unzip.

12.4. Product identification

Header := **CH** + Product_identification(14Bytes) + Control_information(16Bytes)

Product_identification (ASCII) := TFS (3Bytes) + DATE (9Bytes) + Q(1Byte) + C(1Byte)

TFS := Type (1Byte) + Format (1Byte) + Source (1Byte)

DATE := Year(2Bytes) + Daynr(3Bytes) + Hour(2Bytes) + Minutes(2Bytes)

Q := Quality code (1Byte)

C := Compression code (1Byte)

Notes:

- only the last two digits are given for the **year** (no century)
- the **day number** is given in the range interval 1 to 365 (or 366)
- the **hour** ranges from 00 to 23

12.5. Product Type

For **image products** we differentiate between PPI and CAPPI categories.

- PPI is for images in Polar Coordinates
- CAPPI is for images in Cartesian Coordinates

Product Type	Product Name	Product Content	Image Category	Example	Supported Formats
C	CALIB	Calibration Report	N.A.	CVL982470015	ASCII
N	COUNTP	Cumulated Count of Valid Measurements	PPI	N1D991022355	NY
O	OVERVIEW	Volumetric Instantaneous Reflectivity	CAPPI	O3L982472200	OY
P	RAIN	Estimated 30 min Surface Precipitation Intensity	CAPPI	PHL982472200	PH , PL , PS
R	RAPID	Maximum Vertical Instantaneous Reflectivity	CAPPI	RHL972401655	RH , RL , RS

Operational Use of Radar for Precipitation Measurements in Switzerland

S	STATUS	Status Report	N.A.	SVL972472200	ASCII
T	TODAY	3-Views Maximum Projection of Instantaneous Reflectivity	CAPPI	TGC982472200	TG
U	POLARU	Doppler Instantaneous Velocity	PPI	U3L982480717	UY
V	VISIBP	Cumulated Precipitation Quantity	PPI	V1D991022355	VY
W	WIND	Profile of Wind Velocity	N.A.	WDA990400000	ASCII
Z	POLARZ	Instantaneous Reflectivity	PPI	Z3L982480717	ZY

12.6. Image format

Type+Format -> image array_size(rows x cols) + pixel_size(length x width) + pixel_content(coding-table)

Type+Format	rows	columns	pixel_size	coding-table	interval
NY	360	f(elevation)	1° x 1km	valid counts-coding	24 h
OY	200	200	2km x 2km	4 bit Z-coding	5 min
PH	400	400	1km x 1km	4 bit Z-coding	5 min
PL	305	269	2km x 2km	4 bit Z-coding	5 min
PS	305	269	1km x 1km	4 bit Z-coding	5 min
RH	400	400	1km x 1km	4 bit Z-coding	2.5 min
RL	305	269	2km x 2km	4 bit Z-coding	2.5 min
RS	305	269	1km x 1km	4 bit Z-coding	2.5 min
TG	320	256	2km x 2km	3 bit Z-coding	5 min
UY	360	f(elevation)	1° x 1km	velocity-coding	5 min
VY	360	f(elevation)	1° x 1km	4 bit R-coding	24 h
ZY	360	f(elevation)	1° x 1km	4 bit Z-coding	5 min

12.6.1. Volumetric Cartesian format

For the product named **OVERVIEW** the format code Y indicates the altitudes of 1 km thick horizontal planes in correspondence of their centers:

Y	1	2	3	4	5	6	7	8	9	A	B	C
Height [m a.s.l.]	1000	2000	3000	4000	5000	6000	7000	8000	9000	10000	11000	12000

The maximum of the reflectivity values in the vertical is reported in a 13th plane with the Y code set to **M**.

12.6.2. Volumetric Polar format

Elevation-dependent maximum range [km] for polar reflectivity (ZY), valid measurements count (VY) and cumulated precipitation (NY) data										
Format Code Y	1	2	3	4	5	6	7	8	9	A
gates (columns)	230	230	162	112	85	68	51	37	27	20
Elevation angle [degrees]	-0.3	1.5	3.5	5.5	7.5	9.5	13.0	18.3	25.3	34.5
Format Code Y	B	C	D	E	F	G	H	I	J	K
gates (columns)	230	205	133	97	76	59	43	31	23	18
Elevation angle [degrees]	0.5	2.5	4.5	6.5	8.5	11.0	15.5	21.6	29.6	40.0

Elevation-dependent maximum range [km] for polar Doppler (UY) data										
Format Code Y	1	2	3	4	5	6	7	8	9	A
gates (columns)	130	130	130	112	85	68	51	37	27	20
Elevation angle [degrees]	-0.3	1.5	3.5	5.5	7.5	9.5	13.0	18.3	25.3	34.5
Format Code Y	B	C	D	E	F	G	H	I	J	K
gates (columns)	130	130	130	97	76	59	43	31	23	18
Elevation angle [degrees]	0.5	2.5	4.5	6.5	8.5	11.0	15.5	21.6	29.6	40.0

12.7. Pixel content

Pixel values are present in coded form within image products.

12.7.1. Coding of reflectivity

For instantaneous **reflectivity** data given in **dBZ**, code values in the 4-bit and 3-bit coding-tables are indicated for the upper and lower bounds of the class; the **rain rates** given in **mm/h** as resulting from the formula $Z=316R^{1.5}$ refer to the class center.

4-bit coding-table for instantaneous reflectivity data																
CODE	0	1	2	3	4	5	6	7	8	9	10	11	12	13	14	15
[dBZ]	<13	13-16	16-19	19-22	22-25	25-28	28-31	31-34	34-37	37-40	40-43	43-46	46-49	49-52	52-55	>55
[mm/h]	0.0	0.20	0.32	0.50	0.80	1.3	2.0	3.2	5.0	8.0	13	20	32	50	80	130

For the 3-bit coding scheme of instantaneous reflectivity data the code value = 7 is reserved for the graphical layout of the product.

3-bit coding-table for instantaneous reflectivity data								
CODE	0	1	2	3	4	5	6	7
[dBZ]	<17.5	17.5-25	25-32.5	32.5-40	40-47.5	47.5-55	>55	-
[mm/h]	0.0	0.56	1.78	5.6	17.8	56	178	-

12.7.2. Coding of cumulated precipitation

For cumulated **Precipitation** data, code values C_i are related to the precipitation amount R_i through the formula:

$$R_i = 10^{(0.02 \times (C_i - 1) - 1.6666)}$$

expressed in **mm** of total precipitation amounts collected during the cumulation period.

The quality code taken from the product identification gives an indication about the number of cumulated volumes per day.

12.7.3. Coding of Doppler data

For **Doppler** data, code value C_i corresponds to a velocity laying within the two boundary values given by V_i in the formula:

$$V_i = (V_n / 255) \times (2 \times C_i - 256 \pm 1) \text{ for } C_i = 1..255 \text{ where } V_n \text{ is the Nyquist velocity, } C_i = 0 \text{ meaning missing value.}$$

For example $C_i=1$ corresponds to the velocity interval $\sim V_n \times [-1.000, -0.992]$ and $C_i=128$ to $\sim V_n \times [-0.004, +0.004]$

The Nyquist velocity depends from the elevation angle of the antenna because the Pulse Repetition Frequency changes as indicated in the scan strategy table.

Nyqvist velocity V_n in dependence from the antenna elevation angle (first half scan)										
Format code Y	1	2	3	4	5	6	7	8	9	A
Elevation angle [degrees]	-0.3	1.5	3.5	5.5	7.5	9.5	13.0	18.3	25.3	34.5
V_n [m/s]	8.27	8.27	11.03	11.03	16.54	16.54	16.54	16.54	16.54	16.54

Nyqvist velocity V_n in dependence from the antenna elevation angle (second half scan)										
Format code Y	B	C	D	E	F	G	H	I	J	K
Elevation angle [degrees]	0.5	2.5	4.5	6.5	8.5	11.0	15.5	21.6	29.6	40.5
V_n [m/s]	8.27	8.27	11.03	11.03	16.54	16.54	16.54	16.54	16.54	16.54

12.7.4. Coding of valid measurements count

For **Valid Measurements Count** data, code values C_i are related to the number of times N_i that the pixel i is detected free of clutter (as resulting from the clutter detection algorithm) during the cumulation period (usually **one day**) as follow:

$$C_i = N_i - 33$$

Thus, assuming a volume scan of 5 minutes corresponding to 288 images per day, one pixel without any clutter contamination would have a coded value of 255 during one day when all images were available. A count of 0 indicates the presence of a fixed and permanently identified clutter on a given pixel location.

The quality code taken from the product identification gives an indication about the number of cumulated volumes per day.

12.8. Georeferencing

The projection used by **Cartesian products** is a conformal cylindric projection with oblique axis, the coordinates of the old observatory of Bern being set to 600000/200000 [m]. For details and formulas see the document *Swiss National Cartographic Projection*.

Pixel sequence within an image:

- For **Cartesian** products: sequence of rows from North to South. Within each row pixels are sequenced from West to East.
- For **Polar** products: sequence of rays with the axis going from azimuth 0 degrees (North) to azimuth 359 degrees. Within each ray the centers of the gates of 1 km in depth

Operational Use of Radar for Precipitation Measurements in Switzerland

are sequenced by increasing range starting from the distance of 1km from the radar station up to an elevation and product dependent distance.

Type+Format+Source(**TFS**) -> [W/E-coordinate, S/N-coordinate] of the most SW image pixel at its center.

TFS	W/E-coordinate [km]	S/N-coordinate [km]
OYA	481.5	38.5
OYC	298.0	-99.0
OYD	297.5	-57.5
OYL	507.5	-99.5
PHA	481.5	38.5
PHD	297.5	-57.5
PHL	507.5	-99.5
PLC	298.0	-99.0
PSA	529.5	103.5
PSD	345.5	8.5
PSL	555.5	-34.5
RHA	481.5	38.5
RHD	297.5	-57.5
RHL	507.5	-99.5
RLC	298.0	-99.0
RSA	529.5	103.5
RSD	345.5	8.5
RSL	555.5	-34.5
TGA	482.0	9.0
TGC	298.0	-31.0
TGD	298.0	-87.0
TGL	508.0	-129.0

Example:

The geographic location of the area delimited by columns 150 to 165 and rows 0 to 10 for the product PHD (RAIN/Dôle) can be found by knowing the coordinates of the bottom left hand image pixel (at its center) and the geometry of the product, the image being oriented with the North on the top:

NW-pixel(center) of the area : (297.5+150, -57.5+399)

SE-pixel(center) of the area : (297.5+165, -57.5+399-10)

the image size being 400 x 400, the pixel size 1km x 1km the column and row indices going from

Operational Use of Radar for Precipitation Measurements in Switzerland

0 to 399 and the coordinates being given in km based on the Swiss Cartographic Projection.

For **PPI products** the georeferenciation depends from the location of the pixel (range-azimuth-elevation values) as well as from the location of the radar station which is:

Station	Latitude	Longitude	CH-coordinate W/E [km]	CH-coordinate S/N [km]	Altitude [m]	WMO Index Nr.
ALBIS	47.285N	8.513E	681.193	237.593	928	06 661
LA DOLE	46.426N	6.100E	497.057	142.408	1680	06 699
LEMA	46.042N	8.834E	707.957	99.762	1625	06 768



Formulas relating polar coordinates to Cartesian coordinates are under construction...

Additional remarks:

- **Word length of pixels for images in GIF:** 8 bit
- **Volume scan interval:** 5 minutes (for polar data look at the scan strategy)
- **Time indications:** are in UTC and refer to the end of the volume scan
- **Start of continuous operation activity:** from September 1993 to November 1995 (dependend from the station)

12.9. Format of Wind Profile data

For VAD products, data are saved in records of following sequence:

```
Items      date,      rh,      hei,      vh,      dir,      vv,      rms,      naz
-----
Formats    yydddhhmm DDDDD DDDDD DD.D DDD      ±DD.D DD.DD DDD
-----
Units      string    m      m      m/s    degrees m/s      m/s      #
```

where "yydddhhmm" => year-daynr-hour-minute and "D" => decimal digit

and with following meaning:

- date: starting date+time of the swap [UTC]
- rh : horizontal range of the gate centre
- hei : altitude a.s.l. of the gate centre
- vh : horizontal component of the radial velocity (>0 towards)
- dir : azimuth of the wind direction (0->North,>0 clockwise)
- vv : vertical component of the radial velocity (>0 towards)
- rms : root mean square of the difference between the radial velocity and the fitted sinus function divided by the radial velocity or values 99.x for flagging factors of bad quality
- naz : number of approved azimuthal samples

each field being separated by 1 blank.

12.10. Quality Indicator

For products COUNTP and VISIBP the quality indicator Q is in range 1 to 9 and corresponds to the percentual number of accumulated volumes with respect to the value 288 (which is the number of 5 minutes volumes in 24 hours) divided by 10.

A low value of Q indicates a small number of cumulated volumes (due for example to a downtime of the radar station for the considered day); a value of 9 corresponds to more than 90% of uptime for the cumulated product.



... under construction for other products

12.11. Visibility maps

Visibility maps gives indications about the degree of non-occultation at locations in space illuminated by the radar beam.

They can be estimated using a numerical model which simulate the radar irradiation impact with the surrounding terrain.

The maps given here results from a very simple model which use a digital terrain model with spatial resolution of 250 m and a beam with uniformly distributed energy in a spatial angle of 1 degree which scans the volume around the radar station under normal propagation conditions. For each used elevation and each radar station there is a map giving the percentual degree of non-occultation for the points laying over the scanned conical surface. For example the visibility map for the radar station La Dôle at -0.3 degrees elevation indicates good visibility conditions in the Northwest direction and worse conditions to the Southeast.